Universidad de Huelva

Departamento de Ingeniería Química, Química Física y Química Orgánica

High pressure rheology of drilling fluids

Memoria para optar al grado de doctor
presentada por:

Juan Hermoso Limón

Fecha de lectura: 18 de julio de 2014

Bajo la dirección de los doctores:

Francisco José Martínez Boza
Críspulo Gallegos Montes

Huelva, 2014

REOLOGIA DE FLUIDOS DE PERFORACION A ALTA PRESION

HIGH PRESSURE RHEOLOGY OF DRILLING FLUIDS

Universidad de Huelva

PROGRAMA OFICIAL DE DOCTORADO EN PROCESOS Y PRODUCTOS QUÍMICOS

Juan Hermoso Limón

University of Huelva

Department of Chemical Engineering

A thesis submitted for the degree of Doctor of Philosophy

in Chemical Engineering at the University of Huelva,

by Juan Hermoso Limón

Supervisor:

Dr. Francisco José Martínez-Boza, Professor in Chem. Eng.

Dr. Críspulo Gallegos Montes, Professor in Chem. Eng.

Huelva, 2014

AUTORIZACIÓN PARA LA DEFENSA DE LA TESIS DOCTORAL EMITIDA POR LA COMISIÓN ACADÉMICA DEL PROGRAMA DE DOCTORADO

DATOS DEL/ DE LA DOCTORANDO/A:

Apellidos y nombre: Hermoso Limón, Juan	NIF/ Pasaporte: 48931637B	Nacionalidad: Española
Dirección a efectos de notificaciones: Glorieta de los Rederos nº4 1º A		
Teléfono: 620610199	EMAIL: juan.hermoso@diq.uhu.es / djuanhl@yahoo.es	

DATOS DE LA TESIS DOCTORAL:

Título: High Pressure Rheology of Drilling Fluids
Programa Oficial de Doctorado al que se adscribe y órgano responsable: Procesos y Productos Químicos
Línea de investigación a la que se adscribe y órgano responsable: Caracterización y Procesado de Productos derivados del Petróleo
Director/a: Dr./Dra. Francisco Martínez Boza Dr./Dra. Críspulo Gallegos Montes Dr./Dra.

A CUMPLIMENTAR POR LA COMISIÓN ACADÉMICA DEL PROGRAMA DE DOCTORADO:

Una vez valorada la Tesis Doctoral presentada por el/la Doctorando/a y haber incorporado éste/a las modificaciones y/o cambios que esta Comisión Académica le pudiera haber indicado, **se AUTORIZA**, en reunión de fecha , **LA DEFENSA** de la misma.

En Huelva a, _____ de _____ de 2014

Firma del/de la Presidente/a de la Comisión Académica

Fdo. Dra. Concepción Valencia Barragán

Agradecimientos

Me gustaría expresar mi más sincera gratitud a mi tutor en esta Tesis doctoral, Dr. Francisco Martínez-Boza por su crítica constructiva, apoyo y estímulo fueron fundamentales para la consecución de esta Tesis. También, me gustaría dar la gracias a mi segundo tutor Dr. Críspulo Gallegos Montes por su estupenda labor supervisora y su enorme entendimiento en la materia. Gracias a ellos he sido capaz de tener una sólida formación en el campo de la investigación, la cual, será sin duda esencial para mi futura carrera.

También me gustaría agradecer al Programa de Proyectos Excelencia de la Junta de Andalucía FEDER (Proyecto de Investigación P08-TEP-3898, Junta de Andalucía, España) por la aportación económica recibida.

En segundo lugar, mi gratitud está dirigida a todos los compañeros que me han ayudado profesional y emocionalmente durante la realización de la Tesis Doctoral en el laboratorio de Ingeniería de Fluidos Complejos de la Universidad de Huelva. Entre todos ellos, quiero dar las gracias especialmente al Dr. Enrique (1979) y Gema (1987). Fuera de este laboratorio, quiero agradecer también a Antonia (1955) y Encarni (1983) su paciencia, apoyo y acertados y cariñosos consejos.

En tercer lugar, estoy muy agradecido al Dr. Edo Boek (1965) por recibirme durante mi estancia de tres meses en el Imperial College London. Gradezco su dirección y valioso consejo. Asimismo, me siento agradecido por el buen trato recibido por parte de mis compañeros del grupo del Centro de Investigación Qatar Carbonates and Carbon Storage, especialmente a Christine (1985). Ha sido un gran placer trabajar con todos y cada uno de ellos durante mi estancia.

Finalmente, quiero dar las gracias a mis amigos, los cuales los considero una extensión familiar y un pilar en mi vida. De igual modo, expreso aquí mi más profundo aprecio y gratitud a todos los miembros de mi familia, a mi Madre, Padre y mi hermana Ana (1983) por su interminable Apoyo y la Confianza puesta en mi todos estos años. Es

también de agradecer a mi cercana abuela Catalina (1911) por su incondicional Amor. Esta Tesis Doctoral está dedicada a su memoria.

Por encima de todo y siendo lo más importante, me siento agradecido al Creativo Dios $(-\infty, +\infty)$ quien me sostiene y apoya en todo. Gracias porque lo mejor está aún por llegar.

Quien es de verdad Maestro, no se toma ninguna cosa en serio más que en relación con sus discípulos, ni siquiera consigo mismo.

(Friedrich Nietzsche)

Acknowledgements

I would first like to express my sincerest gratitude to my PhD supervisor Prof. Francisco José Martínez-Boza. His insightful direction, support and encouragement were integral to this thesis. I would also like to thank my second supervisor Prof. Críspulo Gallegos Montes for his great supervision and his fabulous insight. Thanks to them I have been able to develop a solid formation in the field of researching which will be essential for my later career development.

I also thank FEDER-Excellence Projects Programme (Research project P08-TEP-3898, Junta de Andalucía, Spain) for the financial support.

Secondly, my gratitude goes to all the colleagues who have helped me professionally and emotionally during the realization of the present Thesis in the Complex Fluids Engineering Laboratory at University of Huelva. A special mention goes to Dr. José Enrique (1979) and Gema (1987). Outside this laboratory, I would like to thank Antonia (1955) and Encarni (1984) for their patience, support and charming advice.

Thirdly, I am very grateful to Dr. Edo Boek (1965) to receive me during my three months stay at the Imperial College London. I thank for his guidance and valuable advice. My gratitude also goes to my colleagues of the Qatar Carbonates and Carbon Storage Research Centre group, especially to Christine (1985).

Finally, I would like to thank to my friends who are part of my family and an indispensable pillar in my life. Besides, I would like to express my deepest appreciation and gratitude to all members of my family, my Mum, Father and my sister Ana (1983) for their never-ending Support and Confidence deposited into me. Likewise, I would like to thank my lovely grandma Catalina (1911) for her Love. This Thesis is dedicated to her memory.

Above all and most, I am always thankful to the Imaginative God (-∞, +∞) who always strengths and supports me with everything. Thank you for the best is yet to come.

He who is a teacher from the very heart takes all things seriously only with reference to his students - even himself.

(Friedrich Nietzsche)

Contents

1. Introduction

Resumen

Generalmente, los fluidos de perforación son mezclas multicomponentes complejas (emulsiones, suspensiones, espumas, etc), constituidas por un fluido base (agua o aceite), un espesante/diluyente (arcillas) y diversos aditivos (sales inorgánicas y otros), diseñados para lubricar durante la perforación y eliminar los recortes entre otras tareas. Las propiedades de los fluidos de perforación se optimizan para conseguir el mejor rendimiento de la operación de perforación, teniendo en cuenta las condiciones particulares de temperatura y presión en el pozo. Desde el punto de vista del ingeniero de campo, la optimización de propiedades del fluido mediante la selección los componentes principales de la suspensión base es una tarea clave. En este sentido las arcillas, principalmente esmectitas, son componentes claves en el desarrollo de propiedades. En el caso de los fluidos en base aceite, las organoarcillas se han utilizado preferentemente dada su facilidad de dispersión y buenas propiedades de transporte de sólidos. Por tanto, el conocimiento del efecto de las organoarcillas sobre las propiedades del fluido de perforación, en función de la temperatura y de la presión es esencial para el diseño de fluido exprofeso en cualquier perforación.

El aumento de las perforaciones de pozos en condiciones extremas de temperatura y presión requiere de un conocimiento exhaustivo del comportamiento volumétrico y reológico de los fluidos de perforación. La previsión de aumento mundial de la demanda de combustibles para los venideros fuerza a la industria del petróleo a perforar en condiciones cada vez más extremas reduciendo los costes. Teniendo en cuenta el coste de los fluidos de perforación sobre el total del proyecto de exploración y producción de pozos de petróleo (entre el 15 y 18% de la inversión), el éxito del proyecto y su coste depende en gran medida de las propiedades de estos fluidos. Así, tanto la predicción como el control de las propiedades más importantes de los fluidos de perforación, densidad y viscosidad, con temperatura y presión son esenciales para asegurar el éxito del proyecto.

En consecuencia, este trabajo original de investigación se centra en el estudio de la influencia que ejerce la temperatura y la presión sobre el comportamiento reológico y volumétrico de una serie de suspensiones modelo, formuladas con organobentonitas y aceites minerales, usados comúnmente en la formulación de fluidos de perforación de pozos de petróleo.

Después de una revisión del estado del arte en la materia y la descripción de los sistemas experimentales utilizados, el capítulo 4.1 trata sobre la caracterización del comportamiento no newtoniano de estos materiales reológicamente complejos en función de la presión, aplicando los principios de la reometría de mezclado. Para realizar este estudio se han diseñado y calibrado dos geometrías no convencionales, una cinta helicoidal y una turbina, usando un fluido newtoniano y varias soluciones acuosas de polímeros con distintos índices de flujo a 20ºC. En este sentido, las medidas de viscosidad a presión atmosférica fueron validadas usando un cilindro coaxial convencional, mientras un conjunto de cilindro coaxial-célula de presión fue empleado para verificar las medidas realizadas a alta presión. Estas geometrías especiales fueron validadas en ensayos bajo presión, usando un fluido de perforación modelo en base aceite, formulado con un 5% en peso de la organobentonita B128 y un aceite nafténico denominado SR-10, el cual fue preparado para ser medido bajo condiciones de alta presión. Los resultados obtenidos demuestran que estas geometrías especiales permiten medir el efecto de la presión sobre los parámetros reológicos de los fluidos de perforación, ampliando el rango de medida de velocidades de cizalla que se alcanza con el uso de la geometría de cilindros coaxiales a valores más bajos.

Las propiedades de la arcilla y la composición son los factores principales que determinan las propiedades de fluencia viscosa de los fluidos de perforación. Así, el capítulo 4.2 estudia el efecto del tipo de arcilla y su composición sobre las propiedades reológicas de las suspensiones de arcilla sometidas a alta presión, realizando ensayos de flujo viscoso sobre fluidos de perforación modelo en base aceite, del tipo “all-oil”, sometidos a alta presión. La preparación de estos fluidos modelo se realizó mezclando en aceite SR-10, al 1, 3 y 5% en peso, dos organobentonitas, conocidas por la siglas B34 y B128. Como se esperaba, el comportamiento viscoso de estos fluidos está muy

influido tanto por la organoarcilla como por su concentración. También se comprobó que la relación entre la viscosidad y la presión de estas suspensiones modelo está fuertemente determinada por las propiedades piezoviscosas del aceite base. Un modelo factorial tipo Sisko-Barus, el cual combina la influencia de la cizalla y la presión en la misma ecuación, describe satisfactoriamente los datos experimentales de presión y viscosidad.

Con objeto de profundizar en la reología de los fluidos de perforación tipo "all-oil" bajo condiciones de alta presión y alta temperatura, dada la creciente demanda de la industria petrolera de fluidos de altas prestaciones, el capítulo 4.3 trata de la caracterización reológica de dos fluidos de perforación modelo (5% en peso de organobentonita) en función de la presión y de la temperatura. Los modelos reológicos de Bingham y de Herschel-Bulkley describen satisfactoriamente el efecto combinado de la temperatura y la presión sobre el flujo viscoso de estos fluidos. El modelo factorial WLF-Barus predice satisfactoriamente la evolución de la viscosidad plástica con la presión y la temperatura. Estos resultados se justifican estructuralmente en base a la compresión del medio continuo y a los cambios en la fracción en volumen de la fase dispersa, atribuidos a la modificación de las interacciones entre el polímero de cubrición de las partículas y el aceite con la temperatura.

El efecto de la presencia de agua sobre la reología de los fluidos de perforación es también fundamental en el caso de perforaciones de pozos dónde se produce influjo de agua desde la formación. En este sentido, en el capítulo 4.4 se estudia el efecto que ejerce la fracción acuosa, el contenido de organoarcilla y la presión sobre las propiedades reológicas de emulsiones inversas modelo (conocidas también por barros inversos) preparadas a partir de los fluidos diseñados. Se han formulado varias emulsiones con distintas fracciones en volumen de fase acuosa, usando las suspensiones modelo, con un 1% y 3% en peso, de la organobentonita B128. A partir de los resultados obtenidos, se deduce que, a presión atmosférica, tanto el esfuerzo umbral como el módulo viscoélastico dependen de la fracción en volumen de la fase acuosa y de la concentración de organoarcilla. El modelo de Herschel-Bulkley ajusta el comportamiento de flujo viscoso de estas emulsiones, formuladas abarcando un amplio

rango de fracciones en volumen de fase dispersa, bastante bien. Por otro lado, el modelo de Barus describe la dependencia de la viscosidad de la emulsión con la presión, para distintas fracciones en volumen y concentraciones de organoarcilla, bastante bien. Estos resultados sugieren que el comportamiento reológico a alta presión de estas emulsiones inversas está relacionado con la elasticidad de la interfase que rodea a las gotas emulsionadas.

Similarmente al comportamiento reológico, el conocimiento del efecto que ejerce la presión y temperatura sobre las propiedades volumétricas de los fluidos de perforación es de gran importancia. Sin embargo, la influencia de la naturaleza de la arcilla y su concentración en la densidad no está aún muy bien estudiada. En este sentido, los capítulos finales 4.4 y 4.5 se han dedicado a estudiar la influencia de la naturaleza de la arcilla y de la concentración en la densidad de fluidos de perforación modelo en base aceite, en un amplio rango de presiones y temperaturas. Con este objetivo, se calibró un densímetro vibrante de alta presión, en un rango de temperaturas comprendido entre los 40ºC y los 140ºC, y presiones de hasta 1200 bar. Para ello, se usaron dos fluidos de calibrado (agua y n-dodecano) por estar las densidades del aceite y las suspensiones dentro de los valores de densidad de estos fluidos de calibrado. Por último, la dependencia de las propiedades volumétricas respecto a la presión y temperatura ha sido modelizada en base a diversas ecuaciones de estado como Tait modificada y Murnaghan.

A partir de los datos de presión-densidad-temperatura obtenidos, puede concluirse que, por un lado, la adición de la organoarcilla al aceite base supone un significativo incremento de la densidad en el rango de presión y temperatura estudiado. El comportamiento expansivo no ideal de estas suspensiones parece estar asociado con el hinchamiento macroscópico de cada tipo de organoarcilla en el medio no acuoso.

Finalmente, los datos de presión-viscosidad-temperatura de los fluidos de perforación estudiados se han usado para modelizar la evolución de la viscosidad de estos sistemas en función de la presión y la temperatura mediante modelos basados en la teoría del volumen libre como los modelos de Yasutomi o FMT y modelos empíricos como

WLF-Barus. Desde el punto de vista ingenieril, ambos tipo de ecuaciones modelizan satisfactoriamente la evolución presión-temperatura-viscosidad de estos fluidos.

Abstract

Generally, drilling fluids may be multicomponent suspensions, emulsions and/or foams, basically consisting of a base fluid (oil or water), viscosifiers/thinners (clays, biopolymers, etc) and weighting agents (salts) designed to lubricate during drilling operation and removal the cuttings, among others functions. Further, depending on the particular conditions of temperature and pressure of the wellbore to be drilled the drilling fluid properties have to be optimized for the best performance. Hence the selection of both the base fluid and additives is a critical issue from a mud engineer point of view. In this sense, clays, and particularly smectites, are the most typical additives to achieve fluid properties. In the case of oil-based drilling fluid, organobentonites have been used in model oil-based drilling fluid formulation due to their good dispersing properties in oil media as well as their excellent carrying and suspension capacities. Accordingly, the knowledge of organobentonite effect on the fluid properties as function of pressure and temperature is essential for designing a fit-for-purpose drilling fluid for any particular wellbore challenge.

The increasing number of wells being drilled under extreme conditions of pressure and temperature requires a comprehensive understanding of the volumetric and rheological behaviour of oil-based drilling fluids. The increasingly worldwide oil demand in the future years has forced the oil industry to drills more challenging wells reducing overall operation costs. Due to the significant impact of drilling fluid on the total drilling costs of petroleum wells (between 15% and 18%), the successful completion and cost of oil well notably depends on the fluid properties. In addition, controlling and predicting the evolution of the two most important properties, density and viscosity, with pressure and temperature, is crucial in ensuring the success of the project.

Consequently, this Thesis focuses on the influence that both pressure and temperature exerts on the rheological and volumetric behaviour of model suspensions, formulated with organobentonites and mineral oils, commonly used as oil-based drilling fluids.

After an intense review about both the drilling fluid state-of-art and the experimental description, chapter 4.1 deals with the characterization of the non-Newtonian flow behaviour of these rheologically complex materials as function of pressure applying the approach of the mixing rheometry. In order to do that, two non-conventional geometries, such as helical ribbon and blade turbines, were designed and calibrated using a Newtonian fluid and several aqueous polymer solutions with different flow indexes at 20ºC. In this sense, the atmospheric pressure viscosity measurements were validated using a conventional coaxial cylinder, whereas coaxial cylinder-pressure cell was employed to verify rheological measurements under pressure. The special geometries were validated under high pressure conditions, using a model oil-based drilling fluid, composed of 5% by weight of B128 organobentonite and naphthenic oil base named SR-10. The results demonstrate that these special geometries enable to measure the effect of pressure on rheological parameters of drilling fluids, extending the experimental shear-rate window covered by coaxial cylinders to lower values.

Clay properties and composition are the main key factors that control the development of the flow properties of drilling fluids. Thus, chapter 4.2 studies the effect that organobentonite nature and concentration exert on the rheological properties of oil-based suspensions submitted to high pressure, performing viscous flow measurement of model oil-based drilling fluids, known as “all-oil”, under high pressures. The model all-oil drilling fluids were prepared by mixing in oil SR-10, at 1, 3 and 5% weight, two organobentonites, denoted as B34 and B128. As expected, the viscous flow behaviour of oil-based fluids is strongly influenced by organobentonite nature and concentration. In addition, the pressure-viscosity behaviour of these oily model suspensions is mainly affected by the piezo-viscous properties of the oil and the properties of the continuous phase. A factorial Sisko-Barus, which combines the shear and pressure influences in the same equation, fits the experimental pressure-viscosity data, fairly well.

In order to get further insight into the complex rheology of all-oil drilling fluids at high pressure and high temperature conditions, and consequently satisfies the increasingly requirements of drilling industry to deal with more technically difficult wells, chapter 4.3 deals with the rheological characterization as function of temperature and pressure,

of two model all-oil drilling fluids (5% by weight of organobentonite). Two well-known rheological models, Bingham and Herschel-Bulkley models, satisfactorily describe the combined effect of pressure and temperature on the viscous flow behaviour of these fluids. Further, a factorial WLF-Barus model satisfactorily predicts the temperature/pressure evolution of the plastic viscosity for both drilling fluids. These results have been explained on the basis of the compression of the continuous media and thermally-induced changes in effective disperse volume fraction, being the latter attributed to changes in solvency between polymer-covered particles and the oil media with temperature.

The effect of water content on drilling fluids rheology is also vital to detect and solve drilling problems related to water influx from rock formation. In this sense, chapter 4.4 is devoted to study the influence of aqueous phase volume fraction, organobentonite concentration and pressure on rheological properties of model invert oil emulsions (also known as invert-muds). Accordingly, several emulsions were formulated with different aqueous volume fractions using the model 1% and 3% B128-based oily suspensions. At atmospheric pressure, both apparent yield stresses and linear viscoelastic modulus are highly influenced by the aqueous disperse phase volume fraction, as well as organoclay concentration. The Herschel-Bulkley model fits the viscous flow behaviour of these emulsions in a wide range of internal aqueous phase volume fraction, fairly well. Barus' model describes the pressure dependence of emulsion viscosity, for different disperse phase volume fractions and organoclay concentration, fairly well. These results suggest that the high pressure rheological behaviour of these invert emulsions may be related to the elasticity of the interfacial layer surrounding the emulsified droplets.

Similarly to rheological behaviour, the knowledge of the effect of high pressure and high temperature on the volumetric properties of drilling fluids is a critical issue worth to be studied. However, the influence of both clay nature and concentration on density is not well understood yet. Hence, the last chapters 4.4 and 4.5 have been focused on the influence of organoclay nature and concentration on the density of the model all-oil drilling fluids, in a wide range of pressure and temperature. With this aim, a high-

pressure vibrating densimeter was calibrated in a temperature range comprised between 40ºC and 140ºC, and pressures up to 1200 bar. To do that, two calibration fluids (water and n-dodecane) were used due to the oil and suspensions densities are inside the density range defined by these calibration fluids. In addition, the pressure-temperature dependence of the volumetric properties of the model fluids was modelled by using different Equation of State such as modified-Tait and Murnaghan.

From pressure-density-temperature data obtained, it can be concluded that, organobentonite addition to the oil base yielded a significant increase in density values in the whole range of temperature and pressure tested. The non-ideal expansive volumetric behaviour of these suspensions seems to be associated with the particular macroscopic swelling of each organoclay in non-aqueous media.

Finally, pressure-viscosity-temperature data of oil-based drilling fluids were used to predict the evolution of viscosity of these systems as function of pressure and temperature using both free-volume based models such as Yasutomi's and FMT's models and empirical model such as WLF-Barus' model . The pressure-temperature-viscosity behaviour is successfully modelled by using the different both kinds of models for engineering purpose.

2. Literature Review

2.1. Drilling Fluids Overview

Drilling fluids are used in oil well drilling operations to extract the oil from the reservoir. These systems are multicomponent emulsions and/or suspensions which are usually classified as "complex fluids" from a rheological point of view. Drilling fluids are related either directly or indirectly to most of drilling problems. The successful drilling operation of an oil well and its cost is significantly influenced by the properties of the drilling fluid (Caenn et al., 2011). The proper formulation of a drilling fluid system which withstands drilling in any particular environment is very challenging. Hence, the knowledge of principal properties of this type of fluids, such as density and viscosity, is a key component of design to accomplish its functions efficiently with minimal costs. Rather, the appropriate selection of a drilling fluid involves safety, high pressure/high temperature conditions or loss zones among others.

2.1.1. Functions of Drilling Fluids

Many requirements are placed on the drilling fluids. The first and only objective of the drilling fluid along decades was to serve as vehicle for removal of cuttings from the bore hole. Nowadays, most of drilling fluids textbooks and manuals list from 10 to 20 functions that drilling fluids performs while drilling a well (Caenn and Chillingar, 1996). However, in rotary drilling, the main functions carried out by the drilling fluid are (Lyons, 2010):

Cool and Lubricate.
When the bit drills into the rock formation, considerable heat and friction is generated at bit between the drill string and wellbore. Likewise, the continuous contact between the drill string and wellbore create significant torque and drag during trips. During the circulation, the heat generated is dissipated by the drilling fluid, reducing the chance of

premature bit failures and pipe damage (Lyons, 2010). The drilling fluid also serves as a lubricant between the wellbore and drill string, decreasing torque and drag.

Clean the Bit and the Bottom of the Hole.

If the cuttings generated at the bit face are not immediately removed, they will be ground very fine, stick to the bit, and generally reduce the penetration rate.

Suspend Solids and Transport Cuttings.

When circulation needs to be stopped (connections, bit trips or loggings runs), the drilling fluids must have the capacity to suspend weight materials and drilled solids. If the drilling fluid is unable to suspend the weight materials it could imply reduction of the drilling mud density, and consequently can lead to kicks and potential of a blowout. Any drilling fluid must be able to transport cuttings out of the hole at a reasonable velocity that minimizes their disintegration and incorporation as drilled solids into the drilling fluid system.

Stabilize the Wellbore and Control Subsurface Pressures

Borehole instability is a natural characteristic of the unequal mechanical stresses and physical-chemical interactions and pressure created when supporting material and surfaces are exposed in the process of drilling a well. The drilling fluid must succeed the trend for the hole to collapse from mechanical failure or from chemical interaction of the formation with the drilling fluid. Borehole stability is sustained by controlling the loss of filtrate and using proper chemicals in the drilling fluid formulation. Then, large volumes of drilling fluid filtrate and filtrates which are incompatible with the formation or formation fluids might destabilize the formation. Instability of formation can cause several serious problems, including, stuck pipe, difficulty in running casing and poor cement jobs (Lyons, 2010).

2.1.2. Types of Drilling Fluids

Traditionally, drilling fluids have been classified into three groups according to the base fluid used in their preparation. In a broad sense, drilling fluids can be divided into three principal categories (Caenn et al., 2011):

Water-Based Fluids (WDFs)

This type of drilling fluid consists of water or brine as the base fluid. Oil may be emulsified in the water, in which case water is the continuous phase. Water-based drilling fluids may contain several soluble additives, including alkalis, salts, surfactants, organic polymers, and various insoluble materials such as barite. Their formulation has to be customized to suit the drilling process and reservoir conditions.

Oil-Based Fluids (OBFs)

Oil-based drilling fluids contain oil (refined from crude such as diesel, mineral or synthetic-base oil) as the continuous phase and may be amounts of water as the dispersed phase. Generally, the percentage of water is less than 5% v/v. Oil-based drilling fluids are usually a mixture of base oil, organophilic clay and lignite, although they could also have other additives to formulate more complex fluids. Only mineral oil-based fluids are investigated in this research.

All-Oil Muds

These muds are formulated with diesel, mineral or synthetic-based oil, a viscosfier agent such as organophilic clay and no water phase (Hermoso et al., 2014).

Oil Muds

These fluids are mixtures composed of diesel, mineral or synthetic-based oil, emulsifiers and water between 2-10% by weight.

Invert Emulsions or Invert Muds

Invert muds are water-in-oil emulsions which have oil as the continuous phase. These muds are stabilizing by adding a surfactant (Caenn et al., 2011). They may contain several additives and water up to 40% by weight. At early 90s, synthetic base oils began to replace the traditional mineral oils in order to reduce the toxicity and improve their biodegradation level, particularly at the bottom of the ocean (Friedheim, 1997). There are four chemical types that are being used to replace diesel or mineral oils muds: esters, ethers, olefins and detergents alkylates (Caenn and Chillingar, 1996).

Gas-Based Fluids (GDFs)

These drilling fluids are also known as reduced-pressure Drilling Fluid. The most common gas used as drilling fluid is air. Gas-Based drilling fluids can be grouped as function of the gas nature and classified into: Dry gas; Mist, which carries droplets of water or mud in the air stream; Foam, in which air bubbles are surrounded by film of water containing a foam stabilizing agent; Gel Foam, in which the foam contains film-strengthening agents such as organic polymer or bentonite.

2.1.3. Drilling Fluid Components

Since the birth of the mud industry, additives have been offered to perform one or several functions for different drilling fluids (Caenn et al., 2011). However, nowadays, there are more than 1400 trade-named additives commercially available to fulfil demands from any particular applications of the oil well, such as high pressure high temperature conditions or extraction in environmentally sensitive zones.

Drilling fluid or muds are complex aqueous or oil-based suspensions designed to deal with a number of important functions during the oil extraction process as commented in previous section. The control of mud performance by manipulating the mud composition and the properties of the components is essential to achieve a required behaviour. Besides, whichever continuous phase is used, the drilling fluid will commonly consists of the following components:

- A mineral to control the density of the mud
- A bridging solid to support the formation of a filter cake within the well
- Wetting and thickening agents to adjust the rheology of the mud.
- Salts to aid well stabilisation particularly for shale formations.

Water

Water is the most important single component presented in drilling fluids. Water could be either a limiting factor in drilled formation (air drilling) or the principal substance of the drilling fluid. The particular characteristics of water influence on each step in the

drilling operation from spud-in to completion. Hence, its content in drilling fluids must be considered for planning stages (Caenn et al., 2011).

Oil

Oil is the common alternative fluid use to overcome the disadvantages of water-based muds, such as dissolve salts, promote dispersion of clays or corrode drill pipes, drill collars and drill bits (Apaleke et al., 2012). Base oils contain a broad spectrum of lineal, ramified, cyclic, saturated and/or unsaturated hydrocarbon molecules, whose distribution depends on crude oil source and refinery processes (Totten et al., 2003). Physical and chemical properties of oils basically rely on structure of these molecules. Interestingly, flow properties of lubricant strongly reflect the composition of the oil base. Regarding to major hydrocarbon molecule oils can be classified as follow:

Mineral oils

Generally, mineral oils are obtained from petroleum, even though they can also manufacture from similar sources such as oil shales and tar-sands (Lansdown, 2004). The chemical compounds making up mineral oils are principally hydrocarbons with carbon and hydrogen atoms. Mineral oils can be divided into the following groups according to proportion of paraffin chains and naphthene rings (Lansdown, 2004):

Paraffinic oils: These oils consist of saturated hydrocarbons molecules with at least 75% percentage of paraffinic components in their composition and less than 25% w/w of naphthenic nature components. These oils are characterized by good viscosity/temperature ratio and good stability (Mortier et al., 2010).

Naphthenic oils: They consist of saturated and unsaturated cyclic hydrocarbon molecules. Naphthenic oils contain over 70% of naphthenic and aromatic hydrocarbons in their composition. Two principal characteristics of naphthenic base oils are their low pour points and exceptional solvency powers. Their viscosity/temperature properties are inferior to paraffinic oils with lower viscosity index. In Figure 2.1 the principal types of hydrocarbon molecules are shown.

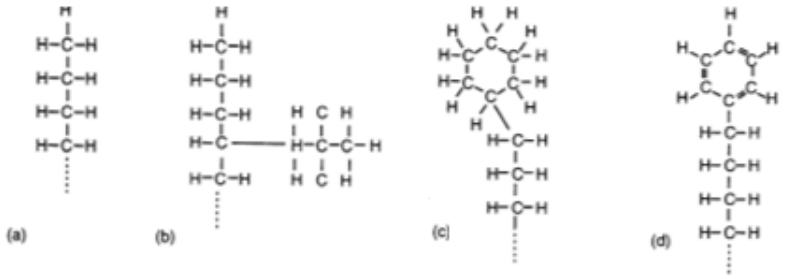

Figure 2. 1. Main types of hydrocarbon molecules

Synthetic oils. Synthetic base oils started to replace mineral oils in drilling at early 1990s due to less toxic and faster degradation (Friedheim, 1997). The high toxicity of mineral oils due to its high aromatic content limits their use in certain types of exploitation wells, such as off-shore drilling of North Sea Regions and Gulf of Mexico.

Synthetic oils are a combination of synthetic base oils plus thickeners and additives which contribute to developed several performance advantages compared to conventional mineral oils. There are four chemical types which are being used to replace diesel and mineral oils in muds: synthetic hydrocarbons, esters, ethers and acetals.

Weighting Agents or inactive solids

Drilling fluids must control the formation fluid pressure in order to prevent blowouts. The density of the mud must be increased as much as necessary to stabilize incompetent formations. A weighting agent is any material denser than water which has not oppositely effects on mud properties and is used to raise the density of the mud to some extent (Caenn et al., 2011). There are several practical factors which affects the use of a substance as a weighting material. Firstly, the weighting agent should have enough density to maintain the well-bore stability without negatively influences on the ratio of perforation (ROP) (Growcock and Harvey, 2005). Additionally the material should be chemically inert, affordable prices, available in large quantities, easily triturate in properly particle-size distribution and relatively nonabrasive.

Barite

Barite is a relatively inert mineral consisting of barium sulphate ($BaSO_4$). It has an average density of 4.5 g/cm^3. Commercially available barite usually contains several iron materials which might increase the specific gravity of the product. Inert solids, as barite or silt, are presented in drilling fluids with sizes normally ranging from 1 to 50 μm. In addition, drilling grade shall be deemed to meet the requirements of the International Standard norm (API Specification 13A) conforms to the chemical and physical features shown in Table 2.1.

Table 2. 1. Barite physical and chemical specifications

Test parameter	**Specification**
Density	4.20 g/cm^3, minimum
Residue greater than 75 μm	Maximum mass fraction 3.0 %
Particles less than 6 μm in equivalent spherical diameter	Maximum mass fraction 30 %
Total soluble alkaline earth metals, as calcium	Maximum 250 mg/Kg

Hematite

Hematite is high-density weighting material composed of iron oxide (Fe_2O_3). This mineral is usually a dark red to brown/black powder with an average density of 5.05 g/cm^3. Its higher density enables faster rates of penetration since the volume of weight material in a mud is less than that mud formulated with barite of the same weight. Hematite, used as a weight material can not be magnetic, because causes interference with electric logs and clogging of fluids lines (Tovar et al., 1999).

Siderite

Siderite consists of ferrous carbonate ($FeCO_3$). The mineral generally contains small amounts of iron oxides, such as dolomite, calcite and quartz. It has a specific gravity of 3.7 to 3.9. Its higher density enables the formulation of both oil- and water base drilling muds up to 2.28 g/cm^3. (Kogel et al., 2006). It is highly soluble in acids, a property considered desirable in completion fluids (Caenn et al., 2011). Table 2.2 shows the range of values of both density and hardness for the most commonly used weighting agents.

Table 2. 2. Weighting agents density and their hardness

Weighting agent	Density (g/cm^3)	Mohs Hardness
Barite	4.5	3.0 – 3.5
Hematite	5.1	5.0 – 6.0
Siderite	3.7 – 3.9	3.5 – 4.0
Galena	7.4 – 7.7	2.5 – 2.8
$CaCO_3$	2.6 – 2.8	3.0
Ilmenite	4.5 – 5.1	5.0 – 6.0

Polymers

Organic polymers are commonly used in drilling fluids to several functions, such as, filtration reduction, clays stabilization and drilled solids flocculation or as emulsifier among others. Generally, they develop highly swollen gels in low concentrations. Some of them are also adsorbed by clay particles and allow preservation from flocculation by salts (Caenn et al., 2011). Polymer used should be safe and environmentally acceptable, easy to be handled and mixed, and economically effective. The most common are:

Starch

Starch is a natural polymer composed of two types of polysaccharides, amylose and amylopectin. This polymer is generally used in strongly alkaline and salt saturated muds to reduce filtration in shallow drilling. It degrades by agitation and by temperature above 93 ºC, and consequently losses its effectiveness in filtration control. Other derivate polymers of starch have been proposed for use in drilling and workover fluids (Caenn et al., 2011). Starch is used in concentrations between 6 to 28 kg/m^3.

Guar gum

Guar gum is a nonionic, branched-chain polysaccharide. The molecular structure is formed by repeating units of mannose and galactose, with short side-branches of galactose residues. Guar gum develops viscous solutions in either fresh or salty water at concentrations of 3 - 6 kg/m^3 (Mallory et. al., 1960). Guar gum is also used to lower filtration rate improving hole stability. Its application is limited to shallow wells due to

its thermal degradation (temperature ≥ 150 ºC). Its influence on viscosity is lower when temperature increases.

Xanthan Gum

Xanthan gum is composed of a linear backbone of glucose residues linked with alternative residues having attached a three-unit-long side chain. This gum is used as a thickener or suspending agent for the drill cuttings due to its ability to build viscosity in fresh or salty water by cross-linking and its excellent shear thinning properties (Deily et al., 1967). The typical concentration of xanthan gum in drilling fluids is ranged from 0.6 to 6 kg/m^3.

Sodium Carboxymethylcellulose (CMC)

Carboxymethylcellulose is a water soluble modified cellulose, which consists of repeating anhydroglucose rings with three hydroxyl groups capable of substitution. It has different degree of substitutions and molecular weight that suit various purposes. The higher the molecular weight is, the higher the viscosity of the suspension is. CMC is normally used to raise the mud viscosity and reduce filtration rate (Kaveler, 1946). The effectiveness of CMC in reducing filtration and increasing viscosity decreases as salt concentration increases because of the coiling of chain. Besides, it is thermally degradable as temperature approaches 150 ºC. The concentration range of this polymer can be very broad, from 0.6 to 14 kg/m^3.

Rheology modifiers or active solids

The active solids are those that have electrically charged surfaces and are reactive with their environment. They can interact with others components to form a gel structure within a fluid, and consequently, to modify the rheology of the mud.

Clays are the primary source of active solids in a drilling fluid. Due to their characteristics, they exhibit a dominant role in determining the rheological and filtration properties of a mud. For this reason, it is necessary to understand basic clay chemistry in order to properly control the properties of the drilling fluid. Thus, the structure and properties of clay mineral and their chemical modifications will be discussed in detail in the next chapter.

Surfactants

Surfactants are ambiphilic compounds which have one part that has an affinity for nonpolar media and one part that has an affinity for polar media. These substances adsorb between two immiscible phases altering their interfacial properties. The unusual properties of aqueous surfactants solutions can be explained on basis of both the hydrophilic head group and the hydrophobic chain in the molecule (Schramm et al., 2003). According to their hydrophilic group, surfactants can be classified into different groups: anionic, cationic, nonionic and amphoteric. Most of water-based drilling surfactants are anionic or nonionic, or mixtures of them.

Surfactants are utilized in all types of drilling fluids for several objectives. They can be used as emulsifiers, foamers, wetting agents or corrosion inhibitors. The concentration of surfactant in drilling fluids can vary widely from mere traces to over 30kg/m^3.

2.1.4. Rheological Behaviour of Drilling Fluids

Drilling fluids usually are classified as "complex" materials due to their wide variety of rheological response, such as shear-thinning and thixotropy effects. These fluids generally have the ability to undergo a solid-liquid transition when they are submitted to a sufficient stresses, which is known as apparent yield-stress. The importance of rheological properties and its effect on the performance of drilling fluids was investigated by Zhongying and Songran (1986). There are two factors closely related to the rheological behaviour of drilling fluids in the annulus which has notable influence on the successful of drilling operation: the cuttings lifting and the annular dynamic pressure. The former denotes the capability of the mud for carrying cuttings as well as the concentration of the cuttings in the mud. A poor lifting capability leads to several problems, such as alteration of rheological performance or increase the probability of pipe sticking. The annular dynamic pressure indicates the effect of the annular pressure loss on the pressure regime down hole. The annular pressure has two contributions: dynamic and static. The dynamic pressure is concurrent with the flow of the mud and will disappear when the circulation stops. Otherwise, static pressure is the pressure of

the mud column, which is the basic pressure, required for controlling the formation and it is continuous and independent of the circulation of the fluid.
The properties of the drilling fluid should be optimized in order to obtain the best overall performance. Therefore rheological properties should be controlled to: minimize pumping cost, maximize bit penetration rate, lift drill cuttings efficiently, lower swab and surge pressures and pressure required to break circulation, separate drill solids and entrained gas at the surface and minimize hole erosion (Caenn et al., 2011).

Shear thinning behaviour is a desirable characteristic in the drilling fluid. This is because of the effective viscosity will be relatively low at the high shear rates prevailing in the drill pipe, thereby reducing pumping pressure. Otherwise, the low shear rates predominating in the annulus leads to high effective viscosity values increasing cuttings carrying capacity. In the oil field, the degree of shear thinning can be evaluated either from flow index, *n*, or from the ratio of apparent yield-stress to the plastic viscosity. Generally, this ratio is increased by reducing the plastic viscosity rather than increasing the yield stress.

The apparent yield stress is a critical rheological parameter to be taken into consideration in order to suspend the drill cuttings and weighting materials when circulation is stopped. For this reason, its value should be maintained to values just high enough. This parameter can also be used to account changes in particle interactions which affect the flow behaviour in the annulus. Apparent yield stress values are mainly associated with the hole cleaning capability and the pressure control. Thus, higher yield stresses increase the carrying capability as well as the circulating pressure drop in the annulus. Nevertheless, the rise in yield point is detrimental to the problems of lost circulation related to swab pressure in the course of a drilling cycle. Besides, drilling industry usually utilizes gel strength as a complementary parameter to yield stress. Gel strength is a measurement of the shear stress at 10 second and 10 minutes required to initiate flow of a fluid that has been quiescent (API Recommended Practice 13D, 2009). High gel strengths are undesirable because it retards the separation of cuttings and entrapped gases at the surface. Further, the determination of

both yield stress and gel strength permit the evaluation the pressure necessary to re-establish circulation as well as the magnitude of swab and surge pressure.

High-shear viscosity, or more commonly used in drilling fluid, plastic viscosity, is principally a function of both the media viscosity and the volume solids. Additionally, maintaining the viscosity at a low value is a major factor in promoting fast penetration rate for the bit mainly because of good scavenging of the cuttings from under the bit.

2.1.4.1. Drilling Fluid around the well bore

In rotary drilling operation, the bit is pressed against the bottom of the hole and is rotated by the drill pipe, which extends all the way to the surface. The drilling fluid circulates down the inside of the drill pipe, out through the openings in the bit and up through the annular space between the walls of the hole and the drill pipe. The cuttings are lifted to the surface, by the drilling fluid through the annulus, where they are separated from the drilling fluid through a shaker screen or any other mechanical removal equipment (Growcock and Harvey, 2005). Then the drilling fluid is passed to the pit from where it is pumped up by a mud pump and is recirculated down the drill pipe to the bit.

During circulation of the drilling fluid around the wellbore, the flow can vary in different sections. In the drill pipe the flow is turbulent, the effective shear rate in the wall ranges from 200 to 1000 s^{-1}, whereas in the annulus the flow is laminar and the shear rate range is 50-150 s^{-1}. In the annulus, the shear rate might change in each section, depending on the drill pipe and on the degree of the hole enlargement. The velocity through the bit nozzles is extremely high and corresponds to a shear rate of the order 100.000 s^{-1}. In addition, the eccentric rotation of the drill causes a pseudo-helical flow which influences on the velocity profile of the drilling fluid.

2.1.4.2. Rheology of Water-based Drilling Fluids

The rheological behaviour of water-based drilling fluids is very complex. The flow behaviour of these systems result from the microstructure developed which essentially depend on the interaction between their media and components, mainly clays. The clay particles present in drilling fluids, such as montmorillonite, can develop structures even

at low solid concentrations. Essentially, these materials behave as either stabilized or flocculated suspensions. Four factors principally affect their rheological response: the type of electrolyte/s in the mud, pH of drilling fluid, the type of clay used and the presence of polymers or polyelectrolytes.

Naturally, the rise in clay concentration will lead to an increase of all rheological properties (Abend and Lagaly, 2000). Likewise, both yield stress and plastic viscosities tend to increase with increasing clay concentration in typical water-based drilling fluids formulated with typical bentonite (Briscoe et al., 1994; Mahto and Sharma, 2004). The experimental work performed by Van Olphen (1964) showed that both apparent yield stress and viscosity increases with NaCl concentration gradually. At very high salt content, these systems displayed a reduction in apparent yield stresses. Similarly, Yildiz et al. (1999) observed that low NaCl concentration reduce the viscous flow parameters, while above 0.29 % w/w NaCl addition has an opposite effect on rheological properties. These results were explained on basis of changes in type association due to electrostatic attraction between edges and faces surfaces of the clay platelets. Vali and Bachmann (1988) suggested that the yield stress and thixotropy degree of clay suspensions is due to "band-type" aggregates whose size is modified by adding NaCl. This type of microstructure model explained successfully the effect of Ca^{2+} ions in alkaline medium on the enhancement of shear stress values. The creation of an interlayer Ca^{2+} between platelets and the formation of thicker aggregates was presumably the condition to lead to this yielding behaviour. Recently, it has been found that bentonite dispersions might shift from shear-thinning to shear-thickening behaviour depending on the nature of electrolyte and its concentration in solution (Abu-Jdayil, 2011).

For Na-montmorillonite suspensions, non-Newtonian behaviour was shown in the pH range from 4 to 10, exhibiting a reduction in viscosity as pH increases (Tarchitzky and Chen, 2002). Water drilling fluids, mainly consisted of smectites, are affected by pH in different manners. Thus, drilling fluids shows gel characteristics exhibiting shear thinning behaviour at low pH, and Newtonian viscosity at high pH (M´Bodj et al., 2003).

The addition of polymers in drilling fluids considerably alters the flow behaviour of these fluids. Generally, drilling fluids consisting of polymers, such as xanthan gum or carboxymethylcellulose, exhibit remarkably reducing friction property depending on the concentration and polymer structure (Caenn et al., 2011; Znou and Shah, 2004). In general, the more polymer content, the higher rheological properties. Xanthan gum is a biopolymer commonly used due to its exceptional ability to develop high viscosity solutions, at low shear rate, with remarkable shear-thinning behaviour. In case of drilling fluids formulated with carboxymethylcellulose, it seems that this polymer has a little influence on apparent yield stress (Kelessidis et al., 2011), or even could remove the apparent yield stress values (Benyounes et al., 2010). The changes in yielding behaviour for both xanthan and carboxymethylcellulose, suggests an interaction between the charged surface of clay particles and the anionic nature of these polymers (Benchabane and Bekkour, 2006). Further, the flow behaviour at higher shear rates has been related to alignment and deformation of elongated chains.

In addition, water-based drilling fluids can be formulated with either polyacrylamide (PA) or partially hydrolyzed polyacrylamide (PHPA) in order to reduce the flow pressure. Kelessidis described the rheological behaviour of PHPA by using Herschel-Bulkley model. He found that the polymer addition cause a viscosity increase and notable decrease in apparent yield stress (Kelessidis and Chatzistamou, 2013). This increase in shear viscosity might due to a bridging interaction between clay particles and polymer, whereas the observed yield stress reduction could be related to the destruction of the regular stacking through polymer adsorption (Mostafa and Assaad, 2007).

2.1.4.3. Rheology of Oil-based Drilling Fluids

Flow properties of oil-based drilling fluids are strongly influenced by the organoclay content of the formulation. Nevertheless, there are few studies concerning the relationship between composition and rheological behaviour in oil-based drilling fluids. Incorporation of organoclays, even at low concentration, might promote thixotropic behaviour as well as the ability to develop rapidly a gel-like material retaining suspended particles, such barite or cuttings. In addition oil-based muds can

contain water up to 40% by weight, emulsifiers and/or polymers. In case of these complex systems, the rheological response seems to be mainly governed by interactions between the three major components, water, oil and organoclays (Schmidt and Cline, 1987).

The rheological behaviour of organoclay suspensions is dependent of the shape and concentration of particles, the surface coverage characteristics, the nature media and the physical and/or chemical interactions between covered particles and background base (Moraru, 2001). As in water drilling fluid formulations, apparent yield stress and viscosity of oil-based drilling fluids are increased with increasing the organoclay content, i.e.: organoclay-based dispersions in xylene showed considerable yield stress values at organoclay concentration as low as 1% by weight (Zhong and Wang, 2003). The yielding behaviour of these systems was related to the formation of a percolating network among the exfoliated organoclays. Further, the dosage organoclay has significant influence on shear-viscosity behaviour depending on the clay characteristics. Minase et al. (2008) suggested that the apparent yield stresses and plastic viscosity depend not only on the disperse concentration, but also on the amount of organic cation added. Besides, in order to understanding the microstructure of these suspensions, viscoelasticity measurements have been used by several researchers. In this sense, Burgentzlé et al.(2004) observed that the static properties (elastic modulus and yield stress) of organoclay suspensions are strongly dependent of organic ions/solvent interactions. These authors demonstrated using X-ray diffraction and macroscopic swelling tests that the rheological behaviour of these systems is attributed to the connections between clay assemblies in a microscale instead of of a nanometric swelling process. Likewise, the solid-like character for different organoclay-based suspension in silicone oil is modified by the hydrophobicity surface degree of each organoclay species (Hato et al., 2011). Otherwise, weak interactions clay/media lead to less consistent three-dimensional structures with liquid-like behaviour (Zhang et al., 2003). King et al. (2007) found that organically modified montmorillonite in p-xylene show a plateau modulus that follows a power relation with volume fraction.

Invert muds are prepared by mixing the oily phase with either water or brine. The rheology of these emulsion/suspension systems is influenced by: i) the oil/water ratio, ii) the amount of surfactant added, iii) the organoclay content iv) the interactions in the interface, and v) the size and deformation of the droplets. There are few works in the open literature concerning the effect of these factors on the viscous behaviour of water-in-oil emulsions, particularly stabilized by clays.

Generally, invert muds exhibit a non-Newtonian behaviour with apparent yield stress. Higher apparent yield stresses are obtained by increasing either the volume of emulsified water in invert muds or the organoclay concentration. Viscosity values also rise with higher oil/water ratio, whereas the addition of extra amount of emulsifier could have an opposite effect (Ghalambor et al., 2008).

Recently several studies have dealt with the effect of water and clay concentration on rheological behaviour of these emulsion/suspensions. Bhatt et al. (2013) investigated the influence of the aqueous phase percentage on the rheological parameters of water-in-oil emulsions stabilized by organoclays using both Casson´s and power law models. He reported an enhancement of yield stress as well as a slightly decrease in high-shear viscosity as aqueous phase consisting of water/methanol mixture is raised up to 65% wt%. This rheological behaviour was explained by the ability of water molecules to stabilize the network structure by hydrogen-bond formation between silanol groups at the edges of different layers or platelet aggregates, as has been proposed elsewhere (Sobish and Lerche, 2000). Binks et al. (2005) observed different increase in apparent yield stress with drop volume fraction for the same organoclay dispersed in isopropyl myristate and toluene. In this work, he also reported higher viscosities and more shear-thinning effect as water/oil ratio is raised. He suggested that the small yield stresses and shear-thinning flow behaviour of isopropyl myristate oil-based suspoemulsions were attributed to aggregated structures. By contrast, the highly viscous toluene-based suspoemulsions were presumably consisted of highly elastic network of tactoids and drops. Akkal et al. (2013) showed that concentration and nature of organoclay can modify shear viscosity in whole shear rates ranged, even leading to apparent yield stress by addition of a surfactant. In this study, the decay in viscosity was attributed to

the gradually elongated water droplets in the flow direction instead of orientation of microstructure developed by organoclays. In addition, the elasticity of droplets contributes to oil-in-water emulsion increasing the viscoelastic effects. Shu et al. (2013) reported water-in-oil emulsions showed solid-like behaviour above 0.3 aqueous volume fraction. This elastic behaviour appears to be related to stress transmitted between contacting droplets in a jamming state.

2.1.4.5. High Pressure High Temperature Rheology of Drilling Fluids

The future of oil and gas exploration and production lies greatly in deepwater wells drilled in High-Pressure/High-Temperature (HPHT) environments. In this sense, drilling industry has been working in order to establish the gap between the current available technology and the drill requirements to produce wells in this type of conditions. Besides, proper drilling fluid selection plays a major role in the success of drilling operation, particularly in high-priced HPHT wells. Hence, drilling fluids with suitable rheological properties are essential in challenge HPHT wells.

As it has been previously commented, drilling fluids in the well might experiences extreme pressures and temperatures as well as a wide range of shear rates during the drilling cycles. Consequently, rheology of drilling fluids under downhole conditions needs to be assessed as function of composition, pressure and temperature.

High temperature and high pressure scenario can change the rheological behaviour of both oil-based and water-based drilling fluids in different manner:

Physically: decreases in temperature and/or increases in pressure influence the mobility of drilling fluid leading to an increase of apparent viscosities. In case of oil-based systems the effect of pressure on rheological properties is expected to be greater than water-drilling fluids due to their oil phase compressibility.

Chemically: At temperatures above 94ºC, all hydroxides react with clay minerals. This effect can result in a modification of the structure, hence changes in the drilling fluid rheology, in particular for highly alkaline muds.

Electrochemically: temperature rising intensifies the ionic activity of any electrolyte, as well as the solubility of any partially soluble salts presented in the drilling fluid. The variation of ion and base exchange balance alter the equilibrium between interparticle attractive and repulsive forces, and so the degree of dispersion and flocculation.

Generally, the magnitude and direction of both temperature and pressure effects will vary as function of the particular composition of a given drilling fluid. In early investigations, Combs and Whitmare (1960) studied the combined effect of temperature and pressure on the rheology of oil-based drilling fluids formulated with organophilic clays, and found that the change in continuous phase viscosity was the main controlling factor. Hiller (1963) studied the effect of temperature and pressure on the rheological behaviour of Na-montmorillonite suspensions and other drilling fluids using a HPHT rheometer up to 160°C and the pressures up to 700 bar. He found yield stress and plastic viscosity increased with temperature and the plastic viscosity increased slightly with pressure, as was expected. The enhancement of both rheological properties with temperature where attributed to the dispersion of thicker particles flocculated, whereas the little rise in these properties induced by pressure was due to compression of aqueous media. Annis (1967) investigated the rheology of water-based muds consisting of bentonite up to 150ºC. Annis´s results showed that the flow curves became more non-Newtonian with higher shear-thinning degree as temperature increased, displaying higher yield stresses and lower plastic viscosities. Incorporation of NaCl to water drilling fluid at 100ºC caused a very remarkable increase in shear stresses compared to muds without this salt. These data suggested that high temperatures leaded to flocculation process of bentonite particles depending on of salt content. De Wolfe et al. (1983) fitted the influence of pressure and temperature of several oil muds composed of different low toxicity oils by using the Herschel-Bulkley model. It was observed that both temperature and oil composition are the main factors on viscosity values. Politte (1985) studied the flow behaviour of invert diesel oil mud between 32 ºC and 150 ºC in the pressure ranged comprised from 69 to 1034 bar. He used a multi-term equation with 13 parameters to model the oil viscosity data, and the Bingham model to correlate the flow viscous behaviour of invert muds. He concluded

that the plastic viscosity could be normalized with the viscosity of the oil and the yielding behaviour is a weak function of pressure. Likewise, Houwen and Geehan (1986) described the pressure-temperature effect on rheological properties of invert muds by using several rheological models. He found that Casson's model has the advantage over the Bingham's model that it enabled to estimate the flow curves above 1 s^{-1} in whole range of pressure and temperature tested. Alderman et al. (1988) performed rheological measurements at high pressure high temperature conditions on water-based drilling fluid containing Na- montmorillonite clay using a rheometer. He observed several effects of temperature/pressure conditions on viscous flow behaviour of this type of drilling fluids: i) the high-shear viscosity decreases with temperature rising, and increase with pressure to an extent which relies on mud density, ii) the apparent yield stress do not depend on pressure applied, show a weak dependency with temperature below a critical temperature, T_c. iii) above T_c, the yield stress strongly increases with temperature. The viscosity trend with pressure and temperature was largely governed by the viscosity and compressibility characteristics of the continuous phase. On the other hand, the change on yielding point above the critical temperature was suggested to be due to modification of the electrical double layer surrounding the platelets by releasing of the ions, or changes in dielectrical parameters. Briscoe et al. (1994) carried out rheological measurements at HPHT conditions for fresh concentrated bentonite suspensions using HPHT rolling-ball rheometer at temperatures up to 140ºC and pressure as high as 1400 bar. The pressure effect on apparent Bingham yield stress was negligible at room temperature, whereas plastic viscosity exhibited higher values as the pressure applied increased. This effect was assumed to be a consequence of an effective increase of the solid content due to the volume change of the liquid phase under pressure. Elevated temperatures led yield stress enhancement with pressure. Otherwise, plastic viscosity decreased significantly at higher temperatures, but showed little variation with pressure. It was suggested that the higher amount of cations (Na^+) dissolved from the surface of the particles by increasing temperature provoked both a plastic viscosity reduction and yield stress rising.

Herzhaft et al. (2001) carried out viscous flow curves for several drilling fluid formulations from temperatures as low as 0ºC up to 170ºC, ranging pressures between 3 and 620 bar, showing that the evolution of apparent viscosity with temperature can be predicted if both volume fraction and oil base viscosity are known. Moreover, the shear viscosity followed an exponential function of pressure applied. More recently, Herzhaft et al. (2003) conducted rheological measurements in a wide range of temperatures (0 – 80ºC) at atmospheric pressure for invert muds with different oil nature. He observed that invert oil muds behaved as quasi-Newtonian fluids at low shear rates with shear-thinning behaviour. The onset of shear rate was shifted to higher values as temperature was elevated. It was conclude that the interaction of organoclay with water droplets was the responsible of the changes in the viscous flow behaviour observed in the temperature range studied. This microstructural scheme was confirmed by using oscillatory experiments and cryomicroscopic images. Gandelman et al. (2007) measured the apparent viscosities and gel strength for synthetic drilling fluids between 4.4ºC and 176.7ºC and pressures between 69 and 689.5 bar., concluding that the influence of pressure on gel strength for these fluids is mainly governed by temperature.

2.1.5. Density of Drilling Fluids

Drilling fluids have a wide range of physical properties which are particularly designed for drilling conditions. The suitable properties are obtained by changing the drilling mud formulation. Rather than rheological properties, there are other important physical properties to be studied in drilling fluids, such as density, filtration properties, pH, electrical conductivity or corrosivity. The determination of the drilling fluid density is fundamental in order to prevent the inflow of formation fluids and create a low permeability filter cake on the walls of the hole. The incorporation of formation fluids is avoided when the pressure of drilling fluid column, which is proportional to the mud density, exceeds the pore pressure by at least 14 bar (Caenn et al., 2011). The pore pressure relies on the depth of the porous formation, the density of formation fluids and geological conditions.

In drilling, there are two types of pressure which are function of density, static pressure and dynamic pressure. Static pressure is defined as the pressure exerted by a fluid column as follow:

$$p_s = \rho_m \cdot g \cdot h \tag{2. 1}$$

Where ρ_m is the mud density and h is the depth.

Dynamic pressure, also refers to the equivalent circulating density (ECD), can be defined as the sum of static pressure and the pressure loss in the annulus due to fluid flow. ECD is expressed as follow:

$$\rho_{ECD} = \rho_m + \frac{\Delta P_{frict}}{gh} \tag{2. 2}$$

being ΔP_{frict} is the frictional pressure loss.

The general practice is to measure the volumetric properties under ambient surface conditions and assume that this property is constant throughout the duration of several steps of drilling operation. However, muds experience compression and expansion effects during the circulation, and consequently, this assumption can prove to be in serious error when there is a large variation in the pressure and temperature conditions, such as in HPHT wells (Harris and Osisanya, 2005). At elevated temperature and pressure environments where reservoir pressures may reach 1500 bar and bottom hole temperatures excess 180ºC (Nelemans et al., 2012), the operating window between pore pressures and fracture gradients implies overbalance drilling operations difficult to deal with. Hence, it is vital that both static and dynamic pressures of drilling fluids are accurately modelled as function of both pressure and temperature.

Several authors have investigated the combined pressure and temperature influence on the density of drilling fluids. One the first work carried out on density behaviour of water and oil-based drilling muds at HPHT conditions showed that oil-based ones are quite sensitive to pressure and temperature rather than water-based ones (McMordie et al., 1982). Generally, the studies have used two approaches to relate the density changes with both temperature and pressure of drilling fluids.

On the one hand, a group of researchers has focused on variations of drilling fluid density using empirical equations. In this sense, Sorelle et al. (1982) derived an implicit function to predict densities of diesel oil and water-based drilling muds at high pressure high temperature. Kutasov (1988) proposed an empirical relationship for the density of drilling fluids as an exponential function of pressure and temperature. More recently, Hemprill and Isambourg (2005) developed a general equation to estimate oil- and synthetic-based drilling fluids between 4.4 and 204ºC and pressure ranged 1 to 1655 bar. Demirdal et al. (2007) investigated the behaviour of n-paraffin-based oil and drilling mud under downhole conditions. They concluded that n-paraffin-based oil density and emulsion-driling-fluid density have similar volume variations with temperature and pressure. Demirdal and Cunha (2009) studied the volumetric behaviour of two frequently used olefin-based oils under HPHT conditions and compared with water, brine and mineral oils. They stated that densities of synthetic-based oils show much more sensitivity to downhole environments when compared to those of water, brine and conventional oils.

On the other hand, others authors have used compositional models for analysing the density of drilling fluids under high pressure and high temperature. In this approach, the density change of solids is assumed to be negligible with both temperature and pressure variations. The density-temperature-pressure behaviour of the drilling fluid is interpreted in terms of changing density of liquids (Hoberock, et al., 1982; Peters et al., 1990). Hence the effects of temperature and pressure on density of the mud could be simply determinate by the volumetric behaviour of its liquid components.

2.2. Clay and Organoclays

Clays consist of a heterogeneous mixture of finely divided minerals, such as quartz, feldspars, calcite, pyrites, etc. The clay minerals are hydrous aluminium silicates normally containing alkalies, alkaline earths and iron in appreciable quantities.

Drilling fluids normally contain a number of different types of clays. Most of the clays are added to attain certain physical properties and eliminate hole problems.

2.2.1. Structure

Clay minerals are of a crystalline nature and the atomic structure of their crystals is the main factor that determines their properties. Clays have a mica-like structure and their flakes are composed of tiny crystal platelets stacked together face to face. The atomic structure of the clay minerals consists of two basics units, an octahedral sheet and a tetrahedral sheet (Murray, 2007). A single platelet is called a unit layer.

The octahedral sheet is comprised of closely packed oxygens and hydroxyls in which aluminium, iron, and magnesium atoms are arranged in octahedral coordination, so that they are equidistant from six oxygens or hydroxyls (see Figure 2.1). The oxygen atoms and the hydroxyls groups lie in two parallel planes with the Al or Mg atom between these two planes. When aluminium with a positive valence of three is the cation present in the octahedral sheet, only two-thirds of the possible positions are filled in order to balance the charges. In this case, the mineral is termed dioctahedral. Otherwise, when magnesium with a positive valence of two is present, all three positions are filled to balance the structure and the mineral is termed trioctahedral (Murray, 2007).

The second structural unit is the silica tetrahedral layer which consists of silicon atom coordinated with four oxygen atoms. The oxygen atoms are located on the four corners of a regular tetrahedron, with the silicon atom located in the center. Three of the four oxygen atoms of each tetrahedron are shared by the three neighbouring silicon in one sheet. These tetrahedrons are arranged to form a hexagonal network repeated infinitely in two horizontal directions to form what is called the silica tetrahedral sheet (see Figure 2.2.).

The analogous symmetry and dimensions in the tetrahedral and octahedral sheets allow the sharing of oxygen atoms between sheets. If there is one silica sheet and one alumina sheet the combination is called (1:1 layer mineral), whereas if two silica sheets is combined with one alumina sheet the combination is called (2:1 layer mineral). The combination of an octahedral sheet with one or two tetrahedral sheets is called unit layer. Within each unit layer a certain unit repeats itself in a lateral direction, this unit is called unit cell.

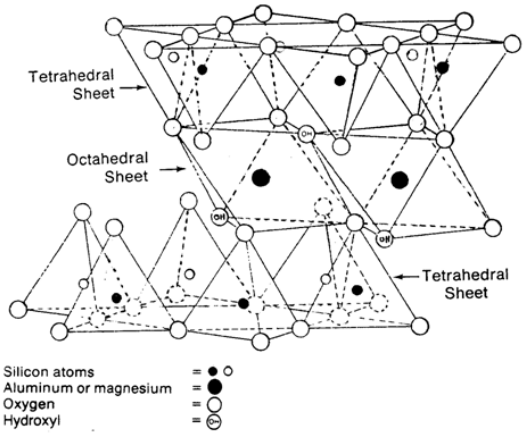

Figure 2. 2. Diagram sketch of bonding one octahedral sheet and two tetrahedral sheets

A schematic representation of the atom arrangements in a unit cell for a three-layer clay such as montmorillonite, is shown in Figure 2.3. This structure is called Hofmann structure (Hofmann et al., 1933).

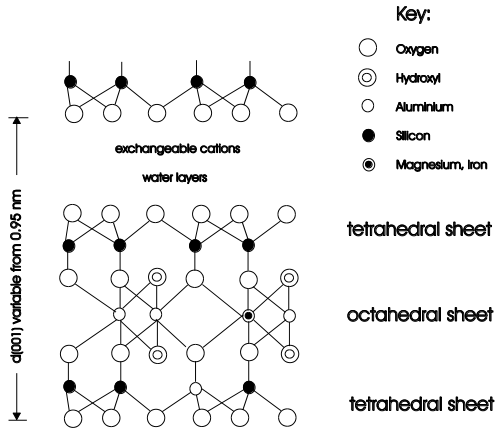

Figure 2. 3. The layer structure of montmorillonite according to Hofmann

The unit layers are stacked together face-to-face to form what is known as the crystal lattice. The distance between the plane in one layer and the corresponding plane in the next layer is called the basal spacing or c-spacing *d(001).* The sheets in the unit layer are tied together by covalent bonds, so that the unit layer is stable.

The layers in the lattice layer are held together only by Van der Waals forces and secondary valences between juxtaposed atoms. Therefore, the lattice cleaves along the basal surfaces, forming tiny mica flakes (see Figure 2.4.)

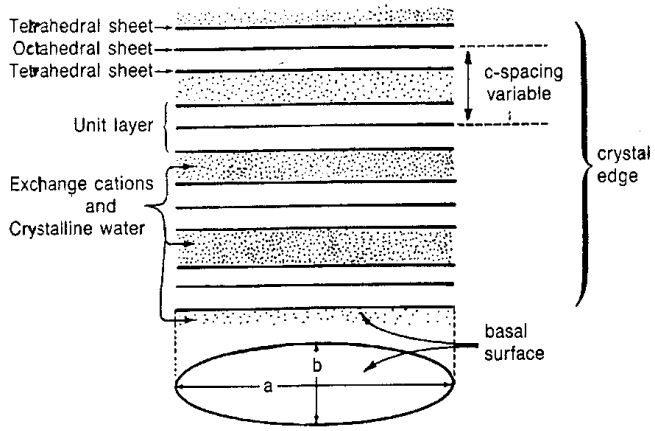

Figure 2. 4. A schematic representation of a 3-layer expanding clay lattice

Clay mineral crystals carry a charge arising from isomorphous substitutions of certain atoms in their structure for other atoms of a different valence (Marshall, 1935). In the tetrahedral sheet, Si^{+4} may be replaced by trivalent cations (Al^{+3} or Fe^{+3}), or divalent cations (Mg^{+2} or Fe^{+2}) may replace Al^{+3} in the octahedral sheet. In this case, a charge deficiency results and a negative potential at the surface of the clay is created. The negative potential is compensated by the adsorption of cations on the surface. In the presence of water, the adsorbed cations can be exchanged with cations of another species in the medium. Those cations are called the exchangeable cations. The total amount of cations adsorbed is expressed in milliequivalents per hundred grams of dry clay and it is known as base exchange capacity (BEC) or cation exchange capacity (CEC) (Van Olphen, 1977).

Substitutions may occur in either the octahedral or the tetrahedral sheets. These substitutions also give rise to innumerable grouping and sub-grouping of clay minerals (Caenn et al., 2011). In addition, the degree of substitutions, the atoms involved and the species of exchangeable cations are of enormous importance in drilling fluids

technology because of their influence on the drilling fluids properties such as swelling, dispersion, rheology and filtration.

2.2.2. Types of Clay Minerals

The most common clays used in drilling fluids formulation are attapulgites and smectites (calcium and sodium montmorillonite). Furthermore, others clays, such as Illites and kaolinites, are incorportated into the drilling fluids from the formation modifying their chemical-physical properties. Generally, clays are added to oil base to increase the viscosity and form a thin, low-permeability filter cake.

Attapulgites

Attapulgites are 2:1 layer silicates which the tetrahedral sheets are linked infinitely in two dimensions. However, they are structurally different from other clay minerals in that octahedral sheets are continuous in only one dimension and the tetrahedral sheets are divided into ribbons by the periodic inversion of rows tetrahedrons (Murray, 2007). Attapulgite particles consist of bundles of "laths", which separate into individual laths (long shaped needles) when mixed vigorously with water. The flow properties of attapulgite suspensions are dependent on mechanical interference between the long laths in drilling fluids, attalpulgite is used for its suspending qualities, particularly in drilling fluids of higher salinity than sea water.

Chlorites

The structure of chlorites is formed by regularly stacked, negatively charged 2:1 layers and a single, positively charged interlayer octahedral sheet that are linked to each other by hydrogen bonds. Chlorites is a 2:1 layer mineral with a interlayer brucite sheet ($Mg_3(OH)_6$) (see Figure 2.5). There is quite a range of cation substitutions in chlorites, most commonly Mg^{2+}, Fe^{2+}, Al^{3+}, and Fe^{3+}. There are some substitutions of Al^{+3} for Mg^{+2} in the brucite layer giving it a positive charge, which is balanced by a negative charge on the three-sheet layer, so that the net charge is very low. The negative charge is derived from the substitution of Al^{3+} for Si^{4+} in the tetrahedral sheet. Whereas, the octahedral sheet in 2:1 layer contributes to balancing the tetrahedral sheet (Bergaya et al., 2006).

Kaolinites

Kaolinites are two-layer clay minerals in which a single tetrahedral sheet and a single octahedral sheet are combined to form a unit. In this unit the tips of the silica tetrahedrons are joined with the octahedral sheet. All of the apical oxygens of the silica tetrahedrons point in the same direction so that these oxygens and/or hydroxyls are shared by the silicons in the tetrahedral sheet and the aluminium in the octahedral sheet. Therefore, there is a strong hydrogen bonding between the layers, which prevent lattice expansion. Additionally, there is a little, if any, isomorphous substitutions, and very few cations are adsorbed on the basal surface.

Illites

Illite is a clay mineral mica, which was named by Grim (1937). The structure is a 2:1 layer in which the substitutions are predominately aluminium for silicon in the tetrahedral sheet, and also substitution of aluminium by magnesium or iron may takes place in the octahedral sheet. The balancing cation is always potassium (Figure 2.7). The size, charge, and coordination number of potassium is such that it fits snugly in the hexagonal ring of oxygens of the adjacent silica tetrahedral sheet (Murray, 2007). The potassium atoms fit in the holes of the oxygen network and form secondary valence links. Hence potassium ion is fixed and can not be exchanged and, consequently, non-expanding lattice and no water penetration between the layers occur.

Smectites

Smectite is the group name for several hydrated sodium, calcium, magnesium, iron and lithium aluminium silicates. Those bentonites which are used for drilling industry are principally composed of either sodium montmorillonite, calcium montmorillonite (bentonite) or lesser extent, hectorite (lithium montmorillonite). The most used commercial clay in drilling fluids is sodium montmorillonite. A 5% addition of montmorillonite generally gives the desired viscosity. Further, this clay has high gel strength and low filter cake permeability.

In their lattice crystal, the tetrahedral sheet of one layer is adjacent to tetrahedral sheet of the next as is shown in Figure 2.5. This means that oxygen atoms are opposite oxygen atoms and consequently, bonding between layers is weak (Caenn et al., 2011). Also, there is a high repulsive potential on the surface of the layers resulting from isomorphous substitution. There can be considerable substitution in the octahedral sheet of Fe^{2+}, Fe^{3+}, and Mg^{2+} for Al^{3+}, which creates a charge deficiency in the layer. Besides, there can be some substitution of silicon by aluminium in the tetrahedral sheets, which again creates a charge imbalance. This net positive charge deficiency is balanced by exchangeable cations adsorbed between the unit layers and on the edges. These two last factors contribute to the increase of the c-spacing between the layers due to the penetration of water. These events have implications for many physical properties of smectites, such as swelling and rheological behaviour.

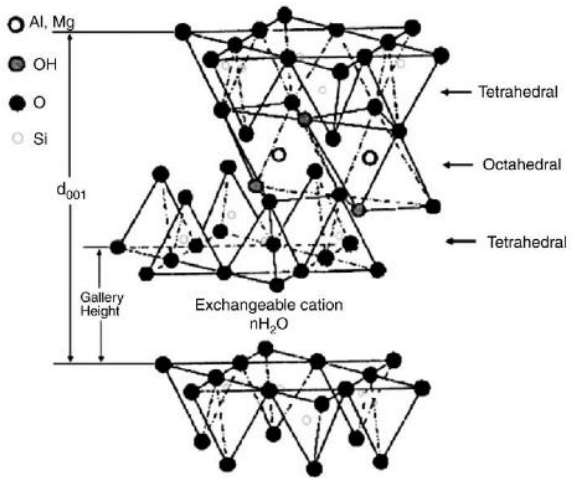

Figure 2. 5. The structure of 2:1 smectite clays

2.2.3. Swelling of Clay Minerals

Swelling of clay minerals is the moving apart or disjoining of the clay particles, especially those in a parallel arrangement until they reach their equilibrium separation under a given pressure (Chen et al., 1987). The swelling behaviour of clay minerals has

been treated in detail by various authors (Norrish, 1954; Van Olphen, 1977; Swartzen-Allen and Matijevic, 1974; Hunter, 2001; Anderson et al., 2010). The majority of these studies have been focused on smectites and particularly with montmorillonite since their expanding lattice.

The swelling can occur via two different regimes: Crystalline and Osmotic swelling. Crystalline swelling can occur in all types of clay minerals. This type of swelling results from the adsorption of monomolecular layers of water on the basal crystal surfaces. The first layer of water is held on the surface by hydrogen bonding to the hexagonal network of oxygen atoms. The next layer is coordinated and bonded to the first and so on with succeeding layers. Simulations have confirmed that crystalline swelling occurs via a stepwise mechanism and that adsorbed water molecules form distinct layers in the interlayer region (Boek et al., 1995; Chávez-Páez et al., 2001; Hensen and Smit, 2002). In addition, the structured nature of the water gives it quasi-crystalline properties, such as a viscosity greater than the free water (Caenn et al., 2011). Swelling in this region is primarily due to hydration of the interlayer cations which probably take up positions between two opposing silicate layers.

The increase in the *c*-spacing, or the degree of expansion of the layers planes depends on the cations located in the interlayer region. If the cations in the interlayer are monovalent and strongly hydrated (Na^+, Li^+), the interplatelet repulsion is stronger, and consequently, the degree of platelet separation is larger (Hunter, 2001). Otherwise, the exchangeable cations can also linkage to crystal surface in competition with the water molecules, disrupting the water structured. Exceptions are Na^+ y Li^+, which are lightly bonded and tend to diffuse away. According to Norrish study (Norrish, 1954), the c-spacing changes can be explained in basis of repulsive swelling force arising from the hydration of the interlayer cations, and opposing attractive forces arising from electrostatic links between negatively charged layer surface and the interlayer cations. Moreover, the equilibrium layer-spacing for a given clay mineral is generally the state in which the thermodynamic potential is a global minimum for the given thermodynamic constraints of temperature, pressure, and water chemical potential

(Anderson et al., 2010). Typical interlayer spacing recorded in the crystalline swelling regime lie in the range 9 to 20 Å.

Osmotic swelling is limited to certain clay minerals which contain exchangeable cations in the interlayer region. Osmotic swelling occurs due to the concentration of cations between the layer is greater than that the bulk solution. As a consequence, water molecules can be drawn into the interlayer to restore the cation equilibrium. Despite no semi-permeable membrane is involved, the mechanism is essentially osmotic, because it is governed by a difference in the electrolyte concentration. This kind of swelling can result in significantly larger volume increase than crystalline swelling, reaching interlayer space of more than 20 to 130 Å. This type of swelling behaviour in Na^+ saturated smectites is the main source of shale deposit instability, which can potentially lead to the collapse of bore-holes in oil well drilling operations (Anderson et al., 2010). On the contrary, K^+ saturated smectites do not swell in this fashion and form crystalline hydrates even in aqueous suspensions (Denis et al., 1991).

Fukushima (1984) carried out an X-ray diffraction studies on a Na^+-montmorillonite suspension to determine the alignment of the clay particles upon swelling. It was found that a straight column model used to describe the swelling behaviour observed by Norrish was applicable only at high Na^+-montmorillonite concentrations. This model failed to describe the swelling at high water content. A zig-zag column model was found to agree with the swelling observed at high and low water content, where the layers swell not only longitudinally but also laterally as is shown in Figure 2.6. (Luckham and Rossi, 1999):

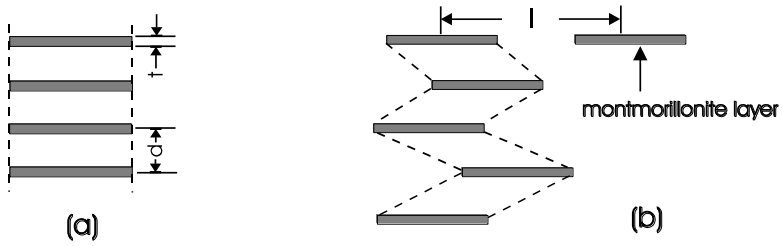

Figure 2. 6. Schematic diagram of (a) straight column model, (b) zig-zag column model for the arrangement of layers in montmorillonite aqueous suspensions

2.2.4. Particle association

There are two types of particles associations, flocculation and aggregation. The term flocculation is referred to the loose association of clay platelets which forms flocs or gel structures. The term aggregation refers to the collapse of the diffuse double layers and consequently the formation of aggregates of parallel platelets.

The gel structures build up with time when particles are oriented towards positions of minimum energy under the effect Brownian motion (Luckham and Rossi, 1999). The velocity of this process depends on the concentration of clay in the medium and the salt content. Thus, if the concentration of clay is high enough a gel structure is developed. For Na-montmorillonite, this concentration is generally above 3% w/w.

There are three modes of clay particle association when plate-like particles, such as montmorillonite, flocculates (Van Olphen, 1964): face-to-face (FF), edge-to-face (EF) and edge-to-edge (Figure 2.7.). Face-to-face associations lead to thicker and larger tactoids, which are aggregates of parallel platelets. Edge-to-edge and edge-to-face lead to three-dimensional structures, known as “house of cards”. Thus, aggregation can be described by the FF associations, while the continuous gel structure is due to EF and EE associations. Nevertheless, other theories describing the modes of interaction between montmorillonite particles have been proposed. These are the different plate-plate linkages proposed:

- Mutual repulsion of the particles as a result of the interactions between their double layers (Norrish, 1954).
- Edge-to-edge association to form cross-linked ribbons, due to the high repulsive potential between basal surfaces (M´Ewen and Pratt, 1957)
- Parallel association of plates, held together by crystalline water between them (Leonard and Low, 1961).

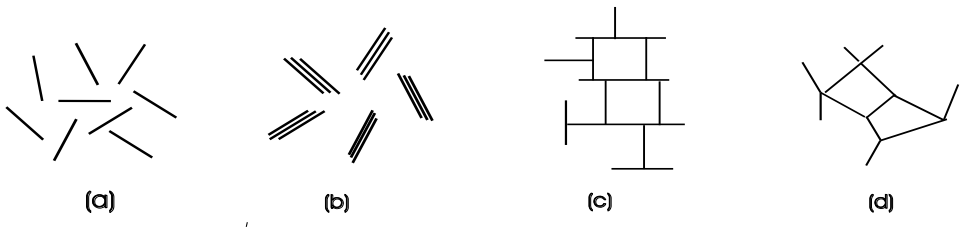

Figure 2. 7. Model of particles associations clay suspensions: (a) dispersed; (b) face-to-face; (c) edge-to-face; (d) edge-to-edge.

The three types of particle association strongly depend on the electrical interaction energy between double layers. In an enough concentrated suspension, neighbouring platelets may flex according to their relative positions and magnitude of their surface and edge potentials. Thus, when the edges are positive, the platelets flex towards a negative face (EE and EF associations). When the edges are negative the platelets are forced to allocate an almost parallel type orientation (FF associations) (Norrish and Rausell-Colom, 1963). Edge-to-edge associations between the poorly or non-charged edges and negatively charged faces of platelets are induced by low NaCl concentration (Tombácz and Szekeres, 2004). Kretzschmar et al. (1998) found using light scattering measurements that: i) pure Na-kaolinite flocculates rapidly even at low electrolyte concentration at pH lower than 5.8 due to edge-to-edge associations; ii) above this pH, particle are electrostatically stabilized and value flocculation rate strongly depends on both pH and ionic strength.

In the presence of an electrolyte, the double layers are compressed, attractive forces predominate, and particles begin to flocculate, or even can aggregate. The critical concentration of a particular electrolyte at which occurs is called flocculation value.

The value of this parameter decrease as the valence of the cations is higher. Baik and Lee (2010) observed that suspensions of natural Ca-bentonite were stable at low ionic strength between 0.01 and 0.001 M $NaClO_4$, but unstable at higher ionic strength of 0.1 M for the whole pH range between 3 and 11. The higher degree of hydration of Na cations from $NaNO_3$ compared to NaCl salt due to water structure breaking effect of nitrate ions results in higher flocculation values (Bergaya et al., 2006). Furthermore, the flocculation process and the resulting microstructures are significantly affected by the species of clay mineral, the exchange cations and the type of salt added.

2.2.5. Organoclays

Organophilic clays are extensively used for their interesting rheological properties in industrial applications, such as cosmetics, inks, paints or drilling fluids (Jones, 1983). They are generally used as flow modifiers in order to reach moderate steady-shear viscosity, together with the formation of a strong gel upon cessation of shear (King et al., 2007). For drilling industry, organoclays were the most contribution to the technology of oil muds. These clays have the property of swelling and dispersing in organic liquids (Hauser, 1950) suspending solids in oil without requiring additional soaps and emulsifiers.

The organoclay complexes are formed by means of cationic exchange reaction. The exchangeable cations of smectite are replaced by cationic groups of the amines, generally long-chain alkylammonium cations, and by further adsorption of the hydrocarbon on the clay lamina surface. Some typical alkylammonium cations used in the synthesis of organoclays are shown in Figure 2.8.

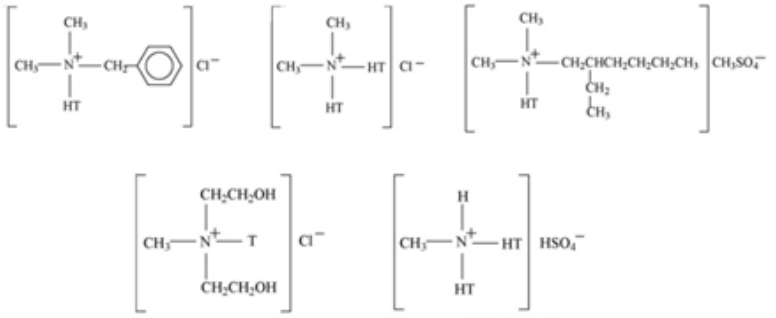

Figure 2. 8. Five types of alkylammonium cations used in the synthesis of organoclays

This modification increases the interlayer distance with the organic chains and change the layer polarity as is shown in Figure 2.9.:

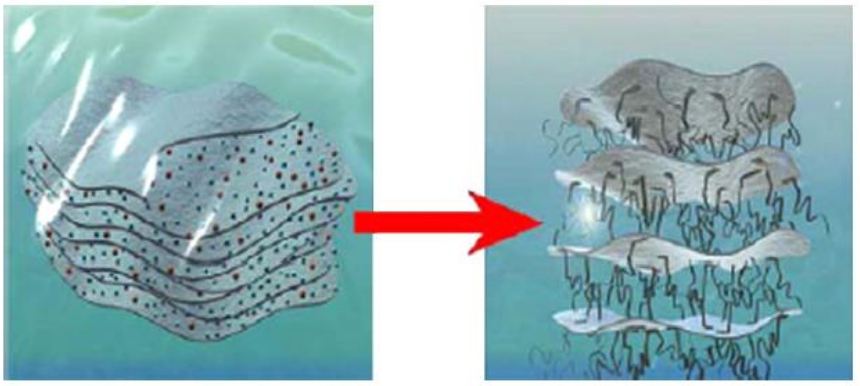

Figure 2. 9. Schematic picture of an ion-exchange reaction. The inorganic small ions are exchanged against more voluminous organic cations

Depending on the layer charge of the clay mineral and the chain length of the organic ions, different arrangements of organic molecules between the layers can be formed. The geometry of the surface and the degree of exchange can also influence. The organic ions may fit flat on the silicate surface as a monolayer or bilayer, pseudotrimolecular layer depending on the packing density and the chain length, as an inclined paraffin-type structure (de Paiva et al., 2008), as is illustrated in Figure 2.10.

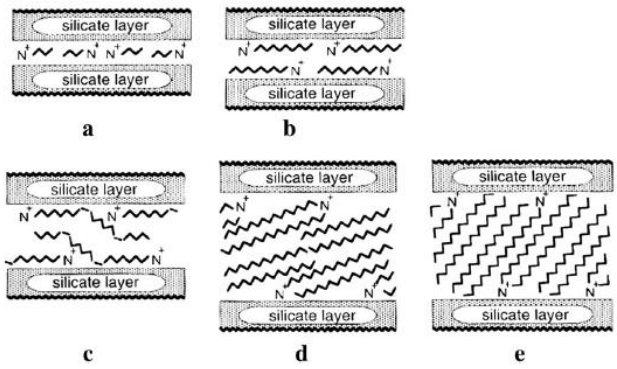

Figure 2. 10. Orientations of alkylammonium ions in the galleries of layered silicates: a) monolayer; b) bilayers; c) pseudotrimolecular layers and d, e)paraffin-type arrangements

Most important characteristics of the organic derivatives of montmorillonite with long alkyl chains are ability for swelling and thixotropic gel formation in organic media (Moraru, 2001). This process is a complex phenomenon influenced by several factors such as the nature of clay, the nature of modifying ions and dielectric constant of the organic media (Gherardi et al., 1996). Likewise, Moraru (2001) specified that the condition for gel formation from alkylammonium montmorillonite in organic liquids is the intercrystalline swelling and dispersion since gel is developed by interactions existing between anisotropic and swollen particles. The chemical nature of the solvent is also a determining factor for gel formation. The early works on gel formation in non-polar medium demonstrated that the addition of polar solvents, such as water, methanol, was efficient for nanoclay dispersion (Burgentzlé et al., 2004).

The dispersion state of organophilic clays plays an important role in rheological behaviour. In this sense, the gel strength increases gradually with the structure changes from the well-dispersed state to the flocculated state and on the aggregate state (Le Pluart et al., 2004).

2.3. Rheology Fundamentals

Rheology is the study of the deformation and flow of matter under the influence of an applied stress. This definition was accepted when the American Society of Rheology

was founded in 1929. The word rheology is derived from the Greek words "ρεω", which translates literally as "to flow" and "λογοσ" meaning "science". Therefore, it literally means "the study of the flow" (Macosko, 1994). The origin of rheology began in 1950s due to the developing and use of complex materials with different flow properties, such as plastics, paints, polymers melts and polymers solutions, biological products, colloidal suspensions, inks, drilling fluids, etc. The general feature of all these examples is that they all exhibit very complicated superimposition of liquid-like and solid-like properties. (Malkin and Isayev, 2006). Therefore, rheology is a science which deal with the relationship between stress and deformation of any type of materials differ from the classical theories of elasticity to the classical theory of hydrodynamics.

Robert Hooke developed his "True Theory of Elasticity" in 1678. His work copes with mechanical properties of elastic solids. He proposed that "the power of any spring is in same proportion with the tension thereof". This means that stress applied is always directly proportional to strain in small enough deformation but independent of the rate of deformation:

$$\tau = G \cdot \gamma \tag{2. 3}$$

where:

τ is the stress (Pa)

γ is the strain

G is the coefficient of proportionality called Young modulus (Pa)

Isaac Newton gave attention to liquids and in the "Principia" (1687), he suggested the following hypothesis to explain the steady simple shearing flow: "The resistance which arise from the lack of slipperiness of the parts of the liquid, other things being equal, is proportional to the velocity with which the parts of the liquid are separated from one another". Basically, it means that the stress is always directly proportional to the rate of strain but independent of the strain itself:

$$\tau = \eta \cdot \dot{\gamma} \tag{2. 4}$$

where:

η is the proportionality constant, called viscosity (Pa·s)

Consequently, the ideas of a liquid and a solid are model representations of two extreme idealizations. Nevertheless, the vast majority of materials show a rheological behaviour that classifies them to a region somewhere between the liquids and the solids.

In summary, rheology is focused on the relationship between forces and deformations (or changes of shape). In order to achieve a model that gives a mathematical formulation is necessary to determinate the rheological properties of any material. Therefore, before classifying the rheological behaviour of fluids, it would be appropriate to define some important concepts.

2.3.1. Simple Shear

Simple shear is a very important type of deformation because movement of all fluids and liquid-like materials is based on the principle of sliding of neighbouring layers relative to each other (Malkin and Isayev, 2006). In this type of shear field, a material element is placed between two parallel plates (Figure 2.11.) where the bottom plate is stationary and the upper plate is displaced in x-direction by applying a force *F* tangentially to the surface *A*. The velocity profile in simple shear with no slip is given by the following velocity components:

$$u_x = \dot{\gamma} \cdot y \qquad u_y = 0 \qquad u_z = 0 \tag{2. 5}$$

The corresponding shear stress is given as:

$$\tau = \frac{F}{A} \tag{2. 6}$$

In this case, the shear rate may be expressed as the velocity gradient in the direction perpendicular to that of the shear force, i.e.,

$$\dot{\gamma} = \frac{du_x}{dy} = \frac{\tau}{\eta} \tag{2. 7}$$

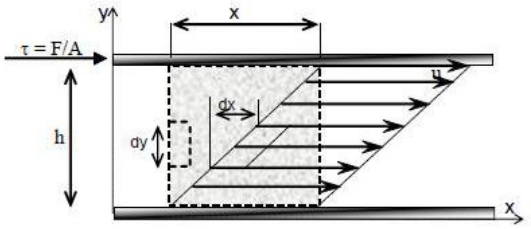

Figure 2. 11. Simple shear between two parallel plates

In this type of field flow the deformation is homogeneous e independent of fluids element, and consequently it can be expressed as a function of the distance between the parallel plates, *h*, and the displacement of upper plate, *x*, as:

$$\dot{\gamma} = \frac{x}{h} \tag{2. 8}$$

2.3.2. Types of Fluid Behaviour

2.3.2.1. Newtonian Fluid Behaviour

Newtonian fluids are characterized by a linear relationship between the applied shear stress and the rate of shear, independently the strain reached. This relationship is expressed by the Newton law as follow:

$$\tau = \eta \cdot \dot{\gamma} \tag{2. 9}$$

The proportionality constant, η, is called shear viscosity. This parameter is only dependent of structure of material, pressure and temperature. Most of fluids composed of either little molecules or simple structures behave as Newtonian fluids. Newtonian fluids also do not show normal stress differences and present proportional viscosities

measured by different types of deformations, such as uniaxial and biaxial extension. Obviously, Newtonian behaviour is an idealization, but it is also a good approach of a large number of common liquids.

2.3.2.2. Non-Newtonian Fluid Behaviour

Non-Newtonian fluids show a non-linear relationship between the shear stress and the shear rate generated. Consequently, the viscosity, named apparent viscosity, depends on the shear rate value applied to, even on the kinematics history of the fluid element under consideration. The apparent viscosity can be defined as the Newtonian case:

$$\eta(\dot{\gamma}) = \frac{\tau}{\dot{\gamma}} \tag{2. 10}$$

Such materials can be generally classified into three groups:

A) Time independent Fluids. These fluids are characterised by shear viscosity is only dependent of the value of shear stress (or shear rate) at that point at that time. They also called as "inelastic" or "Generalized Newtonian Fluids" (GNF).
B) Time-Dependent Fluids. Fluids which show a more complex rheological response. Their shear viscosity depends on shear rate applied as well as the duration of shearing and their kinematic history. They are called "time-dependent fluids".
C) Viscoelastic Fluids. Viscoelastic fluids simultaneously exhibit obvious fluid-like and solid-like behaviour, showing a partial elastic recovery, after deformation.

Time-independent Fluid Behaviour

The flow behaviour of this class of fluids may be described by the following constitutive equation:

$$\tau = \tau(\dot{\gamma}) \tag{2. 11}$$

This equation means that the value of τ at any point within the sheared fluid is determined only by the current value of shear rate at that point or vice versa.

Depending on the mathematical relationship of the previous equation GNF may be further subdivided into three types (See Figure 2.12).

Shear-Thinning Fluids. This is the most frequent time-independent behaviour. Very many substances such as emulsions, suspensions, polymer melts, greases or commercial products belong to this group (Schramm, 1994). Shear-thinning, or pseudoplastic fluids, are characterized by an apparent viscosity decrease with increasing shear rate.

For most fluids, the shear thinning effect is reversible, often with some lag. The most general shear-thinning behaviour is characterized by three regions (Reiner, 1969). These materials might show a Newtonian plateau at low shear rates, called "zero shear viscosity" (η_0), a viscosity reduction with increasing the shear rate and a high-shear rate limiting viscosity (η_∞).

The origin of this phenomenon is due to microstructure changes by the shear field applied to the material. Initially, these structures exhibit a highly disordered state which leads a high resistance to be deformed. When the shear stress increases to such an extent that the deformation leads to the orientation or breakdown of elements of the material (particles, polymer coils) by far exceeds the randomizing initial state change, the viscosity drops drastically. At high shear rates, the structure is completely broken down, a perfect orientation is reached, and there are no particle interactions (Macosko, 1994). Consequently, the material became a Newtonian fluid.

Shear-Thickening Fluids or Dilatant Fluids. This type of materials is also characterized by a shear dependent viscosity with shear rate. Its apparent viscosity increases with increasing shear rate. The parameters which control dilatant behaviour are: particle size distribution, phase volume, shape, interactions, continuous phase viscosity and flow field (Barnes, 1989a). Originally, this class of fluid behaviour was observed in concentrated suspensions. Actually, the literature concerning shear thickening effects has focused on suspensions. Nevertheless, there are very few studies

related to dilatant effects (Barnes, 1989a; Boersma et al., 1990) despite the growing interest in the handling and processing of systems with high solids loadings.

Viscoplastic Fluids. A viscoplastic material is one that shows little or no deformations up to a certain level of stress, called yield stress, τ_c. Truly, as soon as the stress tensor reaches that critical stress value the material flows with a deformation localized along the surfaces where this critical value is reached (Coussot, 2005). On the contrary, such a material will deform elastically when the externally applied stress is smaller than the yield stress.

Materials whose the relationship between stress and shear deformation is lineal are called Bingham plastic fluids. Further, there are viscoplastic fluids showing a yield value with a non-linear stress/shear rate flow curve. Thus, these materials also pose a particular class of shear-thinning behaviour.

The yield stress behaviour is not a simple concept to account for. Actually, it is virtually impossible to ascertain whether any real material has a true yield stress or not. However, the yield stress concept has proved to be a practical parameter to characterize materials with solid-liquid transition in shearing (Barnes and Walters, 1985; Moller, 2008; Malkin, 2013)

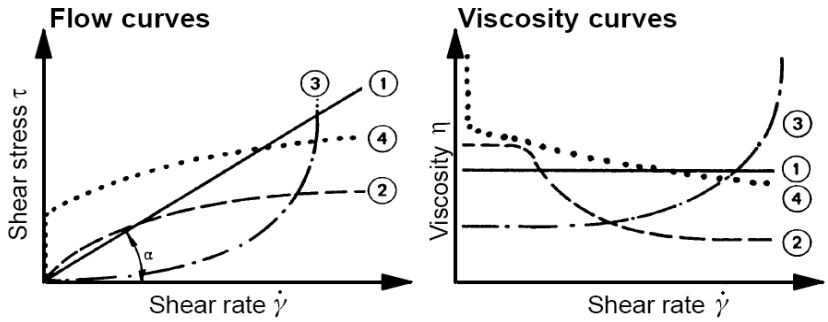

Figure 2. 12. Flow curves (left) and viscosity curves (right) for fluids: (1) Newtonian; (2) Shear-thinning; (3) Shear-thickening and (4) Viscoplastic

Time-Dependent Fluids

Time-dependent fluids are those in which the shear stress is a function of both the shear rate and time shear stress is applied (Johnson, 1998). Time-dependent fluid behaviour may be classified into two classes: Thixotropy and rheopexy, also called anti-thixotropy. They obey the following general expression:

$$\tau = \tau(\dot{\gamma}, t) \tag{2. 12}$$

where *t* is the shearing time.

Thixotropy. Thixotropy is a property of materials which show a continuous decrease of viscosity with time when flow is applied to a sample that has been previously at rest and the subsequently recovery of viscosity in time when the flow is discontinued (Mewis and Wagner, 2009). This means that the viscosity of these materials is shear thinning and time dependent and a yield stress could be included as well. According to this definition the thixotropic effect is reversible.

Thixotropy can be understood on the basis of underlying microstructure. In these systems the rheological response results from complex flow-induced structural changes. A general description model (*Structural kinetics models*) explains the thixotropic effects is based on a balance between hydrodynamics shear stresses pulling structures apart by erosion, and a combination of Brownian and shear forces building the structure up (Goodeve, 1939; Coussot, 2005).

There are several procedures to study the thixotropic effect of a material. The most typical is the hysteresis technique (Green and Weltmann, 1943). It consists of systematically increased and decreased shear rate between two values. When the transient data are represented in the flow the ascending curve is no longer directly underneath the decreasing curve. The thixotropic material will describe a hysteresis loop. The area and shape defines the magnitude of this property indicating the energy required to break down the thixotropic structure. For a given material, this area will depend on shear history, maximum shear rate and the rate of increase/decrease of shear rate.

Rheopexy or Antithixotropy. Those fluids for which their apparent viscosity (or the corresponding shear stress) increase with the time of shearing is said to display *rheopexy* or *antithixotropy*. There are few materials which exhibit this particular flow property (Kanai and Amari, 1995). Flow curve for these materials also depicts a hysteresis loop, but in this case the higher viscosity values correspond to the descending flow curve.

Antithixotropy is a phenomenon due to either the temporary aggregation by collision of attractive particles, or more open flocs structures formed under shearing (Barnes, 1997).

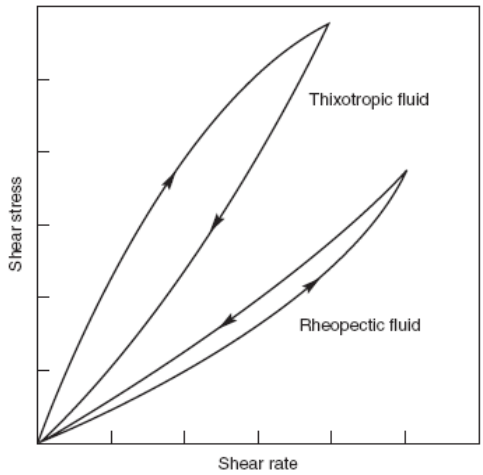

Figure 2. 13. Schematic steady flow curve for time-dependent fluid behaviour

Viscoelastic Fluids

Viscoelastic materials exhibit a behaviour which combines both elastic and viscous characteristics. For these materials, the stress required to maintain a constant deformation applied to the material diminishes gradually with time, or relaxes. Besides, the combined solid and liquid behaviour leads to two effects, some energy input is stored and partially recovered (elastic solid) and some is dissipated as heat (viscous liquid).

The study of these materials implies determinate a constitutive equation which relates stress, deformation and time. When both strain and stress are small enough and microstructure is conserved during the experiment, the relationship between both magnitudes can be described by linear differential equations with constant coefficients, and the material is in linear viscoelastic regime (Ferry, 1980). In this case, the stress-strain relation is simply a function of time and not of stress magnitude (Darby, 1976; Dealy, 1982). Otherwise, the viscoelastic behaviour is called non lineal.

Viscoelastic properties can be characterized by experiments which examine the relationship between stress and strain, and strain rate in time dependent experiments.

$$\tau = \tau(\gamma, \dot{\gamma}, t) \tag{2. 13}$$

Dynamic mechanical analysis is the most widely used method for characterizing viscoelastic behaviour. Dynamic (oscillatory) tests may be performed in stress controlled or strain controlled modes. In oscillatory tests, the sample is deformed sinusoidally by applying a sinusoidal shear deformation or stress, and the resultant stress or strain is monitored with time. When considering tests in the controlled strain mode, the applied strain is expressed according to the following equation:

$$\gamma(t) = \gamma_0 \cdot \sin(\omega \cdot t) \tag{2. 14}$$

where:

ω is the angular frequency (rad/s)

γ_0 is the amplitude of strain applied.

The corresponding stress observed can be expressed as:

$$\tau(t) = \tau_0 \cdot \sin(\omega \cdot t + \delta) \tag{2. 15}$$

Where τ_0 is the amplitude of stress and δ is shift angle.

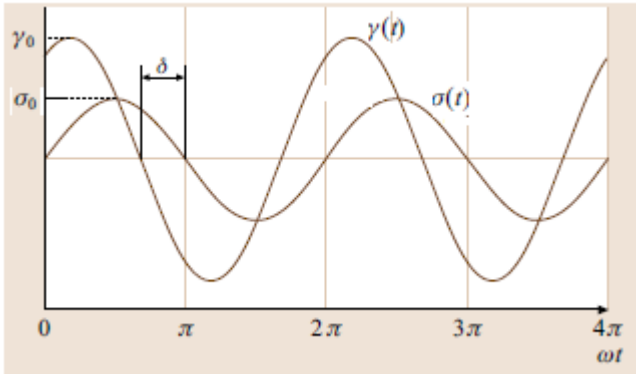

Figure 2. 14. Sinusoidal stress and deformation signals of dynamic test

By employing complex notation, the complex modulus, *G*(ω)*, is defined as

$$G^*(\omega) = \frac{\tau(t)}{\gamma(t)} = G'(\omega) + iG''(\omega) \quad (2.16)$$

$$|G^*(\omega)| = \frac{\tau^*}{\gamma^*} = \sqrt{(G'(\omega))^2 + (G''(\omega))^2} \quad (2.17)$$

Where:

τ(t) is the dynamic oscillatory shear stress

γ(t) is the dynamic oscillatory shear strain

G´(ω) is the real part of the complex function

G´´(ω) is the imaginary part of the complex function

G´(ω) and *G´´(ω)* are two frequency dependent functions, termed the shear storage and loss moduli, respectively. These two rheological functions can be defined:

$$G'(\omega) = \frac{\tau_0}{\gamma_0} \cdot \cos\delta \quad (2.18)$$

$$G''(\omega) = \frac{\tau_0}{\gamma_0} \cdot \sin\delta \quad (2.19)$$

The storage modulus, *G'*, is related to the elastic character of the fluid (energy storage during deformation), whilst the loss modulus, *G''*, is related to the viscous character of the material (energy dissipation during the experiment) (Macosko 1994).

Another commonly used dynamic viscoelastic property, the loss tangent, $tan\delta(\omega)$, denotes ratio of viscous and elastic components in a viscoelastic behaviour:

$$\tan\delta(\omega) = \frac{G''(\omega)}{G'(\omega)} \tag{2. 20}$$

In addition, there is another interesting material function denominated as dynamic viscosity. This function can be expressed either as function of viscous component of viscoelastic response, G'' as:

$$\eta'(\omega) = \frac{G''(\omega)}{\omega} \tag{2. 21}$$

or, as function of G' as:

$$\eta''(\omega) = \frac{G'(\omega)}{\omega} \tag{2. 22}$$

Both functions are the components of a complex number, η^*, called as complex viscosity which can be defined as:

$$|\eta^*| = \sqrt{\eta'^2 + \eta''^2} = \sqrt{\left(\frac{G''(\omega)}{\omega}\right)^2 + \left(\frac{G'(\omega)}{\omega}\right)^2} = \frac{|G^*|}{\omega} \tag{2. 23}$$

Oscillatory tests can be very useful in order to identify the influence of electrostatic effects on drilling fluid. In this sense, it was found that the elastic modulus of montmorillonite suspensions became notably high at different clay concentrations with the same pH values. These high G' values were attributed to a higher degree if dispersion of the platelets in water (Sohm and Tadros, 1989). Besides, it was observed that the G' values followed a power-law index, *n*, between 4 and 5 in the pH ranged Khandal and Tadros (1988). The predominant elastic behaviour of montmorillonite

suspensions, mainly in the acid range, is due to the cohesive energy of the flocs structures in wide range of pH (Duran et al., 2000). Further, static properties of clay dispersions, such as elasticity or yield stress, might be affected by crystal chemistry parameters of the clay (Paineau et al., 2011).

2.3.2.2.1. Rheological Models

Rheological models are mathematical functions of varying complexity which have proposed in order to describe characterize the Non-Newtonian flow behaviour. Many attempts were made to model the rheological response of materials by analytical equations from both theoretical and empirical point of view. The following models are commonly used to correlate the steady-shear viscosity and/or shear stress as function of shear rate.

The power law or Ostwald de Waele model

This model has been the most frequently used to describe the shear-thinning behaviour of different viscous materials, such as melt polymers or drilling fluids. The relationship between shear stress and shear rate for this type of fluids can expressed by a power-like equation over a limited range of shear rate (or stress). The mathematical form for this model is expressed by the following equation:

$$\tau = k \cdot \gamma^{n} \tag{2. 24}$$

For $n < 1$, the fluid exhibits shear-thinning properties

$n = 1$, the fluid shows Newtonian behaviour

$n > 1$, the fluid shows shear-thickening behaviour

Both, k and n are the two empirical curve-fitting parameters known as consistency index and flow index, respectively.

The Sisko model

Generally, the power law model can fit the rheological data over two or three decades. However, this model fails at high shear rates, where the viscosity reaches a constant limiting value. In order to rectify this lack of precision in this shear rate region, Sisko

model was originally proposed adding a limiting high-shear rate viscosity parameter, as follow:

$$\eta = k \cdot \gamma^{n-1} + \eta_{\infty} \tag{2. 25}$$

Where:

η is the shear viscosity.

η_{∞} is the high-shear limiting viscosity.

k is the consistency index.

n is the flow index.

The Cross Model

Many shear thinning fluids show notable deviations from the two parameter power law model at high and low shear rates. In order to model the viscous flow behaviour of these fluids, a model which takes into account viscous behaviour in limiting shear conditions, η_0 and η_{∞}, is necessary. This is analytical expression of this four parameter model:

$$\frac{\eta - \eta_{\infty}}{\eta_0 - \eta_{\infty}} = \frac{1}{1 + \left(\lambda \cdot \dot{\gamma}\right)^p} \tag{2. 26}$$

Where:

η is the shear viscosity.

η_0 is the zero shear viscosity.

η_{∞} is the high-shear limiting viscosity.

λ is a fitting parameter.

s is a fitting parameter related to the slope in that region.

Bingham model

This is the simple and most traditional equation used to fit the viscoplastic behaviour of a fluid with a yield stress, such as drilling fluids (Rossi et al., 2002):

$$\tau = \tau_B + \eta_p \dot{\gamma} \tag{2. 27}$$

Where:

τ_B is the apparent Bingham yield stress.

η_p is the plastic viscosity.

This model is based on the idea that the fluid will not deform, unless the shear stress exceeds a finite critical yield stress, τ_B. Hence, this parameter is related with the tendency of components to build a shear resistant structure. The parameter, η_p, is the slope of the stress-shear rate curve at high shear rate, and is generally associated with base viscosity, concentration and shape of solids in drilling muds.

Herschel-Bulkley model

Generally, the Bingham plastic model does not describe well shear stresses of the fluid at low shear rate overestimating the apparent yield stress value. In order to correct the deviation of this model, a much reliable model with three parameters is used:

$$\tau = \tau_H + k \cdot \dot{\gamma}^n \tag{2. 28}$$

Where:

τ_H is the apparent Herschel-Bulkley yield stress

k is the consistency index.

n is the flow index.

For most practical purposes, the Herschel-Bulkley model can account for the steady-state rheological performance of most of viscoplastic fluids, especially drilling fluids (Kelessidis et al., 2009; Herzhaft et al., 2003). Kelessidis et al. (2007) evaluated the rheological properties of water-based drilling fluid as function of pH using the Herschel-Bulkley model. Yield stress, flow consistency index and apparent viscosity showed a maximum close to the natural pH for 5% and 6.42% bentonite water-based drilling fluids formulated, whereas for the highest alkalinity drilling fluid, the degree flow consistency index drastically drops. In addition, several authors have reported that

raising the polymer content increase the apparent Herschel-Bulkley yield stress and lower the flow index in a wide range of concentration, particularly for higher clay content (Hamed and Belhadri, 2010; Khalil and Jan, 2011).The extra degree of freedom generally enables this model to fit the most rheological data better than any other two-parameter expression. On the other hand, this tree-parameter model is very susceptible to extrapolate beyond the measured shear range.

2.3.3. Suspension Rheology

The interest of suspension rheology has been gradually increasing over the last several decades. These systems play an important role in many industrial applications, in particular their rheological behaviour. In this sense, it is important to know the extent to which a rheological property, such as viscosity, changes with the addition of either colloidal or non-colloidal particles. When a particle is dispersed into a liquid matrix, the flow field is altered, with energy dissipation. There are two factors to be taken into account in order to study suspension rheology: hydrodynamic effect and the Brownian motion. The former refers to the interaction between the dispersed particles submitted to a flow field. Secondly, Brownian effect consists of a stochastic thermal movement which simply influences on particles smaller than 1μm. In this sense, Brownian hard spheres can be considered as dispersion with the simplest interaction potential of any type suspension.

Beyond hydrodynamic interaction and Brownian motion, there are others forces, such as electrostatic interactions. These forces affect the interparticle distances, and consequently when dispersions are subjected to shear stresses their resulting rheological properties changes.

From a rheological point of view, suspensions can be classified according to their volume fraction into three groups: dilute ($\phi \leq 0.05$), semi-dilute ($0.05 \leq \phi \leq 0.15$) and concentrated ($\phi > 0.15$).

2.3.3.1. Dilute Suspensions

The presence of a particle distorts the velocity distribution in a flowing fluid, an increase in energy dissipation and consequently, in viscosity is expected, (Macosko, 1994). This increase in viscosity is due to the stress from main flow and the stress around the particles. The viscous behaviour of dilute suspensions was first addressed by Einstein (1906), who derived the following expression for non-interacting spherical particles:

$$\eta_r = 1 + 2.5\phi \tag{2. 29}$$

In dilute systems, the distance between particles is large enough, the size of particles is not relevant, and the energy dissipation comes from the volume occupied. Hence, the relative viscosity is affected by neither particle distribution nor density. This equation shows a linear increase of viscosity suspension with increasing the volume fraction of disperse phase, although the behaviour remains Newtonian, even for non-colloidal particles.

In order to identify the influence of both hydrodynamics and Brownian motion on rheological behaviour of suspensions, a dimensional number, Peclet number, *Pe*, is defined as follow:

$$Pe = \frac{\sigma a^3}{k_B T} = \frac{\eta \dot{\gamma} a^3}{k_B T} \tag{2. 30}$$

This adimensional number is the ratio of advection by the flow to the rate of diffusion by Brownian motion.

Regarding stable suspensions, the dispersion microstructure is dependent of the balance between hydrodynamics, Brownian motion as well as electrostatic or steric forces, and consequently, these suspensions show a more complex rheology, even in dilute regime concentration. For suspensions stabilized by either electrostatic or steric forces, it is convenient introduce the effective volume fraction, ϕ_{eff}, in order to account for the layer thickness around the particle.

In case of electrostatically stabilized suspensions, the streamlines around the particle are modified by the electric double layer and the viscosity increases (first electroviscous effect). This extra dissipation energy can be described by the following expression:

$$\eta_r = (1 + 2.5(1 + p)) \tag{2. 31}$$

, being p is factor which relies on the electrostatic effects derived from the surface potential and ion-counterion atmosphere particle. For these suspensions, the thermal energy is lower than repulsive forces from the overlapping of electric potentials, and hence, the surfaces of neighbouring particles do touch each other.

The viscous behaviour of sterically stabilized suspensions via polymer adsorption or grafted polymer onto the particle surface at low particle concentration can be approximately considered as hard spheres, showing an hydrodynamics effective volume, ϕ_{eff}. Hence, they exhibit a constant viscosity with shear given by Einstein relationship:

$$\eta_r = (1 + 2.5\phi_{eff}) \tag{2. 32}$$

Where the hydrodynamic effective volume is derived from the hydrodynamic effective particle radius and hydrodynamic effective layer thickness, δ_h, as follow:

$$\phi^h{}_{eff} = \phi\left[1 + \left(\frac{\delta_h}{a}\right)\right]^3 \tag{2. 33}$$

The determination of hydrodynamic layer thickness under shear flow can be obtained from dynamic light scattering, or even more reliable from small angle neutron scattering (Stiger et al., 2004; Kim et al., 2013).

For flocculated suspensions, the attractive forces become larger than the repulsive forces, Brownian motion and/or hydrodynamic interactions, both microstructure and rheology of dispersions overcome a dramatic change. At low volume fractions, the Brownian movement has relatively low and opposite effect compared to the attractive

forces. Thus, zero-shear viscosities experience a notable increase, even inducing yield stress value.

2.3.3.2. Semi-dilute Suspensions

Increasing the solid volume concentration, the flow field of a particle is significantly altered by the presence of neighbouring particles, modifying the rate of energy dissipation. Batchelor and Green (1972) were the first who obtained an expression take account the hydrodynamics effect on semi-dilute suspension microstructure:

$$\eta_r = 1 + 2.5\phi + c_2\phi^2 \tag{2. 34}$$

In this equation the value of c_2 relies on the type of flow field, being 7.6 for extensional flow and 5.0 for shear flow. The coefficient c_2 shows both the contributions from hydrodynamics particle interactions and direct interparticle forces. More recently, Wagner and Woutersen (1994) found a more accurate value of 5.2 for c_2 in their calculations. In semi-dilute regime, the polydispersity of particles has a notable effect on interparticle interactions. The viscosity decreases only slightly with polydispersity (Qi and Tanner, 2012).

A higher-order power series equation describes the viscosity-solid concentration relationship because of multibody interactions, as follow:

$$\eta_r = \sum_{i=1}^{N} c_i \phi^i \tag{2. 35}$$

, where c_i are the concentration-independent expansion coefficients.

In this range of concentration, shear viscosities of sterically dispersions for higher volume fraction disperse phase show notable differences respect to hard spheres dispersions as function of shear rate. In this sense, the high-shear rate limiting viscosity is lower than that expected for Brownian hard spheres viscosity at concentration near maximum packing fraction due to compression of polymer layers (Mewis et al., 1989). Interestingly, the decrease in relative viscosity by increasingly shear rates applied can be modelled a Cross-like equation (see equation 2.26).

Similar to stabilized systems, dispersions with weak attractive potentials show a zero-shear viscosity higher than that Brownian equivalent suspension.

Regarding to oscillatory test, sterically stabilised suspensions might show notably different viscoelastic response with the volume fraction. Thus, semidilute and intermediate concentrated suspensions have a Maxwellian-like behaviour. Besides increasing disperse phase concentration, mechanical response is characterized by an independent storage modulus which reflects higher repulsion when covered particles approach.

Dispersions with weak attractive potentials show a zero-shear viscosity higher than that Brownian equivalent suspension. Semidilute flocculated suspensions can show shear-thinning behaviour exhibiting a transition from the low shear rate region to high shear rates region because of the work required to separate particles. At high-shear rates, the hydrodynamic forces are comparatively higher than attractive interactions, and consequently, particle size decreases yielding a Newtonian behaviour.

2.3.3.3. Concentrated suspensions

Further increasing of volume fraction causes a more remarkable rise in viscosity in hard sphere suspensions. Additionally, viscosity values can diverge at particular volume fraction called maximum packing fraction, ϕ_{max}. Thus, particles are sufficiently close that lubrication hydrodynamic effect becomes the main contribution to stresses. Furthermore, under shear conditions, microstructure of concentrated suspensions is distorted leading to changes in the maximum packing fraction. This shear dependent maximum packing fraction has been included in phenomenological models, such us Krieger and Dougherty (1972) to yield:

$$\frac{\eta_r - \eta_{r,\infty}}{\eta_{r,0} - \eta_{r,\infty}} = \frac{1}{1+(\sigma/\sigma_{cr})^{m(\phi)}} \tag{2. 36}$$

Where, $\eta_{r,0}$ and $\eta_{r,\infty}$ are the relative viscosities at low and high-limiting shear rates, respectively; σ_{cr} is a fitting stress parameter. The exponent *m* increases with volume fraction and range from 0.5 to 0.73. This rheological behaviour was suitable for

suspensions without yield-stress. Moderately concentrated suspensions also show a shear thinning at intermediates shear rates with two plateau viscosity values in the low and high shear rate limits (Figure 2.15).

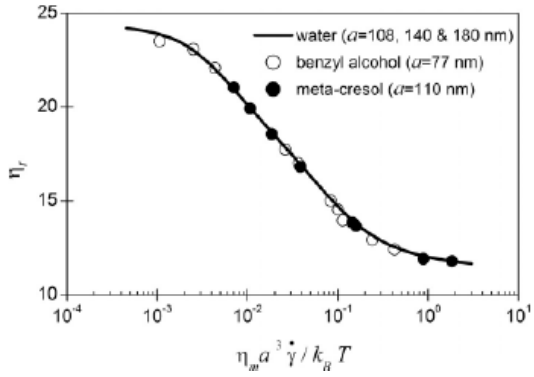

Figure 2. 15. Rheology of polystirene of various sizes volumes at volume fraction of 0.5 in different suspending media

In stabilized suspensions by charges, particles experience a softer potential at relative lower potential, and consequently, viscosity values are lower than hard spheres ones. However, increasing volume fraction leads to stronger repulsive forces between neighbouring particles resulting in more remarkable increase in viscosity. The shear-thinning behaviour is generally more severe in these systems because of the notable differences in microstructure response at low and high shear rates. Thus, zero-shear viscosity is strongly influenced by repulsive forces, whereas viscosity at high stress is practically not affected by potential.

2.3.4. High Pressure Rheology

High-pressure rheology plays an important role in many areas of science and technology. Several industrial processes, such as sedimentation, crystallization or chemical reactions are strongly affected by the fluid viscosity, which depends on both temperature and pressure conditions. For instance, a deep knowledge of the pressure-temperature viscosity relationship is very important in lubrication field, since the lubrication film may be submitted to pressures as much as 10000 – 20000 bar, and

shear rates of 10^{-3} s^{-1}, over a wide range of temperature (Bair, 2007). In the drilling industry, the effect of pressure and temperature on viscosity of drilling fluids must be taken into consideration in order to deal with a wide range of challenges such as, instability problems, surge pressure or sticking the pipe.

The influence of temperature on the shear properties of fluids has been fairly well studied. However, little effort went into the research on the effect of pressure on the mechanical properties of materials. This is mainly due to the well-known difficulty of measuring rheological properties with enough precision under high pressure environments (Tschoegl et al., 2002). For simple materials, such as organic low molecular weight liquids, the combined pressure-temperature-viscosity relationship is well characterized by simple expressions as function of both variables. Nevertheless, Non-Newtonian fluids generally exhibit a more complex rheological response with pressure, and consequently, more sophisticated treatment is necessary (Martinez-Boza and Gallegos, 2010).

2.3.4.1. High-Pressure Rheology Experimental Technique

The study of high pressure rheology implies the use of experimental methods and proper equipment to collect the evolution of viscosity with pressure. In general, all techniques must be reliable for recording pressure values, transmitted torque and deformation of the fluid to be characterized.

Capillary Viscometers

One of the earliest viscosity measurements under pressure (150 bar) was carried out by Warburg and Sachs (1884) using a capillary viscometer. Capillary viscometers measure the pressure change between two points of a capillary duct for a given flow across a length of known circular section. For Newtonian liquids, the viscosity can be calculated directly using the Hagen-Poiseuille equation:

$$\eta = \frac{\pi R^4}{8\Delta L}\frac{\Delta P}{Q} \qquad (2.\ 37)$$

Where ΔP, is the pressure drop, Q is the volumetric flow, R is the radius of the capillary, and ΔL is an equivalent length for correcting the entrance and end effects.

For Non-Newtonian fluids, the true apparent shear rate at the wall depends on the flow properties of the fluid, and it necessary to be account the Rabinowitch´s correction for calculating. Thus, the real apparent shear rate at the wall can be expressed as follow:

$$\dot{\gamma}_w = \left(\frac{4Q}{\pi R^3}\right)\cdot\left(\frac{3}{4} + \frac{1}{4}\frac{d\ln Q}{d\ln \tau_w}\right) \tag{2. 38}$$

Where τ_w is the wall shear-stress.

The shear stress can be expressed as:

$$\tau_w = \frac{\Delta P \cdot R}{2(L + \Delta L)} \tag{2. 39}$$

Novak and Winer (1968) designed a high level pressurized capillary viscometer capable of measuring viscosities at pressures up to 6000 bar, and temperatures up to 150ºC (see Figure 2.16.). This apparatus maintains high pressures at the capillary by the motion of a moveable piston, which causes a known flow, and a fixed one arranged in series at both ends of capillary. The pressures at the both ends of the capillary are detected using strain gauge transducers.

Capillary viscometers extensively use for high pressure high temperature viscosity of melt polymers and oils (Galvin et al., 1981; Song et al., 2011).

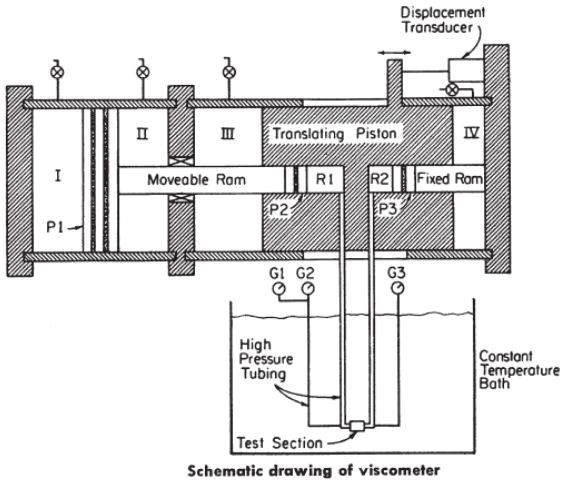

Figure 2. 16. The pressurized capillary viscometer of Novak and Winer

Falling Ball and Rolling Ball Viscometers

The earliest measurements with this type of viscometer were performed by Flowers in 1914. Bridgman also carried out viscosity measurements of several pure liquids up to 12000 bar using a falling ball-like viscometer (Bridgman. 1925).

Essentially, classical falling and rolling ball viscometer measure the Newtonian viscosity by recording the time of fall for which a smooth ball travelling a fixed distance inside a tube (Briscoe et al., 1992a; Briscoe et al., 1992b). In high-pressure conditions, where the pressure containing the vessel must be internally compact, the rolling ball along an inclined tube is preferred due to easier operation and control than the falling ball (Bair, 2007). Many instruments may be utilized with ball travelling both directions by rotating the tube. In this apparatus, the typical inclination (from horizontal) angles comprised 8 – 70º. All studies suggest a similar general form to calculate the viscosity, as follow:

$$\eta = C \cdot (\rho_s - \rho_l) \cdot \Delta t \tag{2. 40}$$

where C is the instrument constant that must be obtained using liquids of known viscosity, Δt is the time taken by the ball to roll through a fixed distance, ρ_s and ρ_l the

densities of the ball and the fluid, respectively. The fluid density, ρ_l, must be independently determinate as function of both pressure and temperature in order to calculate the values of Newtonian viscosity.

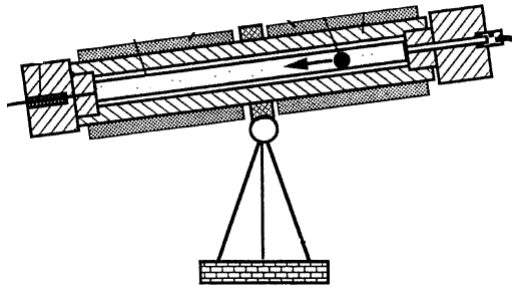

Figure 2. 17. Schematic diagram of a rolling ball viscometer

On the other hand, the use of a rolling ball viscometer for the measurement of Non-Newtonian fluids is still unpopular in spite of the attempts to calculate a mean shear rate and shear stress at the ball (Sestak and Ambros, 1973). In spite of that, good agreements between rolling ball data and other rheometric techniques for different fluids show its potential use (Schurz, 1990; Briscoe et al., 1994; Eguchi and Karino, 2008).

The major distinction among the different rolling or falling ball viscometers designed has been the means for detecting the position of the ball or sinker (Martinez-Boza and Gallegos, 2010). Sawamura et al. (1990) utilized a visible light detector to observe through a pair of sapphire windows the fall of a glass ball across the tube. He was able to measure viscosities up to 4000 bar. Izuchi and Nishibata (1986) used linear variable differential transformers and a steel ball, in a pressure range of up to 10000 bar. Recently, Calvignac et al. (2010) has designed a high pressure falling ball viscometer equipped with sapphire windows, a cold lighting device and a high-speed digital video camera connected to a computer for pressures up to 250 bar.

Rotational Rheometers

These apparatus are devices commonly used to perform rheological test in simple shear. They can operate either, under controlled stress or controlled rate conditions. In first case, a torque (or stress) is applied by the rheometer and the resulting shear rate is measured. On the other hand, for controlled rate version, the rheometer commands a rotational speed, which is proportional to shear rate, and stress is measured. The rheological characterization using this type of equipment requires collecting both torque and/or rotational speed under high pressure environment. Initially, this issue was dealt with closing all the principal parts of the rheometer (motor, geometry and transducer) into a pressure cell (Thomas et al., 1939). This set-up was refined by Hutton and Phillips (1973) introducing several improvements to control the temperature and the response time for torque measurements.

More recently, high-pressure rotational rheometers have been constructed by companies ThermoHaake, Reologica Instruments AB, and TA Instruments, enclosing some parts of the rheometer into a pressurized vessel, called pressure cell. Essentially, this device consists of a static steel vessel with a cylindrical close head. The inner conventional geometry sensor (coaxial cylinder or plate-plate configuration) is equipped at the top, with a secondary magnetic device which is magnetically coupled to a tool outside the cell (Martinez-Boza and Gallegos, 2010). The outer part transmits the torque through the pressure cell by a magnetic coupling (see Figure 2.18). These devices, however, have some constrains due to its design, such as internal friction between materials that in contact in the vessel or limitations in the pressure range of the cell. However, pressure cell rheometers allow an easy way to operate.

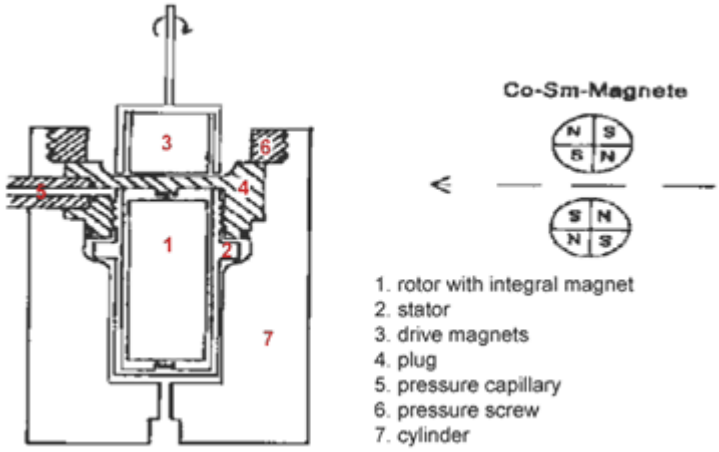

Figure 2. 18. Schematic representation of high pressure rheometer

2.3.4.2. Models for High-Pressure Rheology

There are a wide variety of models for describing the temperature and/or pressure dependence of viscosity. Some of them are empirical equations which correlate the experimental data available within a limited range of temperature and pressure conditions using a number of parameters. Empirical models are based on the data tendency, and their fitting parameters have not a physical meaning. On the other hand, theoretical models are essentially based on molecular theories, such as free volume theory. In the latter case, their parameters have a physical interpretation.

Empirical Models for Isothermal Viscosity

There are several empirical models capable of showing the pressure-viscosity relationships for different materials.

Barus' Model

This a one-parameter exponential model proposed by Barus (1893) to describe the evolution of the isothermal viscosity with pressure:

$$\eta = \eta_0 \cdot \exp\left(\beta (P - P_0)\right) \tag{2. 41}$$

where, η_0 is the viscosity at the reference temperature, β is piezoviscous coefficient, P is the applied pressure and P_0 is the pressure of reference. Barus' model is a proper

equation to correlate pressure dependency of viscosity at low and moderate pressures. The main limitation is due to the exponential increase viscosity prediction with pressure even at high pressures, since viscosity shows either a change in the viscosity-pressure variation or a limiting viscosity values as is reported elsewhere (Bridgman, 1925; Lamb, 1977). The unique fitting parameter,β, is temperature dependent, and generally decrease as temperature rises.

Irving and Barlow's Model

Irving and Barlow proposed a double-exponential model incorporating an inflection to describe the pressure-viscosity response of diesters. Their model possesses four parameters to fit the viscous pressure response at higher pressures:

$$\eta = A_1 \cdot \exp\left(K_1 (P - P_0)\right) - A_2 \cdot \exp\left(K_2 (P - P_0)\right) \tag{2. 42}$$

Where, A_1, A_2, K_1 and K_2 are the four temperature independent parameter of this model.

Sargent's Model

This model was proposed by Sargent (1983) to describe both the concavity and asymptotic viscosity values observed when high pressures are applied:

$$\eta = \eta_0 \cdot \exp\left[\frac{A \cdot (P - P_0)}{B + (P - P_0)}\right] \tag{2. 43}$$

In order to model this pressure-viscosity behaviour at extreme pressure, Irvin model incorporates two fitting parameters independent of temperature, A and B, and the viscosity at the temperature of reference, η_0.

The above models simply take into account the isothermal evolution of viscosity with pressure. Since viscosity strongly depends on temperature, models which fit the temperature on viscosity is very challenging in order to describe the combined effects of pressure and temperature.

Empirical models for non-Isothermal Viscosity

Several equations have been proposed for model the temperature-viscosity behaviour. Vogel, Tamman and Fulcher (1995) proposed the following equation to model viscosity temperature dependence:

$$\eta = \eta_{\infty} \cdot \exp\left[\frac{D_F \cdot T_{\infty}}{T - T_{\infty}}\right] \tag{2. 44}$$

Where, D_f is called the fragility parameter, η_{∞} is the viscosity at the Vogel temperature, and T_{∞} is the Vogel temperature at which the viscosity diverges at low temperature. This temperature parameter has also been referred to as the idealized glass transition temperature and is roughly between 15 and 40º C less than glass transition temperature.

Andrade expression (1930) is an Arrhenius-like equation which describes fairly well the thermal dependence at temperatures near the boiling point and far from the glass transition temperature:

$$\eta = \eta_0 \cdot \exp\left[\frac{\Delta E}{R} \cdot \left(\frac{1}{T} - \frac{1}{T_0}\right)\right] \tag{2. 45}$$

Where η_0 is the viscosity at the temperature of reference, T_0, R is the gas constant, and ΔE is the activation energy to flow.

Williams, Landen and Ferry (1955) originally proposed WLF model which represents an useful modification of the VTF model.

$$\log\left(\frac{\eta}{\eta_0}\right) = -\frac{c_1 \cdot (T - T_0)}{c_2 + (T - T_0)} \tag{2. 46}$$

Where c_1 and c_2 are the WLF constants, η_0 is the viscosity at the temperature of reference, T_0. This model is particularly valid for describing the low temperature viscosity dependency where non-Arrhenius behaviour is characteristic. Besides, it is not strictly an empirical model since its parameters have a physical interpretation as will be discussed below.

Pressure-temperature-viscosity models can be obtained by combining different equations yield, Andrade-Barus model, WLF-Barus model, as example

Andrade-Barus Model

$$\eta = \eta_0 \cdot \exp\left[\frac{\Delta E}{R}\cdot\left(\frac{1}{T}-\frac{1}{T_0}\right)+\beta\cdot(P-P_0)\right] \tag{2. 47}$$

WLF-Barus Model

$$\eta = \eta_0 \cdot 10^{-\frac{c_1\cdot(T-T_0)}{c_2+(T-T_0)}}\cdot\exp\left[\beta\cdot(P-P_0)\right] \tag{2. 48}$$

Theoretical Models

Models for describing the entire pressure range of measurements become more complex with more parameters with any physical meaning. On other hand, theoretical models can provide a more accurate framework for the description of temperature and pressure of viscosity.

Free Volume Model

Ferry-Moonan-Tschoegl Model (FMT model).

Many theories for modelling the effects of thermodynamics variables such pressure or temperature on the time-dependent behaviour of materials are based on the *free-volume* theory (Tschoegl et al., 2002). Initially, this concept was introduced by Doolittle and Dolittle (1957) in their work on the viscosity of liquids. Authors supposed that the variation in viscosity relies on the molecule-size holes in the fluid. The total sum of these holes describes the *free-volume,* which affects the mobility of the liquid molecules. Hence, the viscosity of liquids, η, can be expressed as follow:

$$\eta = A\cdot\exp B\cdot\left(\frac{V_\phi}{V_f}\right) = A\exp B\cdot\left(\frac{1}{f}-1\right) \tag{2. 49}$$

Where A and B are empirical constants, V_ϕ is the *occupied volume* by the molecules of the liquid, and V_f is the free volume, and represents the intermolecular space available

for molecular motion. Therefore, the total macroscopic volume is $V = V_f + V_ø$, being $f = V_f / V$ the *fractional free volume*. The free volume depends on both temperature and pressure. Thus, if f and η represent the viscosity and the fractional volume fraction at a given temperature, T and pressure P, and f_0 and η_0 represent the same quantities at a conveniently chosen temperature, T_0 and pressure P_0, the viscosity ratio can be expressed as:

$$\frac{\eta}{\eta_0} = \exp B\left(\frac{1}{f} - \frac{1}{f_0}\right) \tag{2. 50}$$

This relationship provides a shift factor, a_{TP}, which is also proportional to the relaxation time at the same pressure and temperature conditions, taking into account the approach from the Rouse theory (1953). Hence, the *general shift factor*, a_{TP}, can be expressed as:

$$a_{TP} = \frac{\tau(T,P)}{\tau_0(T_0,P_0)} \tag{2. 51}$$

When pressure is kept constant, the free volume only depends of temperature. Williams et al. (1955) modelled the effect of temperature on the mechanical properties amorphous homopolymers or random copolymers assuming that the fractional free volume of such polymers increases linearly with temperature:

$$f = f_0 + \alpha_f (T - T_0) \tag{2. 52}$$

Where α_f is the thermal expansivity of the fractional free volume. If this equation is substituted into the equation 2.50 leads to:

$$\log\left(\frac{\eta}{\eta_0}\right) = \log a_T = \frac{(B/2.303 f_0)\cdot(T - T_0)}{(f_0/\alpha_f) + T - T_0} \tag{2. 53}$$

where a_T is the *temperature shift factor*.

For experiments performed under constant temperature, the effect of pressure on the mechanical properties must be considered introducing a function of free fractional volume with pressure.

Ferry and Stratton (1960) proposed that the fractional free volume decreases linearly with pressure. Thus:

$$f = f_0 + \kappa_f (P - P_0) \tag{2. 54}$$

where κ_f is the isothermal compressibility of the fractional free volume. Introducing this equation into equation 2.50 the viscosity ratio is given by Ferry-Stratton equation:

$$\log\left(\frac{\eta}{\eta_0}\right) = \log a_P = \frac{(B/2.303 f_0)\cdot(P - P_0)}{(f_0/\kappa_f) - (P - P_0)} \tag{2. 55}$$

where a_P is the *pressure shift factor*.

For low and medium pressures, O´Reilly (1962) found the pressure dependence of shift factor, a_P, can be described by an exponential relationship as follow:

$$a_P = \exp\theta\cdot(P - P_0) \tag{2. 56}$$

where $\theta = 1/\Pi f_0$, and Π is a material-dependent empirical parameter that is considered to be independent of pressure. The logarithmic form becomes:

$$\log a_P = \frac{B}{2.303\Pi f_0}\cdot(P - P_0) \tag{2. 57}$$

Kovacs and its associates (1988; 1990) proposed a variation of *pressure shift factor* from the compressibility of the Tait equation (Tait, 1888) to yield:

$$\log a_P = \frac{B}{2.303 f_0}\cdot\left[\frac{1 + kP/K^*(T)}{1 + kP_0/K^*(T)}\right]^{1/fk} \tag{2. 58}$$

Where K^* is the bulk modulus at zero pressure, and k is an empirical constant that represents the variation of bulk modulus with pressure.

The FMT model (Fillers and Tschoegl, 1977; Moonan and Tschoegl, 1985) is considered as an extension of the WLF equation. In this model, both pressure and temperature are taken into account. Hence, authors assumed the following relations to describe the effect of both variables on the fractional free volume:

$$f = f_0 + f_P(T) - f_{T_0}(P) \tag{2. 59}$$

$$f_P(T) = \alpha_f(P)\cdot(T - T_0) \tag{2. 60}$$

$$f_{T_0}(P) = \kappa_f \cdot (P - P_0) \tag{2. 61}$$

The expression for $f_{T0}(P)$ is obtained by assuming that the compressibility of the fractional free volume, κ_f, is independent of pressure, and can be expressed as the difference between the entire and occupied volume:

$$\kappa_f = \kappa_e - \kappa_\phi \tag{2. 62}$$

where κ_e is the compressibility of the entire volume, and κ_ϕ is the compressibility of the occupied volume. The isothermal compressibility of entire, occupied or free volume is defined as:

$$\kappa = \left[\frac{1}{K^* + kP}\right] \tag{2. 63}$$

Thus, after integrating the above expression between P_0 and P, and substituting into equation 2.50, the FMT equation yields:

$$\log\left(\frac{\eta}{\eta_{00}}\right) = \log a_{TP} = -\frac{c_1^{\,00}\cdot(T - T_0 - \theta(P))}{c_2^{\,00}(P) + (T - T_0 - \theta(P)} \tag{2. 64}$$

where,

$$\theta(P) = c_3(P)\ln\left[\frac{1+c_4P}{1+c_4P_0}\right] - c_5(P)\cdot\ln\left[\frac{1+c_6P}{1+c_6P_0}\right] \quad (2.\ 65)$$

In which:

$$c_1^{\ 00} = \frac{B}{2.303 f_0} \quad (2.\ 66)$$

$$c_2^{\ 00}(P) = \frac{f_0}{\alpha_f(P)} \quad (2.\ 67)$$

$$c_3(P) = \frac{1}{k_e\alpha_f(P)} \quad (2.\ 68)$$

$$c_5(P) = \frac{1}{k_\phi\alpha_f(P)} \quad (2.\ 69)$$

$$c_6 = \frac{k_\phi}{K_\phi^{\ *}} \quad (2.\ 70)$$

$$\alpha_f(P) = \alpha_f^{\ *}\left[1 - \frac{mP}{K_e^{\ *} + k_eP}\right] - m\alpha_\phi^{\ *}P\left[\frac{1}{K_e^{\ *} + k_eP} - \frac{1}{K_\phi^{\ *} + k_\phi P}\right] \quad (2.\ 71)$$

Where, η_{00} is the viscosity at the reference temperature and atmospheric pressure, f_0 is the fractional free-volume at the reference temperature, B is a constant which usually is taken to be 1, $\alpha_f(P)$ is the expansivity of the free volume, considered pressure dependent and temperature independent, $\alpha^*_f(P)$ is the expansivity of the free volume at zero differential pressure and temperature of reference, α^*_ϕ is the expansivity of the occupied volume at zero differential pressure, $K_e^{\ *}$ and K_ϕ* are the bulk modulus of the entire and occupied volume respectively, at zero differential pressure and temperature of reference, m is proportionality constant, k_e and k_ϕ the pressure rate of change of the isothermal bulk modulus at pressure of reference of the entire and occupied volume, which are independent of temperature and pressure.

From the rheological data, all FMT parameters can be determined considering *B* value is 1, using non-linear regression techniques to solve the FMT equation. However, *B* can be determined using Pressure-Volume-Temperature data (PVT), in order to determinate.

Generally, the parameter *m* is assumed to be the same value for either occupied or entire volume. However, this assumption might be erroneous when PVT data are employed, and different values of *m*, for occupied or entire volume, are required, in order to estimate the evolution of expansivity with pressure properly, as is reported elsewhere (Martin-Alfonso et al., 2007).

Yasutomi's Model

Yasutomi et al. (1984) suggested a WLF-like equation for modelling the pressure-temperature mechanical behaviour based on the free volume concept. He assumed that the fractional free volume can be expressed by means the glass transition temperature as follow:

$$f_P(T) = f_g + \alpha_f(P)\cdot(T - T_g) \tag{2. 72}$$

Where f_g and α_f are the fractional free volume and the thermal expansion coefficient, respectively, at the glass transition temperature, T_g. It is well known that the glass transition temperature increases with pressure. In addition, the pressure dependence of this temperature is influenced in different manner if pressure is very high (higher than 10000 bar). Thus, Yasutomi proposed a modified temperature-pressure WLF equation which accounts the material properties at the glassy state:

$$\log\left(\frac{\eta}{\eta_0}\right) = -\frac{c_1\cdot(T - T_g)\cdot F}{c_2 + (T - T_g)\cdot F} \tag{2. 73}$$

Being the glass transition temperature, T_g, a function of pressure:

$$T_g = T_{g0} + A_1 \ln(1 + A_2 P) \tag{2. 74}$$

The dimensionless relative thermal expansivity of the free volume, *F*, is given by an empirical expression (Breuer and Rehage, 1967) for the total thermal expansivity of the liquid, assuming that the temperature dependences of the free volume and total volume change with pressure in the same manner. Being *F* is the free volume expansivity:

$$F = 1 - B_1 \ln(1 + B_2 P) \tag{2. 75}$$

Where T_{g0}, A_1, A_2, B_1 and B_2 a set of parameters to be evaluated.

Bair (2001) used this equation to model the pressure-temperature dependence of viscosity for polyethylene and different lubricant oils. The application of Yasutomi´s WLF-modified equation requires viscosity data at temperatures close to T_g, a thermal range with difficulties to be accomplished.

In addition, the original Yasutomi correlation suffers from the appearance of a zero in the function describing the pressure dependence of relative free volume thermal expansivity. In this sense, Bair et al. (2013) used an improved Yasutomi correlation for viscosity at high pressure. The new expression for the free volume expansivity, *F* is:

$$F = 1 + B_1 (P - P_0)^{B_2} \tag{2. 76}$$

Friction Theory Models

The *f-theory* was presented by Quiñones-Cisneros et al. (2000) in order to model the viscosity of fluids. This new theory is based on friction concepts and Van der Waals theory, to characterize the shear viscosity of fluids, rather than a transport property. The total viscosity is assumed to be separated into two principal contributions, a dilute gas term, η_0, and a friction term, η_f:

$$\eta = \eta_0 + \eta_f \tag{2. 77}$$

where η_0 is the dilute gas viscosity, which derives from the kinetic theory of gases, and η_f is the frictional viscosity associated to the interactions of the moving fluid layers. The latter term is connected to the repulsive and attractive intermolecular forces, which can be expressed as follow:

$$\eta_f = \kappa_a p_a + \kappa_r p_r \tag{2. 78}$$

where κ_a and κ_f are the attractive and repulsive viscous friction coefficients, and p_a and p_r are the attractive and repulsive pressures which can be determinate using different equations of state, such as, for instance, the Soave-Redlich-Kwong (Soave, 1972) or Peng-Robinson-Stryjek-Vera equations (Stryjek and Vera, 1986). This expression, known as *linear friction model equation*, is more convenient for light fluids, at which the attractive part prevails. For dense fluids, the dominant term is due to short-range nature repulsive forces, and a quadratic expression (*the quadratic friction model*) for modelling the friction contribution is preferable:

$$\eta_f = \kappa_a p_a + \kappa_r p_r + \kappa_{rr} p_r^{\,2} \tag{2. 79}$$

Or the generalized form represented by series as:

$$\eta_f = \sum_{i=1}^{n_a} \kappa_{a,i} p_a^{\,i} + \sum_{i=1}^{n_r} \kappa_{r,i} p_r^{\,i} \tag{2. 80}$$

For Newtonian fluids, the κ parameters are temperature-dependent related to friction coefficients between sliding surfaces. The friction theory has been successfully used by Quiñones-Cisneros and Deiters (2006) to model the viscosity of several hydrocarbons in a wide range of pressure and temperature conditions. In addition, an extension of the f-theory approach for modelling the Non-Newtonian behaviour fluids has been applied to reservoir fluids, such as crude oils by Quiñones-Cisneros et al. (2008) at different temperature-pressure environments.

2.4. Volumetric Behaviour of Fluids

2.4.1. Pressure - Volume - Temperature Measurement Techniques

Bellows Volumometer

The first bellows volumometer was described by Bridgman (1931) who employed it for temperatures between 0 and 95ºC and pressures up to 12000 bar. In bellows volumometer the fluid to be compressed is fully contained within measuring cell. This cell, or a part of it, is a flexible bellows which transmits the pressure applied to the fluid. The change in length of the bellows is measured to determinate the compression of the fluid under the pressure applied. Operating with this equipment in a wide range of temperatures requires the determination of volumometer volume by using a liquid of known density at different temperatures. Likewise, some quite small corrections have to be applied to raw data.

There is a wide variety of bellows volumometer which have been used for measurements over a wide range of temperature and pressure. Mopsik (1967) performed density measurements as well as dielectric constant of the fluid that covered the temperature range from -153 to 27ºC and pressure up to 2000 bar. More recently, Yokayama and Uematsu (2003) made density, bubble pressure and vapour pressure measurements for methanol-water mixtures from 47ºC to 143ºC, at pressures up to 2000 bar, using a bellow volumeter to determinate excess molar volume of mixtures as function of pressure and temperature. Sugiyama et al. (2011) also employed a metal-bellows variable volumometer to measure volumetric data for binary mixtures of CO_2 and isobutane.

Vibrating-Wire Densimeter

Initially, the principal use of vibrating-wire sensors was the measurement of fluid viscosity. In order to obtain viscosity data, the vibrating-wire viscometer relates the viscosity of the sample to the damping of free transverse oscillations of an immersed rigid wire. The behaviour of a fluid surrounding the vibrating wire also relies on its density. However, it is not easy to obtain enough sensitivity to the density without compromising the performance of the sensor as a viscometer.

Nevertheless, in the nineties a new design of vibrating-wire sensor with a buoyancy device in the form of a suspended sinker was capable of a precise determination of

density using this technique (Dix et al., 1991). The design of vibrating-wire sensor can be improved to maximize the density sensitivity combining the capability of viscosity measuring since the installation of the buoyancy device has no influence on the viscosity result. In order to measure density, the vibrating-wire sensor is driven in the forced mode of oscillation. In this type of densimeter, once masses, densities and dimensions of all solid parts of the assembly are known and the resonant frequency and damping of the wire in vacuum are determined experimentally, density and viscosity can be obtained accordingly. In addition, because it is supported by a rigorous theory, the vibrating-wire technique does not require extensive calibration for performing density measurements of different fluids, even though at high pressure and high temperature conditions.

After the first attempt to build a densimeter based on the vibrating-wire sensor, Pádua et al. (1994) was constructed to measure density and viscosity simultaneously for three pure liquids in the temperature range of -76ºC to 75ºC and pressures up to 1000 bar. This instrument was also used for determining both viscosity and density of supercritical CO_2-saturated polyethyleneglycol mixtures (Gourgouillon et al., 1998). Audonnet and Pádua (2001) introduced several notable improvements in the vibrating-wire instrument, such as lesser amount of sample required, chemical compatibility improved and enhancement of output signal. In this work, simultaneous measurements of viscosity and density for n-pentane were carried out in the temperature range from 25 to 110ºC and up to 1000 bar. Lately, a newly designed apparatus for accurate simultaneously viscosity and density measurements of gases was built (Seibt et al., 2009). The measuring system was enabled to obtain independently both thermophysical properties using a vibrating-wire viscometer and a single-sinker densimeter mounted in the same measuring cell. The reliability of viscosity-density measurements for helium and nitrogen covering temperatures from -20ºC to 200ºC up to 300 bar was confirmed by comparing with selected data from literature.

Vibrating-Tube Densimeter

The typical vibrating tube densimeter consist of a hollow metallic or glass thin-walled tube in a U or V shape which is isolated from external mechanical perturbations. The sample is introduced into the tube which vibrates perpendicular to its plane in an electromagnetic field. This electromagnetic field is created by a permanent magnet and a wire-coil, which also register the frequency of the tube. The basic relation for a tube vibrating with a period of oscillation, τ, in the harmonic mode can be expressed as:

$$\tau = 2\pi\left(\frac{m_t + \rho V_t}{C}\right)^{1/2} \tag{2. 81}$$

Where m_t and V_t are the mass and inner volume of the tube, respectively, ρ is the density of the fluid, and C is the force constant which relies on the size, shape of the tube and the nature. The density of the fluid can be derived from this equation to yield the following working equation for this type of densimeter:

$$\rho = K\tau^2 + L \tag{2. 82}$$

Both parameters, L and K are function of temperature and pressure:

$$K(T,P) = \frac{C(T,P)}{4\pi^2 V_t(T,P)} \quad L(T,P) = -\frac{m_t}{V_t(T,P)} \tag{2. 83}$$

The determination of temperature and pressure dependence of the K and L can not be calculated exactly. Hence a calibration procedure over the range of temperature and pressure conditions is essential. In addition, reliable data for reference fluids should be chosen carefully in order to achieve a good determination of these parameters. For calibration purposes in a wide range of temperatures and pressure conditions, three procedures have been proposed in literature.

Lagourette et al. (1992) proposed a “classical” calibration performing measurements of oscillating period at vacuum and water to determinate densities at pressure up to 700 bar. He assumed that parameter K is only a function of temperature, and therefore it can be determinate by measuring the oscillating period of the evacuated cell at different temperatures. To obtain accurate density results according to this method, the density

of a reference fluid and the measurement of the period of this substance in the temperature and pressure range scoped should be known. Lagourette used water as reference fluid to yield the following expression:

$$\rho(P,T) = \rho_{water}(T,P) + \rho_{water}(T,1bar)\left[\frac{\tau^2(T,P) - \tau_{water}{}^2(T,P)}{\tau_{water}{}^2(T,1bar) - \tau_{vacuum}{}^2(T)}\right] \quad (2.\ 84)$$

being, τ_{water} and τ_{vacuum} the period of water and the evacuated cell, respectively.

Niesen (1989) proposed method based on the use of empirical polynomial equations which relate density and the period of oscillation (Anton Paar, 2007). A set of parameters must be adjusted using several fluids of well-known density. Finally, a third attempt to calibrate the vibrating-tube densimeters is a semi-empirical approach which takes account mechanical response of the tube. In this model, the correlation parameters obtained by fitting are related to the thermal behaviour and deformations assumptions of the tube material (Holcomb and Outcalt, 1998, Bouchot and Richon, 2001).

In addition, the viscosity of fluids might affect the volumetric measurements, and consequently a correction of the density is necessary. The viscosity influence causes an increase in density measured at both atmospheric and high pressure conditions (Ashcroft et al., 1990; Lundstrom et al., 2005, Anton Paar, 2007). This correction factor, which also depends on the design of the vibrating tube (Comuñas et al., 2008), should be included in the uncertainty of density measurements.

Vibrating-tube densimeter can operate either in dynamic mode or static mode. In the first configuration, fluid density is performed on a stream flowing along the tube. This mode allows faster density determination than static one by comparing the sample density to reference fluid (typically water) at the same temperature and pressure conditions. Hence, dynamic mode is proper when the determination of small differences in density is required, such as dilute solutions. On the other hand, in the static mode, the density measurement is carried out inside the tube without motion at temperature and pressure fixed. This mode is generally employed to measure of pure

fluids and their mixtures. Kratky (1969) was the pioneer to publish density data obtained from a vibrating tube with a permanent magnets attached to the tube and wire-coil electromagnets. His design inspired the commercially vibrating tube densimeter constructed by Anton Paar, which have been employed for PVT measurements of wide variety of fluid systems at temperature up to 200ºC.

Bouchot (1998) measured the density of several pure refrigerants between -20ºC and 150ºC up to 400 bar. This author revised the calibration method for vibrating tube densimeter, and implemented model to minimize the influence of the calibration procedure in the determination of density from measurements of the period (Bouchot, 2001). In his model the mechanical behaviour of constructing material of the tube model was taken account.

More recently, several authors have proposed methods for precise determination of fluid density using this technique. Comuñas (2008) extended the classical calibration procedure for measuring diethyl adipate density between 20 and 120ºC, up to 1400 bar by using water and decane as reference fluids. Sanmamed et al. (2010) carried out a specific calibration procedure in order to deal with the common calibration methods to determinate the high density of high viscous fluids.

2.4.2. Equation of States

Dowson and Higginson equation

This equation of state was obtained by Dowson and Higginson fitting pressure-volume data of a mineral oil up to 3500 bar at constant temperature (Dowson and Higginson, 1966). It is usually used for isothermal simulations to solve elasto-hydrodynamics lubrication for compressible liquid lubricants:

$$\frac{V}{V_0} = \frac{2K_e^* + (k_e - 1)\cdot(P - P_0)}{2K_e^* + (k_e + 1)\cdot(P - P_0)} \qquad (2.\ 85)$$

Where V and V_0 are the specific volume at constant temperature for the pressure applied P, and the pressure of reference, P_0 respectively. K^*_e is the isothermal bulk at P = 0 bar, and k_e is the pressure rate of change of isothermal bulk modulus at P = 0 bar.

In this equation, the ratio V/V_0 reaches a limit (0.74) for sufficiently high pressures, describing the liquid as incompressible, being this behaviour questionable in particular for synthetic lubricants (Ramesh, 1991). Because of this limitation, it is generally employed for describing the compressibility of lubricants at low pressure and temperatures environments (Bair, 2007).

Tait equation

The Tait equation (Tait, 1888) is by far the simplest and most accurate isothermal equation of state for modelling the PVT experimental data for materials in gas, liquid and solid state. There are several equivalent forms to express the pressure-volume-temperature relationship. In this work the Tait-Tamman equation has been used:

$$\frac{V}{V_0} = 1 - C \ln\left[\frac{B+P}{B+P_0}\right] \tag{2. 86}$$

being C a constant which have a "universal" value of 0.0894, and B is adjusting parameter. Several expressions for $B(T)$ and $V_0(T)$ has been proposed to fit high pressure specific volume. Generally, $V_0(T)$ or its inverse function, $\rho_0(T)$, is a second order polynomial function which represent the volume (or density) variation of the material under atmospheric pressure:

$$V_0(T) = \sum_{i=0}^{n} a_i \cdot T^i \tag{2. 87}$$

where a_i are adjusting coefficients. However, polynomial expression has not been the unique type of relation used in Tait-like equation of state for modelling the volume-temperature dependence at atmospheric pressure (Jianguo et al., 2011). Similarly, the function $B(T)$ is commonly expressed as a polynomial relationship as follow:

$$B(T) = \sum_{i=0}^{n} b_i \cdot T^i \tag{2. 88}$$

where b_i are adjusting parameters. In addition, more complex modified Tait-Tamman equation has been used by parameterization of C as function of temperature (Dutour et al., 2003)

Murnaghan's equation

The Murnaghan equation of state (1951) was derived from the linear theory of finite strain. This equation is based on the assumption that the bulk modulus at constant temperature is a linear function of pressure at any temperature. The isothermal volume-pressure relationship is given by the following expression:

$$\frac{V}{V_0(T)} = \left[1 + \frac{k_e^* P}{K_e}\right]^{-1/k_e} \tag{2. 89}$$

According to the Murnaghan equation, the evolution of the bulk modulus of the entire volume, K_e, with pressure follows a linear relationship as follow:

$$K_e(P) = K_e^* + k_e P \tag{2. 90}$$

where k_e is an empirical constant, the Bridgman constant, that implies a linear dependence of the bulk modulus with pressure, and K_e represents the temperature dependence of the bulk modulus of the entire volume.

The Murnaghan equation can be used in a wider pressure range than original Tait's equation, particularly for materials in solid state as has been pointed out by MacDonald (1966). However, the application of both empirical equations is limited at high pressures and low temperatures since they do not account for transitions, such as freezing, glass transition or polymorphic changes. Similarly Tait equation, the range of application of Murnaghan equation can be improved by introducing a thermal dependence for both K_e and V_o. In this sense, Moonan and Tschoegl (1983) used an equation for the bulk modulus as function of temperature in order to model PVT behaviour of three polymers between 25 and 100ºC up to 1600 bar.

$$K_e(T) = K^*{}_e \exp(-\lambda(T - T_0)) \tag{2. 91}$$

Where K_e^* is the bulk modulus at zero pressure and the temperature of reference (T_0), λ is a parameter which defines the temperature dependence of the bulk modulus, K_e, at any given pressure. Further, this constant, $\lambda = m\alpha_e$, with m an empirical constant and α_e the thermal expansivity for the entire volume. More recently, Martin-Alfonso and Martinez-Boza (2011) modelled satisfactorily the volumetric behaviour of fuel oils from -35 to 50ºC up to 1000 bar by introducing a polynomial expression for V_o (T) in Murnaghan equation.

2.5. References

Bergaya, F.; Theng, B.K.G.; Lagaly, G. **2006**. Handbook of Clay Science. First Ed. Elsevier, Amsterdam.

Murray, H.H. **2007**. Applied Clay Mineralogy. Occurrences, Processing and Application of Kaolins, Bentonites, Palygorskite-Sepiolite and Common Clays. First Ed. Elsevier, Amsterdam.

Hofmann, U.; Endell, K.; Wilm, O. **1933**. Kristallstructur und Quellung von Montmorillonit. *Z. Krist.* 86, 340-348.

Marshall, C.E. **1935**. Layer Lattices and Base Exchange Clays. *Z. Krist.* 91, 433-449.

Van Olphen, H. **1977**. An Introduction to Clay Colloid Chemistry. Second Ed. John Wiley & Sons, New York.

Caenn, R.; Darley, H.C.H.; Gray, G.R. **2011**. Composition and Properties of Drilling and Completion Fluids. Sixth Ed. Gulf Professional Publishing, Waltham.

Bradley, W.F. The Structural Scheme of Attapulgite. **1940**. *Am. Mineralogist.* 25, 405-410.

Grim, R.E.; Bray, R.H.; Bradley, W.F. **1937**. The mica in argillaceous sediments. *Amer. Mineral.* 22, 813-829.

Norrish, K. The Swelling of Montmorillonite. **1954**. *Disc. Faraday Soc*. 18, 120-134.

Swartzen-Allen, S.L.; Matijevic, E. **1974**. Surface and colloid chemistry of clays. *Chem. Rev.* 74, 385-400.

Hunter, R.J. Foundations of Colloid Science. **2001**. Oxford Univ. Press. Second Ed. New York.

Anderson, R.L.; Ratcliffe, I.; Greenwell, H.C.; Williams, P.A.; Cliffe, S.; Coveney, P.V. **2010**. Clay swelling – A challenge in the oilfield. *Earth-Sci. Rev.* 98, 201-216.

Chen, S.; Low, P.F.; Cushman, J.H.; Roth, C.B. **1987**. Organic compound effects on swelling and flocculation of Upton montmorillonite. *Soil Sci. Soc. Am. J.* 51, 1444-1450.

Boek, E.S.; Coveney, P.V.; Skipper, N.T. **1995**. Monte Carlo Molecular Modeling Studies of Hydrated Li-, Na- and 1K-Smectites: Understanding the Role of Potassium as a Clay Swelling Inhibitor. *J. Am. Chem. Soc*. 117, 12608-12617.

Chávez-Páez, M.; van Workum, K.; de Pablo, L.; de Pablo, J.J. **2001**. Monte Carlo simulations of Wyoming sodium montmorillonite hidrates. *J. Chem. Phys.* 114, 1405-1413.

Hensen, E.J.M.; Smit, B. **2002**. Why clays swell. *J. Phys. Chem. B* 106, 12664-12667.

Denis, J.H.; Keall, M.J.; Hall, P.L.; Meeten, G.H. **1991**. Influence of potassium concentration on the swelling and compactation of mixed (Na, K) ion-exchanged montmorillonite. *Clay Miner.* 26, 255-268.

Fukushima, Y. **1984**. X-ray Diffraction Study of Aqueous Montmorillonite Emulsions. *Clays Clay Miner.* 32, 4, 320-326.

Luckham, P.F.; Rossi, S. The colloidal and rheological properties of bentonite suspensions. **1999**. *Adv. Colloid Interface Sci.* 82, 43-92.

Van Olphen, H.J. **1964**. Internal mutual flocculation in clay supensions. *J. Coll. Interf. Sci.* 19, 313-322.

M´Ewen, M.B.; Pratt, M.I. **1957**. The gelation of montmorillonite, I. The formation of a structural framework in soils of Wyoming bentonite. *Trans. Faraday Soc.* 53, 535-547.

Leonard, R.A.; Low, P.F. **1961**. Effect of gelation on the properties of water in clay systems. *Clays Clay Miner.* 10, 311-325.

Norrish, K.; Rausell-Colom, J.A. **1963**. Low-angle X-ray diffraction studies of the swelling of montmorillonite and vermiculite. *Clays Clay Miner.* 10, 123-149.

Tombácz, E.; Szekeres, M. **2004**. Colloidal behaviour of aqueous montmorillonite suspensions: the specific role of pH in the presence of indifferent electrolytes. *Appl. Clay. Sci.* 27, 75-94.

Kretzschmar, R.; Holthoff, H.; Sticher, H. **1998**. Influence of pH and humic acid on coagulation kinetics of Kaolinite: A dynamic light scattering study. *J. Colloid Interface Sci.* 202, 95-103.

Baik, M.H.; Lee, S.Y. **2010**. Colloidal stability of bentonite clay considering surface charge properties as a function of pH and ionic strength. *J. Ind. Eng. Chem.* 16, 837-841.

Jones, T.R. **1983**. The properties and uses of clays which swell in organic solvents. *Clay Miner*.18, 399-410.

King Jr., H.E.; Milner, S.T.; Lin, M.Y.; Singh, J.P.; Mason, T.G. **2007**. Structure and rheology of organoclay suspensions. *Phys. Rev. E* 75, 2.

Hauser, E.A. **1950**. Modified gel-forming clay and process of producing same. U.S. Patent No. 2.531.427.

de Paiva, L.B.; Morales, A.R.; Valenzuela Díaz, F.R. **2008**. Organoclays: Properties, preparation and applications. *Appl. Clay Sci.* 42, 8-24.

Moraru, V.N. **2001**. Structure formation of alkylammonium montmorillonites in organic media. *Appl. Clay Sci.* 19, 11-26.

Gherardi, B.; Tahani, A.; Levitz, P.; Bergaya, F. **1996**. Sol/gel phase diagrams of industrial organo-bentones in organic media. *Appl. Clay Sci.*11, 163-170.

Burgentzlé, D.; Duchet, J.; Gérard, J.F.; Jupin, A.; Fillon, B. **2004**. Solvent-based nanocomposite coatings I. Dispersion of organophilic montmorillonite in organic solvents. *J. Colloid Interface Sci.* 278, 26-39.

Le Pluart, L.; Duchet, J.; Sautereau, H.; Halley, P.; Gerard, J.-F. **2004**. Rheological properties of organoclay suspensions in epoxy network precursors. *Appl. Clay Sci.* 25, 207-219.

Macosko, C.W. **1994**. Rheology, principles, measurements and applications. First Ed. Wiley-VCH Publishers Inc., New York.

Caenn, R.; Chillingar, G.V. **1996**. Drilling fluids: State of the art. *J. Pet. Sci. Eng.* 14, 221-230.

Lyons, W.C. **2010**. Working Guide to Drilling Equipment and Operations. First Ed. Gulf Professional Publishing, Burlington.

Hermoso, J.; Martínez-Boza, F.; Gallegos, C. **2014**. Influence of viscosity modifier nature and concentration on the viscous flow behaviour of oil-based drilling fluids at high pressure. *Appl. Clay Sci.* 87, 14-21.

Friedheim, J.E. **1997**. Second-generation synthetic drilling fluids. *J. Pet. Technol.* 49, 724-728.

Apaleke, A.S.; Al-Majed, A.; Hossain, M.E. **2012**. Drilling fluid: State of the art and future trend. Technical Conference and Exhibition 2012. 1, 101-113.

Totten, G.E.; Westbrook, S.R.; Shah, R.J. **2003**. Fuels and Lubricants Handbook: Technology, properties, performance and testing. First Ed. G.E. Totten & Associates, LLC, Seattle.

Lansdown, A.R. **2004**. Lubrication and lubricant selection: A practical guide. Third Ed. Professional Engineering Publishing ASME Press.

Mortier, R.; Fox, M.F.; Orszulik, S.T. **2010.** Chemistry and Technology of Lubricants. Third Ed. Springer, Heidelberg.

Growcock, F.; Harvey, T. **2005**. Drilling Fluids Processing Handbook. Drilling Fluids. First Ed. Gulf Professional Publishing, Burlington.

Tovar, J.; Rodríguez, Z.; Quiroga, F.; Greaves, R.; Meléndez, H.; Arocha, J.; Bland, R.; Hebert, M. **1999**. Orimatita. An improved hematite for drilling fluids. Latin American and Caribbean Petroleum Engineering Conference. SPE 53939.

Kogel, J.E.; Trivedi, N.C.; Barker, J.M.; Krulowski, S.T. **2006**. Industrial Minerals & Rocks: Commodities, Markets and Uses. Seventh Ed. Society for Mining, Metallurgy and Exploration.

Mallory, H.E.; Holman, W.E.; Duran, R.J. **1960**. Low-solids mud resists contamination. *Petrol Eng.* B 25-30.

Deily, F.H.; Holman, W.E.; Lindblom, G.P.; Patton, J.T. **1967**. New biopolymer low-solids mud speeds drilling operation. *Oil Gas J.* 65, 62-70.

Kaveler, H.H. **1946**. Improved drilling muds containing carboxymethylcellulose. *API Drill. Prod. Prac.* 43-50.

Turner, T.; Nahm, J.W. **1973**. Drilling fluids. 19U.S. Patent No. 3.766.229.

Schramm, L.L.; Stasiuk, E.N.; Marangoni, D.G. **2003**. Surfactants and their applications. *Annu. Rep. Prog. Chem. Sect.* 99, 3-48.

Malkin, A.Y.; Isayev, A.I. **2006**. Rheology: Concepts, Methods and Applications. First Ed. ChemTec Publishing, Toronto.

Dealy, J.M. **1982**. Rheometer for molten plastics: A practical guide to testing and property measurement. First Ed.Van Nostrand , New York.

Schramm, G. **1994**. A Practical Approach to Rheology and Rheometry. Second Ed. Gebrueder Haake GmbH, Karlsruhe.

Reiner, M. **1969**. Deformation, Strain and Flow: An Elementary Introduction to Rheology. Third Ed. H.K. Lewis, London.

Barnes, H.A. **1989a**. Shear-thickening ("Dilatancy") in suspensions of non-aggregating solid particles dispersed in Newtonian liquids. *J. Rheol.* 33, 329-366.

Boersma, J.F.; Levan, J.; Stein, H.N. **1990**. Shear-thickening (Dilatancy) in concentrated suspensions. *AIChE J.* 36, 321-332.

Coussot, P. **2005**. Rheometry of Pastes, Suspensions, and Granular Materials. Application in Industry and Environment. First Ed. John Wiley & Sons, Inc. Publication, New Jersey.

Barnes, H.A.; Walters, K. **1985**. The yield stress myth?. *Rheol. Acta* 24, 323-336.

Møller, P.C.F.; Fall, A.; Bonn, D. **2009**. Origin of apparent viscosity in yield stress fluids below yielding. *EPL* 87, 38004-p1 - 38004-p6.

Malkin, A.Y. **2013**. Non-Newtonian viscosity in steady-state shear flows. *J. Non-Newtonian Fluid Mech.* 192, 48-65.

Johnson, R.W. **1998**. The Handbook of Fluid Dynamics. CRC Press LLC Boca Raton.

Mewis, J.; Wagner, N.J. **2009**. Thixotropy. *Adv. Colloid Interface Sci.* 147-148, 214-227.

Goodeve, C.F. **1939**. A general theory of thixotropy and viscosity. Trans. Faraday Soc. 35, 342-358.

Green, H.; Weltmann, R. N. **1943**. Analysis of thixotropy of pigment-vehicle suspensions – Basic principles of the hysteresis loop. *Ind. Chem. An. Ed.* 15, 201-206.

Kanai, H.; Amari, T. **1995**. Negative thixotropy in ferric-oxide suspensions. *Rheol. Acta* 34, 303-310.

Barnes, H.A. **1997**. Thixotropy – A review. J. Non-Newtonian Fluid Mech. 70, 1 – 33.

Ferry, J.D. **1980**. Viscoelastic Properties of Polymers. Third Ed. John Wiley & Sons, New York.

Darby, R. **1976**. Viscoelastic Fluids: An Introduction to Their Properties and Behaviour. First Ed. Marcel Dekker, Inc. New York.

Rossi, S.; Luckham, P.F.; Tadros, Th.F. **2002**. Influence of non-ionic polymers on the rheological behavior of Na+-montmorillonite clay suspensions–I Nonyphenol–polypropylene oxide–polyethylene oxide copolymers. *Colloids Surf., A* 201, 85-100.

Kelessidis, V.C.; Papanicolau, C.; Foscolos, A. **2009**. Application of Greek lignite as an additive for controlling rheological and filtration properties of water-bentonite suspensions at high temperatures: A review. *Int. J. Coal Geol.* 77, 394-400.

Herzhaft, B.; Rosseau, L.; Neau, L.; Moan, M.; Bossard, F. **2003**. Influence of temperature and clay/emulsion microstructure on oil-based mud low shear rate rheology. *SPE J.* 8, 211-217.

Bair, S. **2007**. High Pressure Rheology for Quantitative Elastohydrodynamics, First Ed. Elsevier BV, Oxford.

Tschoegl, N.W.; Knauss, W.G.; Emri, I. **2002**. The effect of temperature and pressure on the mechanical properties of thermo-and/or piezorheologically simple polymeric materials in thermodynamic equilibrium – A critical review. *Mech. Time-Depend. Mater*. 6, 53-99.

Gallegos, C.; Walters, K. **2010**. Encyclopedia of Life Support Systems. Rheology - Vol. I. First Ed. EOLSS Publishers/UNESCO.

Warburg, E.; Sachs, J. **1884**. The Effect of Density on the Viscosity of Liquids. Wiedmanns Annalen., 22, 518-522.

Novak, J.D.; Winer, W.O. **1968**. Some measurements of high pressure lubricants rheology. *J. Lubr. Technol.* 90, 580-591.

Galvin, G.D.; Hutton, J.F.; Jones, B. **1981**. Development of a high-pressure, high-shear-rate capillary viscometer. *J. Non-Newtonian Fluid Mech.* 8, 11-28.

Song, B.Y.; Yang, Q.X.; Qi, Y.L.; Su, D.Z. **2011**. The mechanochemistry of synthetic phosphate oil under high pressure. *Key Eng. Mater.* 450, 185-188.

Bridgman, P.W. **1925**. The effect of pressure on the viscosity of forty-three pure liquids. *Proc. Am. Acad. Arts Sci.* 61, 57-99.

Briscoe, B.J.; Luckham, P.F.; Ren, S.R. **1992a**. The falling of spheres through Bingham fluids. *Colloids Surf.* 65, 69-75.

Briscoe, B.J.; Luckham, P.F.; Ren, S.R. **1992b**. An assessment of a novel rolling-ball rheometer for studying non-Newtonian fluids. *Colloids Surf.* 62, 153-162.

Schurz, J. **1990**. The yield stress – An empirical reality. *Rheol. Acta* 29, 170-171.

Briscoe, B.J.; Luckham, P.F.; Ren, S.R. **1994**. The properties of drilling fluids at high pressures and high temperatures. *Philos. T. Roy. Soc. A* 348, 179-207.

Eguchi, Y.; Karino, T. **2008**. Measurement of rheologic property of blood by falling-ball blood viscometer. *Ann. Biomed. Eng.* 36, 545-553.

Sawamura, S.; Takeuchi, N.; Kitamura, K.; Taniguchi, Y. **1990**. High pressure rolling-ball viscometer of a corrosion-resistant type. *Rev. Sci. Instrum.* 61, 871-873.

Izuchi, M.; Nishibata, K. **1986**. A high pressure rolling-ball viscometer up to 1GPa. *J. Appl. Phys.* 25, 1091-1096.

Calvignac, B.; Rodier, E.; Letourneau, J-J.; Vitoux, P.; Aymonier, C.; Fages, J. **2010**. Development of an improved falling ball viscometer for high-pressure measurements with supercritical CO_2. *J. Supercrit. Fluids* 55, 95-106.

Thomas, B.W.; Ham, W.R.; Dow, R.W. **1939**. Viscosity-pressure characteristics of lubricating oils. *Ind. Eng. Chem.* 31, 1267-1270.

Hutton, J.F.; Phillips, M.C. 1973. High pressure viscosity of a polyphenyl ether measured with a new couette viscometer. *Nature Phys. Sci.* 245, 15-16.

Barus, C. 1893. Isothermals, isopiestics and isometrics relative to viscosity. Am. J. Sci. 45, 87-96.

Lamb, J. **1977**. Viscoelasticity and lubrication: A review of liquids properties. *J. Rheol.* 22, 317-347.

Sargent, L.B. **1983**. Pressure-viscosity coefficients of liquid lubricants. *A.S.L.E. Trans.* 26, 1-10.

Andrade, E.N. **1930**. The viscosity of liquids. *Nature*, 125, 309-310.

Williams, M.L.; Landel, R.F.; Ferry, J.D. **1955**. The temperature dependence of relaxation mechanism in amorphous polymers and other glass-forming liquids. *J. Amer. Chem. Soc.* 77, 3701-3707.

Doolittle, A.K.; Doolitle, D.B. **1957**. Studies in Newtonian flow. Further verification of the three-space viscosity equation. *J. Appl. Phys.* 28, 901-905.

Rouse, P.E. **1953**. A theory of the linear viscoelastic properties of dilute solutions of coiling polymers. *J. Chem. Phys.* 21, 1272-1280.

Ferry, J.D.; Stratton, R.A. **1960**. The free volume interpretation of the dependence of viscosities and viscoelastic relaxation times on concentration, pressure, and tensile strain. *Kolloid-Z.* 171, 107-111.

O´Reilly, J.M. **1962**. The effect of pressure on glass temperature and dielectric relaxation time of polyvinyl acetate. *J. Polym. Sci.* 57, 429-444.

Tait, P.G. **1888**. Report on some of the physical properties of fresh water and sea water. *Phys. Chem.* 2, 1-76.

Fillers, R.W.; Tschoegl, N.W. **1977**. The effect of pressure on the mechanical properties of polymers. *Trans. Soc. Rheol.* 21, 51-100.

Moonan, W.K.; Tschoegl, N.W. **1985**. The effect of pressure on the mechanical properties of polymers. IV. Measurements in torsion. *J. Polym. Sci. Polym. Phys. Ed.* 23, 623-651.

Martin-Alfonso, M.J.; Martinez-Boza, F.J.; Navarro, F.J.; Fernández, M.; Gallegos, C. **2007**. Pressure-temperature-viscosity relationship for heavy petroleum fractions. *Fuel* 86, 227-233.

Yasutomi, S.; Bair, S.; Winer, W. **1984**. An application of a free volume model to lubricant rheology. *ASME J. Tribol.* 106, 291-303.

Breuer, H.; Rehage, G. **1967**. Zur thermodynamic der glasigen erstarrung. *Kolloid-Zeitschrift & Zeitschrift für Polymere*. 216-217, 159-179.

Bair, S. **2001**. The high-pressure, high-shear stress rheology of polybutene. *J. Non-Newtonian Fluid Mech.*97, 53-65.

Bair, S.; Mary, C.; Bouscharain, N.; Vergne, P. **2013**. An improved Yasutomi correlation for viscosity at high pressure. *Proc. Inst. Mech. Eng.* 227, 1056-1060.

Quiñones-Cisneros, S.E.; Zéberg-Mikkelsen, C.K.; Stenby, E.H. **2000**. The friction theory (*f-theory*) for viscosity modelling. *Fluid Phase Equilib.* 169, 249-276.

Soave, G. **1972**. Equilibrium constants from a modified Redlich-Kwong equation of state. *Chem. Eng. Sci.* 27, 1197-1203.

Stryjek, R.; Vera, J.H. **1986**. PRSV: An improved Peng-Robinson equation of state for pure compounds and mixtures. *Can. J. Chem. Eng.* 64, 323-333.

Quiñones-Cisneros, S.E.; Deiters, U.K. **2006**. Generalization of the theory for viscosity modeling. *J. Phys. Chem. B* 110, 12820-12834.

Quiñones-Cisneros, S.E.; Schmidt, K.A.G.; Creek, J.; Deiters, U.K. **2008**. Friction theory modeling of the non-Newtonian viscosity of crude oils. *Energy Fuels* 22, 799-804.

Einstein, A. **1906**. Eine neue bestimmung der moleküldimensionen. *Ann. Phys.* 19, 289-306.

Batchelor, G.K.; Green, J.T. **1972**. The determination of the bulk stress in a suspension of spherical particles to order c^2. *J. Fluid Mech.* 56, 401-427.

Wagner, N.J.; Woutersen, T.J.M. **1994**. The viscosity of bimodal and polydisperse suspensions of hard spheres in the dilute limit. *J. Fluid Mech.* 278, 267-287.

Qi, F.; Tanner, R.I. **2012**. Random close packing and relative viscosity of multimodal suspensions. *Rheol. Acta* 51, 289-302.

Barnes, H.A.; Hutton, J.F.; Walters, K. **1989b**. An Introduction to Rheology. First Ed. Elsevier Science Publishers B.V. Amsterdam.

Krieger, I.M. **1972**. Rheology of monodisperse lattices. *Adv. Colloid Interface Sci.* 3, 111-136.

Zarraga, I.E.; Hill, D.A.; Leighton, D.T. **2000**. The characterization of the total stress of concentrated suspensions of non-colloidal spheres in Newtonian fluids. *J. Rheol.* 44, 185-200.

Kim, C.J.; Sondergeld, K.; Mazurowski, M.; Gallei, M.; Rehahn, M.; Spehr, T.; Frielinghaus, H.; Stühn, B. **2013**. Synthesis and characterization of polystyrene chains on the surface of silica nanoparticles: comparison of SANS, SAXS, and DLS results. *Colloid. Polym. Sci.* 291, 2087-2099.

Stiger, M.; Pedersen, J.S.; Lindner, P.; Ritchtering, W. **2004**. Are thermoresponsive microgels model systems for concentrated colloidal suspensions? A rheology and small-angle-neutron scattering study. *Langmuir* 20, 7283-7292.

Mewis, J.; Frith, W.J.; Strivens, T.A.; Russel, W.B. **1989**. Rheology of suspensions containing polymerically stabilized particles. *AIChE J.* 35, 415-422.

Ogawa, A.; Yamada, H.; Matsuda, S.; Okajima, K.; Doi, M. **1997**. Viscosity equation for concentrated suspensions of charged colloidal particles. *J. Rheol.* 41, 769-785.

Buscall, R. **1991**. Effect of long-range repulsive forces on the viscosity of concentrated lattices: comparison of experimental data with an effective hard-sphere model. *J. Chem. Soc. Faraday Trans.* 87, 1365-1370.

Raynaud, L.; Ernst, B.; Vergé, C.; Mewis, J. **1996**. Rheology of aqueous lattices with adsorbed stabilizer layers. *J. Colloid Interface Sci.* 181, 9-11.

Maranzano, B.J.; Wagner, N.J. **2000**. Thermodynamic properties and rheology of sterically stabilized colloidal dispersion. *Rheol. Acta* 39, 483-494.

Mandelbrot, B.B. **1975**. Les Objects fractals: Hasard et dimension.

Tolpekin, V.A. Duits, M.H.G.; van den Ende, D.; Mellema, J. **2004**. Aggregation and breakup of colloidal particle aggregates in shear flow, studied with video microscopy. *Langmuir*, 20, 2614-2617.

Varadan, P.; Solomon, M.J. **2001**. Shear-induced microstructural evolution of a thermoreversible colloidal gel. *Langmuir* 17, 2918-2929.

Vermant, J.; Solomon, M.J. **2005**. Flow-induced structure in colloidal suspensions. *J. Phys.: Condens. Matter* 17, 187-216.

Poon, W.C.K.; Haw, M.D. **1997**. Mesoscopic structure formation in colloidal aggregates and gelation. *Adv.Colloid Interface Sci.* 73, 71-126.

Cichocki, B.; Felderhof, B.U. **1990**. Diffusion coefficients and effective viscosity of suspensions of sticky spheres with hydrodynamic interactions. *J Chem. Phys.* 93, 4427-4432.

Krishnamurthy, L.N.; Wagner, N.J. **2005**. The influence of weak attractive forces on the microstructure and rheology of colloidal dispersions. *J. Rheol.* 49, 475-499.

Trappe, V.; Sandkühler, P. **2004**. Colloid gels: Low density disordered solid-like states. *Curr. Opinion Colloid Interf. Sci.* 8, 494-500.

de Gennes, P.G. **1980**. Scaling Concepts in Polymers Physics. First Ed. Cornell University Press. New York.

Feng, S.; Sen, P. **1984**. Percolation on elastic networks: new exponent and threshold. *Phys. Rev. Lett*. 52, 1891-1894.

Zhongying, W.; Songran, T. **1986**. The flow effect of mud in annulus and the selection of rheological parameters. International Meeting on Petroleum Engineering, 1986 Beijing.

API Recommended Practice 13D. Rheology and hydraulics of oil-well drilling fluids. **2009**.

API Specification 13A. Specification for drilling-fluids materials. **2008**.

Abend, S.; Lagaly, G. **2000**. Sol-gel transitions of sodium montmorillonite dispersions. *Appl. Clay Sci.* 16, 201-227.

Mahto, V.; Sharma, V.P. **2004**. Rheological study of a water based oil well drilling fluid. *J. Pet. Sci. Eng.* 45, 123-128.

Yildiz, N.; Sarikaya, Y.; Çalimli, A. **1999**. The effect of the electrolyte concentration and pH on the rheological properties of the original and the Na_2CO_3-activated Kütahya bentonite. *Appl. Clay Sci.* 14, 319-327.

Vali, H.; Bachmann, L. **1988**. Ultrastructure and flow behavior of colloidal smectite dispersions. *J. Coll. Interf. Sci.* 126, 278-291.

Abu-Jdayil, B. **2011**. Rheology of sodium and calcium bentonite-water dispersions: Effect of electrolytes and aging time. *Int. J. Miner. Process*. 98, 208-213.

Kelessidis, V.C.; Tsamantaki, C.; Dalamarinis, P. **2007**. Effect of pH and electrolytes on the rheology of aqueous Wyoming bentonite dispersions. *Appl. Clay Sci.* 38, 86-96.

Tarchitzky, J.; Chen, Y. **2002**. Rheology of sodium-montmorillonite suspensions: Effects of humic substances and pH. *Soil Sci. Soc. Am. J.*66, 406-412.

M´Bodj, O.; Ayadi, M.; Benna, M.; Ariguib, N.K.; Trabelsi Ayadi, M. **2003**. Characterization and rheological study of a Tunisian bentonite for its use in the drilling fluids. *Asian J. Chem.* 15, 1251-1265.

Sohm, R. Tadros, Th.F. **1989**. Viscoelastic properties of sodium montmorillonite (Gelwhite H) suspensions. *J. Colloid Interf. Sci.* 132, 62-71.

Khandal, R.K.; Tadros, Th. F. **1988**. Application of viscoelastic measurements to the investigation of the swelling of sodium montmorillonite suspensions. *J. Colloid Interface Sci.* 125, 122-128.

Duran, J.D.G.; Ramos-Tejada, M.M.; Arroyo, F.J.; Gonzalez-Caballero, F. **2000**. Rheological and Electrokinetic properties of sodium montmorillonite suspensions. I.

Rheological properties and interparticle energy of interaction. *J. Colloid Interface Sci.*229, 107-117.

Paineau, E.; Michot, L.J.; Bihannic, I.; Baravian, C. **2011**. Aqueous suspensions of natural swelling clay minerals. 2. Rheological characterization. *Langmuir*. 27, 7806-7819.

Znou, Y.; Shah, S.N. **2004**. Rheological properties and frictional pressure loss of drilling, completion and stimulation fluids in coiled tubing. J. Fluid Eng. Eng-T. ASME 126, 153-161.

Hamed, S.B.; Belhadri, M. **2010**. A comparison between two biopolymers used in drilling muds. *Pet. Sci. Technol.* 28, 723-730.

Khalil, M.; Jan, B.M. **2011**. Herschel-Bulkley rheological parameters of a novel environmentally friendly lightweight biopolymer drilling fluid xanthan gum and starch. *J. Appl. Polym. Sci.* 124, 595-606.

Kelessidis, V.C.; Poulakakis, E.; Chatzistamou, V. **2011**. Use of Carbopol 980 and carboxymethyl cellulose polymers as rheology modifiers of sodium-bentonite water dispersions. *Appl. Clay Sci.* 54, 63-69.

Benyounes, K.; Mellak, A.; Benchabane, A. **2010**. The effect of carboxymethylcellulose and xanthan gum on the rheology of bentonite suspensions. *Energy Sources, Part A* 32, 1634-1643.

Benchabane, A.; Bekkour, K. **2006**. Effects of anionic additives on the rheological behaviour of aqueous calcium montmorillonite suspensions. *Rheol. Acta* 45, 425-436.

Kelessidis, V.C.; Chatzistamou, V. **2013**. Optimization of drilling fluid rheological and fluid loss properties utilizing PHPA polymer. 18th Middle East Oil & Gas Show and Conference, 2013 Baharain.

Mostafa, B.A.; Assaad, F.F. **2007**. Efficiency of Egyptian drilling muds in the presence of cationic polyethylene imine and anionic polyacrylamide. *J. Appl. Polym. Sci* . 104, 1487-1495.

Schmidt, D.D.; Cline, J.T. **1987**. Interaction of water with organophilic clay in base oils to build viscosity. SPE Annual Technical Conference and Exhibition, 1987 Dallas.

Zhong, Y.; Wang, S-Q. **2003**. Exfoliation and yield behaviour in nanodispersions of organically modified montmorillonite clay. *J. Rheol.* 47, 483-495.

Minase, M.; Kondo, M.; Onikata, M.; Kawamura, K. **2008**. The viscosity of organic liquid suspensions of trimethyldococylammonium-montmorillonite complexes. *Clays Clay Miner*. 56, 49-65.

Hato, M.J.; Zhang, K.; Ray, S.S.; Choi, H.J. **2011**. Rheology of organoclay suspension. *Colloid Polym. Sci.* 289, 1119 - 1125.

Zhang, L-M.; Jahns, C.; Hsiao, B.S.; Chu, B. 2003. Synchrotron SAXS/WAXD and rheological studies of clay suspensions in silicone fluid. *J. Colloid Interface Sci.* 266, 339-345.

Ghalambor, A.; Ashrafizadeh, S.N.; Nasiri, M. **2008**. Effect of basic parameters on the viscosity of synthetic-based drilling fluids, SPE International Symposium on Formation Damage Control, 2008, Lafayette.

Bhatt, J.; Somani, R.S.; Hares, M.M.; Bajaj, H.C. **2013**. Rheological study of organoclays prepared from Indian bentonite: Effect of dispersing methods. *Appl. Clay Sci*.83-84, 106-114.

Sobish, T.; Lerche, D. **2000**. Application of a new separation analyser for the characterization of dispersions stabilized with clay derivates. *Colloid Polym. Sci.* 278, 369-374.

Binks, B.P.; Clint, J.H.; Whitby, C.P. **2005**. Rheological behaviour of water-in-oil emulsions stabilized by hydrophobic bentonite particles. *Langmuir*. 21, 5307-5316.

Akkal, R.; Cohaut, N.; Khodja, M.; Ahmed-Zaid, T.; Bergaya, F. **2013**. Rheo-SAXS investigation of organoclay water in oil emulsions. *Colloids Surf., A* 436, 751-762.

Shu, R.; Sun, W.; Wang, T.; Wang, C.; Liu, X.; Tong, Z. 2013. Linear and nonlinear viscoelasticity of water-in-oil emulsions. Effect of droplet elasticity. *Colloids Surf., A* 434, 220-228.

Hiller, K.H., **1963**. Rheological measurements of clay suspensions at high temperatures and pressures. *J. Petrol. Technol.* 15, 779-788.

Annis, M.R. **1967**. High temperature properties of water-base drilling fluids. *J. Petrol. Technol.* 228, 779-789.

Combs, G.D.; Whitmire, L.D. **1960**. Capillary Viscometer Simulates Bottom-Hole Conditions . *Oil Gas J.* 108 - 113.

De Wolfe, R.C.; Coffin, G.B.; Byrd, R.V. **1983**. Effects of temperature and pressure on rheology of less toxic oil muds. Offshore Europe Conference 1983, Aberdeen.

Politte, M.D. **1985**. Invert Oil Mud Rheology as a Function of Temperature and Pressure, SPE/IADC Drilling Conference, 1985, New Orleans.

Houwen, O.H.; Geehan, T. **1986**. Rheology of Oil-Base Muds. SPE Annual Technical Conference and Exhibition, 1986, New Orleans.

Alderman, N.J.; Gavignet, A.; Guillot, D.; Maitland, G.C. **1988**. High-temperature, high-pressure rheology of water based muds. *SPE J.* 18035, 187 - 195.

Herzhaft, B.; Peysson, Y.; Isambourg, P.; Delepoulle, A.; Toure, A. **2001**. Rheological properties of drilling muds in deep offshore conditions. SPE/IADC Drilling Conference, 7p.

Gandelman, R.A.; Leal, R.A.F.; Gonçalves Aragão, A.F.; Lomba, R.F.; Martins, A.L. **2007**. Study on gelation and freezing phenomena of synthetic drilling fluids in ultradeepwater environments. SPE/IADC Drilling Conference, Amsterdam.

Harris, O.O.; Osisanya, S.O. **2005**. Evaluation of equivalent circulating density of drilling fluids under high-pressure high-temperature conditions. SPE Annual Technical Conference Exhibition, 2005, Texas.

Nelemans, A.; Hovland, S.; Haukland, B.; Rosbak, A.I. **2012**. Extreme fast track: Combined subsea HPHT horizontal production and exploration well. IADC/SPE Asia Pacific Drilling Technology Conference and Exhibition, 2012, Taijin.

McMordie, W.C. Jr.; Bland, R.G.; Hauser, J.M.; **1982**. Effect of Temperature and Pressure on the Density of Drilling Fluids. SPE Annual Technical Conference and Exhibition, 1982, New Orleans.

Sorelle, R.R.; Jardiolin, R.; Buckley, P. Barrios, J.R. **1982**. Mathematical field model predicts downhole density changes in static drilling fluids. SPE Annual Technical Conference and Exhibition, 1982, New Orleans.

Kutasov, I.M. **1988**. Empirical correlation determines downhole mud density. *Oil Gas J.* 86, 61-63.

Hemprill, T.; Isambourg, P. **2005**. New model predicts oil synthetic mud densities. *Oil Gas J.* 103, 56-58.

Demirdal, B.; Miska, S.; Takach, N.; Cunha, J.C. **2007**. Drilling fluids rheological and volumetric characterization under downhole conditions. Proceedings of the SPE Latin America and Caribbean Petroleum Engineering Conference, 2007, Buenos Aires.

Demirdal, B.; Cunha, J.C. **2009**. Olefin-based synthetic-drilling-fluids volumetric behavior under downhole conditions. *SPE Drill. Completion* 24, 239-248.

Hoberock, L.L.; Thomas, D.C.; Nickens, H.V. **1982**. Bottom-Hole Mud Pressure Variations due to Compressibility and Temperature Effects. IADC Drilling Technology Conference, 1982, Houston.

Peters, E.J.; Chenevert, M. E.; Zhang, C. **1990**. A model for prediction the density of oil-based muds at high pressures and temperatures. *SPE Drill Eng.* 5, 141-148.

Bridgman, P.W. **1931**. The volume of eighteen liquids as a function of pressure and temperature. *Proc. Am. Acad. Arts Sci.* 66, 185-233.

Mopsik, F.I. **1967**. Dielectric constant of n-hexane as a function of temperature, pressure and density. *J. Res. NBS Sect. A.* 71, 287-292.

Yokayama, H.; Uematsu, M. **2003**. Thermodynamic properties of {$x$$CH_3OH$ + (1-x)H_2O} at x = (1.0000, 0.8005, 0.4002 and 0.2034) in the temperature range from 320 K to 420 K at pressures up to 200 MPa. *J. Chem. Thermodyn.* 35, 813-823.

Sugiyama, T.; Orita, S.; Miyamoto, H. **2011**. (p, ρ, T, x) properties for CO2/n-butane binary mixtures at T= (280 to 440) K and (3 to 200) MPa. *J. Chem. Thermodyn.* 43, 645-650.

Dix, M.; Fareleira, J.M.N.A. Takaishi, Y.; Wakeham, W.A. **1991**. A vibrating-wire densimeter for measurements in fluids at high pressures.. *Int. J. Thermophys.* 12, 357-370.

Pádua, A.A.H.; Faraleira, J.N.M.A.; Calado, J.C.G.; Wakeham, W.A. **1994**. A vibrating-wire tube densimeter for liquids at high pressures: The density of 2,2,4-trymethylpentane from 298.15 to 348015K and up to 100MPa. *Int. J. Thermophys*.15, 229-243.

Gourgouillon, D.; Avelino, H.M.N.T.; Faraleira, J.M.N.A.; Nunes da Ponte, M. **1998**. Simultaneous viscosity and density measurement of supercritical CO2-satured PEG 400. *J. Supercrit. Fluids* 13, 177-185.

Audonnet, F.; Pádua, A.H. **2001**. Simultaneous measurement of density and viscosity of n-pentane from 298 to 383K and up to 100MPa using a vibrating-wire instrument. *Fluid Phase Equilib.*181, 147-161.

Seibt, D.; Herrmann, E.V.; Bich, E.; Hassel, E. **2009**. Simultaneous measurements on helium and nitrogen with newly designed viscometer-densimeter over a wide range of temperature and pressure. *J. Chem. Eng. Data*. 54, 2626-2637.

Lagourette, B.; Boned, C.; Saint-Guirons, H.; Xans, P.; Zhou, H. **1992**. Densimeter calibration method versus temperature and pressure. *Meas. Sci. Technol.* 3, 699-703.

Niesen, V.G. **1989**. (Vapor + liquid) equilibria and coexisting densities of (carbon dioxide + n-butane)at 311 to 395 K. *J. Chem. Thermodyn.*21, 915-923.

Private Communication from Anton Paar. , **2007**.

Holcomb, C.D.; Outcalt, S.L. **1998**. A theoretically-based calibration and evaluation procedure vibrating-tube densimeters. *Fluid Phase Equilb.*150-151, 815-827.

Bouchot, C.; Richon, D. **2001**. An enhanced method to calibrate vibrating tube densimeters. *Fluid Phase Equilb.* 191, 189-208.

Ashcroft, S.J.; Booker, D.R.; Turner, J.C.R. **1990**. Density measurement by oscillating tube. Effects of viscosity, temperature, calibration and signal processing. *J. Chem. Soc., Faraday Trans.*, 86, 145-149.

Lundstrom, R.; Goodwin, A.R.H.; Hsu, K.; Frels, M.; Caudwell, D.R.; Trusler, J.P.; Marsh, K.N. **2005**. Measurement of the viscosity and density of two reference fluids, with nominal viscosities at T = 298 K and p = 0.1 MPa of (16 and 29 mPas), at temperatures between (298 and 393) K and pressures below 55 MPa. *J. Chem. Eng. Data.* 50, 1377-1388.

Comuñas, M.J.P.; Bazile, J.-P.; Baylaucq, A.; Boned, C. **2008**. Density of diethyl adipate using a new vibrating tube densimeter from (293.15 to 493.15) K and up to 140 MPa. Calibration and measurements. *J. Chem. Eng. Data.*53, 986-994.

Kratky, O.; Leopold, H.; Stabinger, H. **1969**. *Z. Agnew. Phys.* 27, 273.

Bouchot, C.; Richon, D. **1998**. Direct pressure-volume-temperature and vapour-liquid equilibrium measurements with a single equipment using a vibrating tube densimeter up to 393 K and 40 MPa: Description of the original apparatus and new data. *Fluid Phase Equilb.* 191, 189-208.

Sanmamed, Y.A.; Gonzalez-Salgado, D.; Troncoso, J.; Romani, L.; Baylaucq, A.; Boned C. **2010**. Experimental methodology for precise determination of density of RTILS as a function of temperatura and pressure using vibrating tube densimeters. *J. Chem. Thermodyn.* 42, 553-563.

Dowson, D.; Higginson, G.R. **1966**. Elastohydrodynamic Lubrication. First Ed. Pergamon Press. Oxford.

Ramesh, K.T. **1991**. The short-time compressibility of elastohydrodynamic lubricants. *ASME J. Tribol.* 113, 361-371.

Jianguo, Y.; Wu, J.; Meng, X.; Abdulagatov, I. **2011**. Compressed liquid density measurements of dimethyl ether with a vibrating tube densimeter. *J. Chem. Thermodyn.* 43, 1371-1374.

Dutour, S.; Carrier, H.; Daridon, J.L. **2003**. Compressibilities of liquid pentadecylcyclohexane from high pressure speed of sound and density measurements. *J. Chem. Thermodyn.* 35, 1613-1622.

Murnaghan, F.D. **1951**. Finite Deformation of an Elastic Solid. First Ed. Wiley, New York.

MacDonald, J. R. **1966**. Some simple isothermal equations of state. *Rev. Mod. Phys.* 38, 669-679.

Fillers, R.W.; Tschoegl, N.W. **1977**. The effect of pressure on the mechanical properties of polymers. *Trans. Soc. Rheol.* 21, 51-100.

Moonan, W.K.; Tschoegl, N.W. **1983**. Effect of pressure on the mechanical properties of polymers. 2. Expansivity and compressibility measurements. *Macromolecules* 16, 55-59.

Martínez-Boza, F.J.; Martín-Alfonso, M.J.; Gallegos, C.; Fernández, M. **2011**. High-pressure behavior of intermediate fuel oils. *Energy Fuels* 25, 5138-5144.

3. Materials and Methods

3.1. Materials

3.1.1. Base Oil (SR-10)

The base oil employed in this study was a naphthenic oil from crude oil distillation provided by Verkol Lubricantes (Spain) (Figure 3.1.). The base oil used was stored at ambient temperature.

Figure 3. 1. SR-10 naphthenic mineral base oil

Some physical properties provided by the supplier are reported in the Table 3.1.:

Table 3. 1. Base oil physical properties

Physical property		Standard Method	Weight percentage (% w/w)
Aromatic content		ASTM D2140	11
Hydrocarbon Analysis	C_A	IR*	16
	C_N	IR	40
	C_P	IR	44
Polynuclear aromatic hydrocarbons (PAH)		IP346	20
Sulfur content		D2622	0.06
Acidity		D974	< 0.01 KOH

*IR: infrared spectroscopy

3.1.2. Organoclays

The two organomodified clays used in this research was supplied by Elementis (Belgium). Both organoclays are powders used directly without any purification for sample preparation. Powders were stored at room temperature in a dry container protected from sunlight. These organoclays have been extensively used as rheological additive in drilling industry.

Bentone® 34

This organoclay is the product resulting from the reaction between bentonite clay and dimethylditallow ammonium cations. Table 3.2 shows the formula of both compounds:

Table 3. 2. Chemical formula for clay and organic ion of Bentone® 34

Compound	Formula
Bentonite clay	$[(Al_{4-x}Mg_x)(Si_{8-y}Al_y)O_{20}(OH)_{4-f}F_f]$
Dimemthylditallow ammonium cation	$(CH_3)_2N^+(CH_2CH_3)_{13,15,17})_2$

Where $0 < x < 1.10$, $0 < y < 1.10$, $0.55 \leq x + y \leq 1.10$; $f \leq 4$, and $C_{14} \sim 5\%$, $C_{16} \sim 25\%$, and $C_{18} \sim 70\%$.

Bentone®34 is a rheological modifier principally used in drilling fluids formulation, particularly in all-oil, invert diesel and mineral oil muds. It also used in formulation of different materials, such as adhesives, anticorrosive paints and greases. This organoclay is specifically designed for low to intermediate polarity non-polar systems to overcome moderate and high temperatures.

Bentone® 128

This organoclay is the product resulting from the reaction between bentonite clay and dimethylbenzytallow ammonium cations. Table 3.3. shows the formula of the modifying ion:

Table 3. 3. Chemical formula of organic cation used in Bentone®128

Compound	Formula
Dimemthylditallow ammonium cation	$(CH_3)_2N^+(CH_2C_6H_5)(CH_2CH_3)_{13,15,17}$

Bentone® 128 is a rheological additive designed to viscosify all-oil drilling fluids and invert muds formulated with diesel, mineral and polyalphaolefins base fluids. This organobentonite possesses rapid dispersion and good sag resistance property at low temperatures. For invert-mud systems, water can act as a polar activator to ensure proper flow viscous properties.

In Table 3.4. some physical properties of both organoclays provided by the manufacturer are reported:

Table 3. 4. Some physical properties of both organoclays

Organoclay	**Color**	**Form**	**Density (g/cm3)**	**Moisture (%)**
Bentone® 34	Cream White	Finely divided powder	1.7	3
Bentone® 128	Very light cream	Finely divided powder	1.6	3

3.1.3. Samples prepared

Two types of drilling fluids were prepared: all-oil drilling fluids and invert muds. The all-oil drilling fluids were prepared by dispersing 1, 3 and 5% by weight of each organoclay in the base oil.

The invert-muds formulated are composed of 1% and 3% w/w Bentone® 128 dispersing in base oil, as background media, and different amount of aqueous phase. The aqueous phase of these invert-muds, which acts as a polar activator, consists of methanol-water mixture (5/95 v/v). Two sets of invert muds with 5/95, 15/85 and 30/70 aqueous/oil ratio were formulated from the all-oil drilling fluids at 1% and 3% organoclay content. These aqueous/oil ratios correspond to the following volume fractions, ϕ = 0.047, ϕ = 0.142 and ϕ = 0.286, respectively. The corresponding volume fractions were calculated according to the following expression:

$$\phi = \frac{x_{aq} \cdot \rho_{org}}{x_{aq} \cdot \rho_{org} + x_{org} \cdot \rho_{aq}} \qquad (3.\ 1)$$

Where x_{aq} is the mass fraction of aqueous phase, x_{org} is the mass fraction of organic phase, ρ_{aq} is the density of aqueous phase, and ρ_{org} is the density of organic phase.

3.2. Processing

3.2.1. All-oil Drilling Fluids

All-oil drilling fluids were obtained by mixing, at room temperature, different concentrations of organoclays with SR-10 base oil, using a high shear mixer T-25 Ultraturrax (Ika, Germany), at 9000 rpm for five minutes. Before this mixing step, the organoclays were wetted in the oil in a low shear mixing to guarantee the good dispersion of the clay into the base oil. After high shear processing, the homogenous all-oil drilling fluids were stored at room temperature. Figure 3.2. depicts the all-oil suspensions prepared.

3.2.2. Invert-Muds

The invert-muds were obtained from the 1% and 3% w/w Bentone® 128 all-oil drilling fluids by addition of different amount of aqueous phase. The aqueous phase added, a mixture of distillate water and methanol at 5/95 v/v, was prepared by mixing both liquids in a batch during five minutes at room temperature. The oily phase was emulsified by adding slowly the aqueous phase with a pipette using the high-shear mixer T-25 Ultraturrax for five minutes at room temperature. The invert muds prepared were stored at room temperature far from sunlight (see Figure 3.2.).

Figure 3. 2. High-shear processing set-up sketch; All-oil suspension picture and Invert-mud picture

3.3. Rheological Characterization

3.3.1. Rotational Rheometry

The rheological characterization of drilling fluids were carried out in a controlled stress rheometer "MARS II" (Thermo Scientific, Germany) using different geometries. The viscous flow behaviour and viscoelastic response of these materials, at atmospheric pressure, were performed using conventional geometries: plate-plate and coaxial cylinder. The high-pressure rheological characterization was carried out by using coaxial cylinder and two calibrated non-conventional geometries: four blade impeller and double helical ribbon.

Prior to any test, samples were always maintained at the testing temperature (±0.1ºC) for at least 10 minutes by using a circulating silicone bath. Two replicates of each rheological test were performed on fresh samples in order to assure repeatability of the results.

3.3.1.1. Equipment

MARS II

The rheometer MARS II is a controlled stress rotational rheometer from Thermo Scientific (Germany). The rheometer applies a controlled stress to the test substance by

means of a low inertia torque motor. The temperature of the sample is controlled via rheometer hardware which commands the set-point temperature to a circulating bath.

Figure 3. 3. Controlled-stress rheometer Mars II

Tests

Steady-state viscous flow curves

Viscous flow measurements between 40ºC and 140ºC were conducted in MARS II (Figure 3.3.) by applying a constant shear stress on the sample for two minutes, achieving a constant shear-rate after this shearing time. The geometries used were a serrated plate-plate geometry of 35 mm diameter and 1 mm gap (Figure 3.4.), and a coaxial cylinder geometry of 41 mm outer diameter and 1.00 mm gap (see Figure 3.4.). In order to avoid evaporation and assure a constant temperature in the sample a glass cover for plate-plate geometry was used.

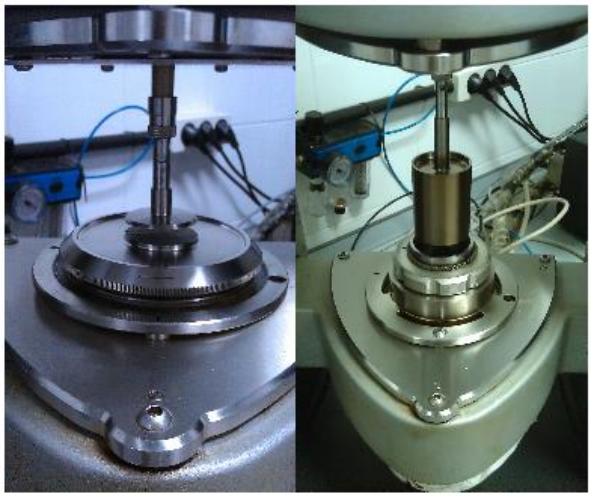

Figure 3. 4. Serrated plate-plate geometry (left); Coaxial cylinder geometry (right)

Dynamic tests

The linear viscoelastic region (LVR) was determined by stress sweep test, using a plate-plate geometry (60 mm diameter, 1 mm gap).

Frequency sweep test of each sample was performed between 0.02 and 100 rad/s at a fixed stress value within LVR previously determined by stress sweep test.

Frequency sweeps resulted in the measurement of the dynamic shear storage and loss moduli, *G'* and *G''*, respectively, over the entire range of frequencies tested.

3.3.2. High-pressure Rheometry

3.3.2.1. High pressure cell

The high-pressure rheological characterization was conducted in a high-pressure cell DC 400/200 (Thermo Scientific, Germany), capable of measuring sample viscosity up to 400 bar and temperature as high as 200ºC. This cell consists of a static vessel of 39 mm diameter hermetically closed. Both conventional and non-conventional geometries used in this research are set in the pressure cell and supported by a lower and an upper sapphire bearing to achieve an optimal radial stability. The high pressure sensors are equipped, at the top, with a secondary magnetic cylinder (36 mm diameter, 8 mm lenght), magnetically coupled to a tertiary cylinder outside the cell, which is connected

to the motor transducer of the rheometer. The maximum of torque transmitted by the rheometer measuring head to the inner sensor is of 120000 µNm. The following picture shows a schematic representation of pressure cell and the magnetic coupling:

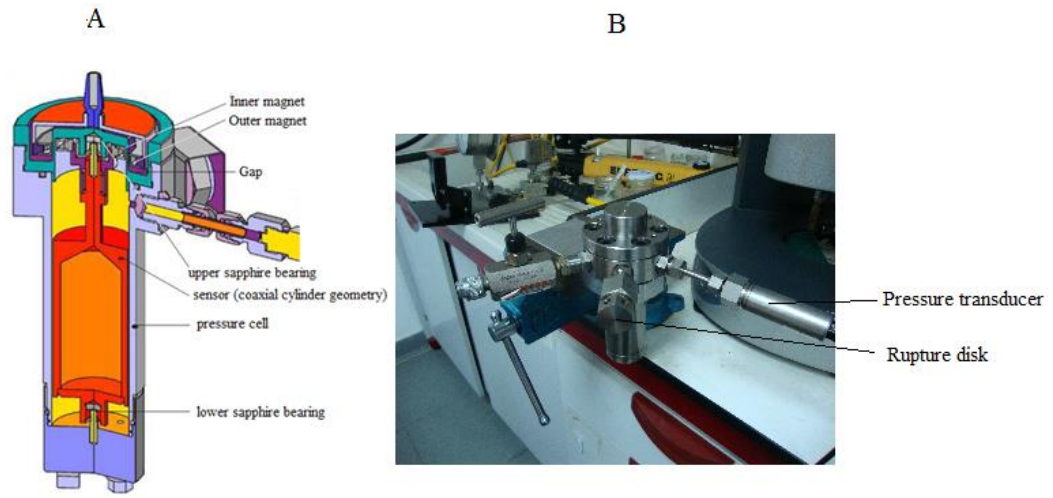

Figure 3. 5. A) Schematic drawing of the pressure cell with magnetic coupling; B) Picture of the pressure cell

In addition, the pressure cell is equipped with a rupture disk as safety device against excess pressure as well as a digital pressure transducer able to measure differential pressure ranged 0 to 400 bar (see Figure 3.5). All the main parts of pressure cell (i.e. the main body of the cell and upper lid) as well as the conventional measuring geometry are made of titanium.

3.3.2.2. Pressurization systems

In the present research, the pressure cell was connected to two pressurization systems. Prior to high pressure measurements, leakage and watertightness checking of both set-ups were verified. All materials used in the pressurization system were designed to support pressure at least 700 bar.

Pressurization system 1

It was the first set-up used to increase the pressure up to 400 bar. This system essentially consists of two main parts connected by a high pressure line: a high

pressure needle control valve (Enerpac, USA), located before the pressure cell and a hand pump (Enerpac 11-400, USA). A high pressure valve connected to this pump is employed to fill the sample from a fitted syringe (see Figure 3.6.). Firstly, the pressure cell with the sensor inside is filled by introducing the sample from the syringe. In order to assure there are no bubbles in the vessel, the hand pump primed with same base fluid as sample is manually operated. Once the pressure cell is completely filled, it is closed, and subsequently, the pressure is increased using the same sample as the pressurizing media. After high pressure measurements, the high pressure valve connected to the hand pump is used as a relief valve.

Figure 3. 6. Picture of the pressurization system 1 connected to the pressure cell mounted in the MARS II rheometer

Pressurization system 2

This pressurization system was designed in our laboratory. In this case a reservoir, where hydraulic pressurizing oil is stored, feed the hand pump. The pressurization system is composed of the following parts which connect the high pressure cell to the hand pump: three high pressure valves, high pressure pipe line circuit and a mixing chamber especially constructed for this set-up. The three high pressure valves, one of them connected to a syringe with some volume of sample (V_1), the second one, which is used to connect the high pressure pipeline circuit to a vacuum pump (V_2), and the

third one, located just before the high pressure cell (V_3) showed in Figure 3.6, are initially locked (see Figure 3.7).

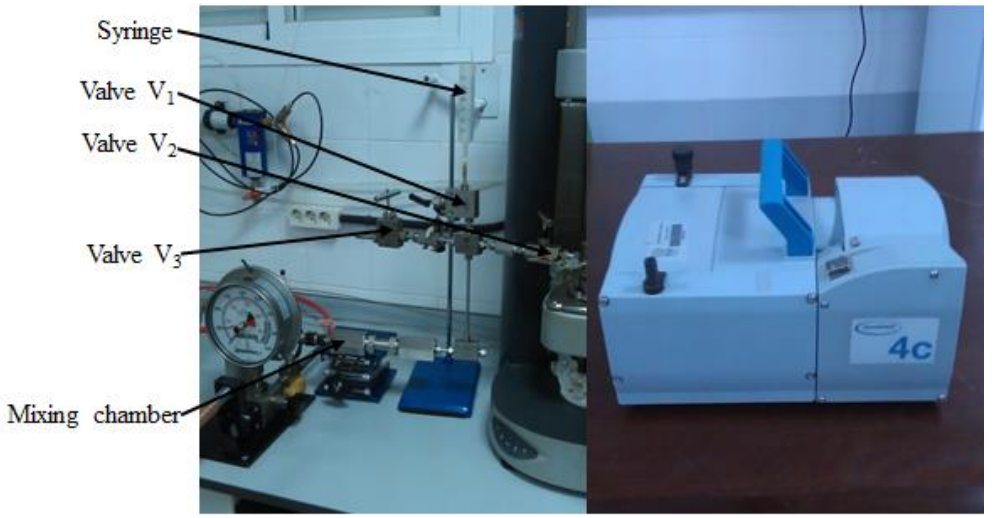

Figure 3. 7. Picture of the pressurization system 2 (left) and the vacuum pump (right).

Between the hand pump and the high pressure circuit, a mixing chamber, consisting of a cylinder fitted with a piston separates the pressurizing fluid and the sample. The pressure applied is transmitted to the sample by the piston displacement along the cylinder fitted in the mixing chamber (Figure 3.8).

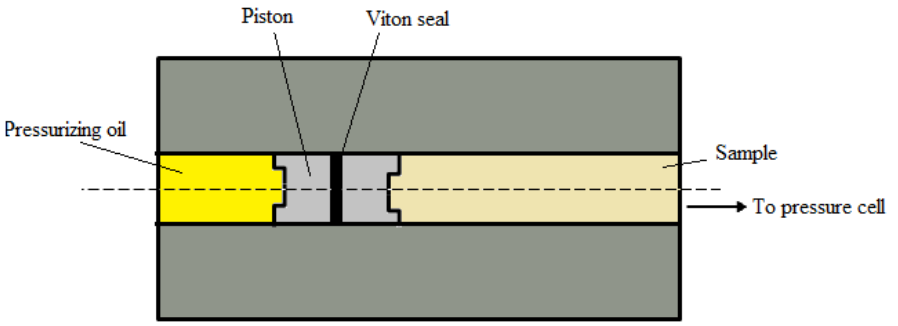

Figure 3. 8. Schematic representation of the mixing chamber

Prior any high pressure measurement, the following procedure was followed in order to guarantee the maximum reproducibility: the sample is poured into the pressure cell from a bottle and the corresponding geometry is put in contact to the lower sapphire bearing. Afterwards, the lid is closed and the high pressure valve (V_3) before the cell is

locked. Before pressurizing, the vacuum pump is switched on for 30 seconds to extract the air in the circuit. Subsequently, the whole circuit is filled from the attached syringe by suction.

3.4. PVT Characterization

3.4.1. Atmospheric Densimeter

The density measurements at atmospheric pressure were carried out by using a densimeter DMA-5000 (Anton Paar, Switzerland) which is based on the U-tube measuring principle (Figure 3.9.). The densimeter consists of U-shapped borosilicate glass tube inside of a thermostated jacket. The sample volume required was 1 ml. This densimeter was capable of measuring density up to 3 $g \cdot cm^{-3}$ with an accuracy of $5 \cdot 10^{-6}$ $g \cdot cm^{-3}$ between 0 and 90ºC, providing a temperature precision of ±0.001ºC by using high-precision platinum thermometer. Before performing the test, the sample was heated up and maintained a constant temperature for five minutes. In order to assure the maximum reproducibility for high temperature density measurements, samples were maintained for 20 minutes for every 10 ºC change.

Density measurements were carried out in the temperature range between 20ºC and 80ºC. Prior the density results, the densimeter was calibrated a two temperatures (20ºC and 60ºC) using both bi-distillate water and dry air. In addition, the effect of sample viscosity on the oscillating U-tube densimeter due to the increasing apparent volume of the cell was automatically corrected by a damping factor implemented in this equipment.

Figure 3. 9. Picture of the Densimeter Anton Paar DMA 5000

3.4.2. High-Pressure High-Temperature Densimeter

The high pressure high temperature density characterization was performed using a high-pressure vibrating tube, DMA HPM densimeter (Anton Paar, Switzerland), enable to measure sample density from 0 to 3 $g \cdot cm^{-3}$ up to 1400 bar and temperatures between -10ºC and 200ºC. The DMA HPM consists of two parts: a measuring cell and an interface module. In order to withstand a wide pressure and temperature range, the cell is made of Hastelloy C-276. The cell containing a 2 ml U-tube is surrounded by a steel jacket whose temperature is regulated using a circulating silicone bath AC150 (Thermo Scientific, Germany) with a precision of ± 0.01ºC. The interface module, which is directly connected to the cell, generates the period of oscillation and measures the period of oscillation and the temperature of the cell. This device is also linked to the mPDS 2000 V3 evaluation unit, which displays the oscillation period and the cell temperature from a built-in thermocouple with an error less than 0.1ºC.

3.4.2.1. Pressurization Set-up

The pressurization system was designed in order to withstand elevated pressure within safe limits. This system is composed of: a manual piston intensifier enable to increase pressure up to 4137 bar (HiP 37-5.75-60, USA), four high pressure valves, 1/4” outer diameter high pressure tubes and several high pressure accessories, such as pipe elbows and union tees. Two high pressure valves, V_4 and V_5, (NovaSwiss, Switzerland) were

used for depressurizing and filling the high pressure elements, and the others two valves, V_6 and V_7 (HiP, USA), were used to clean the system (see Figure 3.10).

Samples were introduced into the pressurization set-up using a syringe (see Figure 3.10), and the piston-type intensifier was employed to apply and control the pressure , which was measured using a pressure transducer model HP-2-S (Wika, Germany) with an uncertainty of less than 0.5% between 1 and 1600 bar.

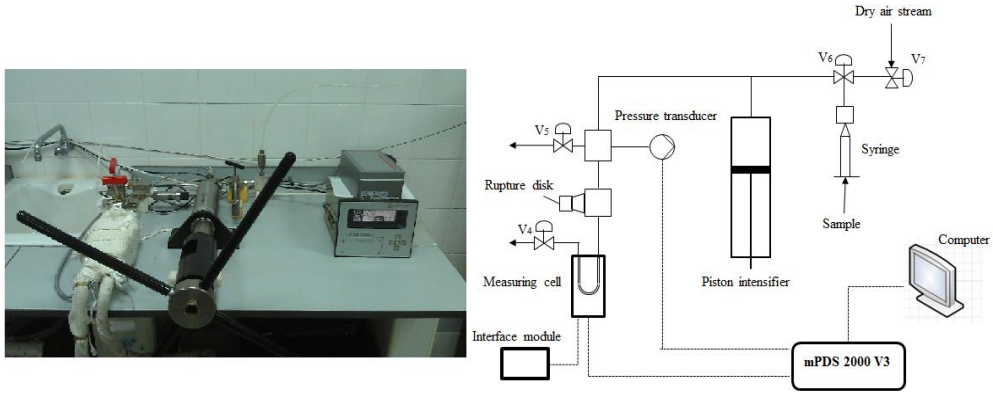

Figure 3. 10. Picture of pressurization system used for PVT measurements (left) and schematic representation (right)

3.4.2.2. Calibration

The calibration method to determinate density at high pressures and high temperatures was based on empirical equation provided by Anton Paar (2007). According to this procedure, at least two reference samples of known density in the range of temperature and pressure to be analysed are required. In this research, bi-distillate degassed water and n-dodecane were used to calibrate the vibrating tube densimeter in temperature range comprised between 40ºC and 140ºC up to 1200 bar. The reference values for water density were obtained from the equation state of Wagner and Pruss (2002), while the equation of state proposed by Lemmon and Huber (2004) was utilized for n-dodecane density values. These fluids have been commonly used as density standards fluids (Lemmon, 2004; Wagner, 1995). In addition, the studied samples have density values between them.

The values of temperature, pressure and oscillating period, measured by the DMA HPM were collected in a computer. The equation used to convert the vibrating periods into density values is given by:

$$\rho = A_1 + A_2 T + A_3 T^2 + A_4 P + A_5 P^2 + A_6 \cdot T \cdot P + (A_7 + A_8 T + A_9 T^2 + A_{10} P + A_{11} P^2 + A_{12} T \cdot P) \cdot \tau^2 \quad (3.\ 2)$$

where, ρ is the density of the fluid in g·cm^{-3}, T the measured temperature in ºC, P is the pressure applied in bar, τ is the oscillation period in ms, and A_i calibration parameter to be determined using density standards. The coefficient determination was conducted using non-linear fitting procedures (Figure 3.11) developed with the help of the Origin 8.1. software.

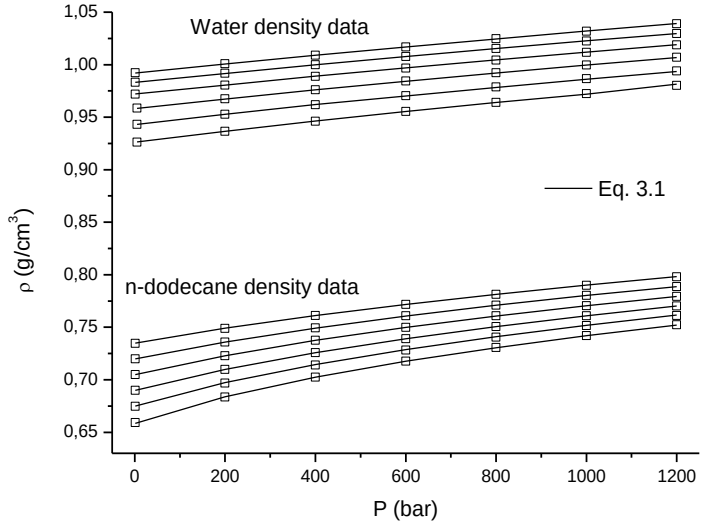

Figure 3. 11. Calibration results at high-pressure high-temperature conditions using equation 3.1. for calibrating fluids.

Density measurements

High pressure high temperature density data were performed in the calibrated region of the high-pressure vibrating tube densimeter (40 - 140 ºC and 1- 1200 bar). Prior any PVT measurement, both the measuring cell and the pressurization system were cleaned in three steps. Hexane was used as first cleaning fluid. Secondly, a flow of a dry air

stream is passed through the circuit for 10 minutes. Finally, a second cleaning liquid (acetone) was used to remove the first cleaning liquid. In order to clean completely the both vibrating densimeter and high pressure elements, a dry air steam was flowed through for 20 minutes. Moreover, a vacuum pump (Vacuubrand, Germany) was connected to the pressurization system to extract air to 0.5 mbar of pressure before the next measurement.

The samples were introduced into the measuring cell at a temperature slightly higher than cell temperature to prevent outgassing during measurements. The high pressure measurements were carried out isothermally starting from the lowest temperature (40ºC). After collecting the high pressure data, pressure applied was slowly reduced to avoid bubbles in the samples, and the measuring temperature was increased 20ºC waiting one hour to assure a homogeneous temperature profile in the sample. Once the temperature and pressure are stabilised, three stable raw period values are collected and average to be converted into the density value.

3.5. Thermal Analysis

3.5.1. Differential Scanning Calorimetry (DSC)

Thermal analysis is a term used to cover a group of techniques in which a physical property of a substance and/or its reaction product(s) is measured as a function of temperature. This experiment is confined to the area of differential thermal analysis (DTA) and, more specifically, its quantitative development, differential scanning calorimetry (DSC) (Sandler, 1998).

DTA/DSC curves reflect changes in the energy of the system under investigation, changes that may be either physical or chemical in origin. DSC measures the heat required to maintain the same temperature in the sample versus an appropriate reference material in a furnace (Pearce, 1982).

A number of important physical changes may be measured by DSC. These include the glass transition temperature (T_g), the crystallization temperature (T_c), the melt temperature (T_m), and the degradation or decomposition temperature (T_D). Chemical changes due to polymerization reactions, degradation reactions, and other reactions

affecting the sample can be determined. A typical DSC trace showing these transitions is shown in Figure 3.12.

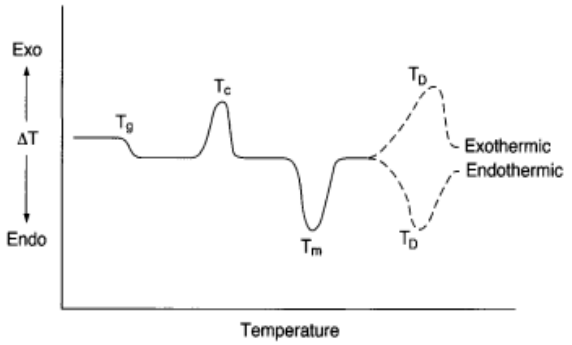

Figure 3. 12. A generic DSC curve depicting several transition types

DSC tests were performed with a TA Q-100 (TA Instruments, U.S.A.) (Figure 3.13). The sample was purged with dry nitrogen at a flow rate of 50 mL/min to avoid any condensation of moisture. Samples of 5-10 mg were always subjected to the following testing procedure: the pans where placed onto the cell at room temperature, then were heated at 80ºC, kept at this temperature for 5 minutes to reach the thermodynamic equilibrium, and subsequently, the samples were quenched-cooled to –80ºC, at 10ºC/min, kept for 5 minutes at this temperature to reach the equilibrium, and, finally, heated, at 10ºC/min, up to 180ºC.

Figure 3. 13. DSC Q-100

3.6. Microstructural Characterization

3.6.1. Particle Size Distribution

Laser diffraction technique is based on the fact that the spatial distribution of scattered light, or also commonly called scattering pattern, is a function of the particle size of the anlyzed sample. This pattern depends on ratio of particle diameter d_p, and the wave length of inciden light, λ. Thus, it can be distinguished among the Fraunhofer, Mie and Rayleigh scattering depending on the d_p/λ.

The Fraunhofer scattering occurs of particle size is at least 5 o 6 times larger than λ, while Mie scattering occurs if d_p/λ ratio is around one. The Rayleigh scattering occurs when the particle size is considerably smaller than λ (10 times).

In order to analyse the scattering pattern of a particle, the intensity of either diffracted or scattered light is taken into account according to the Mie´s theory:

$$I(\theta) = E\left[k^2 d^2{}_p J1^2\theta + (K_1\theta) + (K_2\theta)^3 + (K_3\theta)^5 + \frac{k^4 d^6{}_p (m-1)^2 \theta^6}{8\pi} \right] \qquad (3.\ 3)$$

Where I is the scattered light intensity, E is the flux of the incident light per unit area, k and K_i are constants, d_p is the diameter of the particles, $J1$ is the Bessel function of the first order, θ is the scattering angle and m is the complex refractive index.

Particle size was determined with Mastersizer 2000 analyzer (Malvern Instruments, UK) by laser diffraction (ISO 13320). This instrument contains two laser light sources emitting at wavelengths of λ = 632.8 and 466 nm. The scattered light is detected at various angles by using photodiode detectors (Figure 3.14). The instrument, which is operational only for a range of colloidal particle size and concentration, gives the size distribution using Mie´s theory.

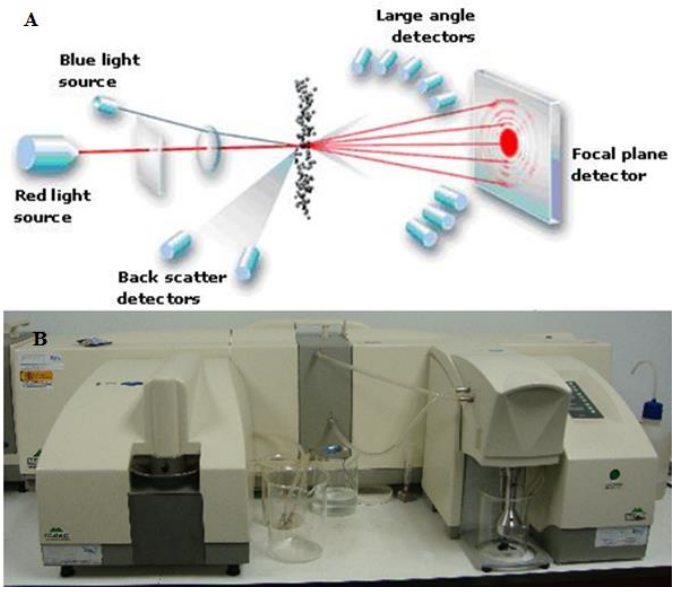

Figure 3. 14. A) Measuring principle of Mastersizer; B) Picture of Mastersizer 2000 with two unit dispersions Hydro 2000S (left) and Hydro 2000MU (right)

3.6.2. Optical Microscopy

Optical microscopy is a technique which is thought to enlarge microscopic objects. Generally, the light is passed through the sample and its image is collected by a primary lens (objective) and magnifying using a set of lens (eyespiece). In this sense, optical microscopy technique can be used to determine the shape, size and size distribution of microscopic dispersed particles, droplets or aggregates as smaller as 0.5 µm (Scharman, 2005). Additionally, it has been used in particulate systems to study creaming, sedimentation, coalescence and/or inversion process.

In this study, optical microphotograhs were carried out by using an Olympus BX52 microscope (Japan) (Figure 3.15), which can be operate either in transmitted and reflected mode. It possesses a built-in transmitted Koehler illumination consisted of a 100W halogen bulb as a light source. In addition, the instrument was equipped with an Olympus C5050Z camera and several objectives from 4X to 50X magnification with a maximum resolution of 0.37 µm.

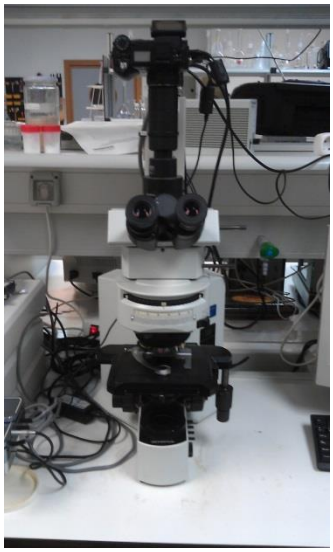

Figure 3. 15. BX-52 Olympus microscope

3.6.3. X-Ray diffraction (XRD)

X-ray diffraction is a powerful technique used to characterize the crystalline structures in solids such as clays, organoclays or composites among others (Starodoubtsev, 2006; Pavlidou, 2008). This technique is based on the detection of the X-ray scattered interference in solid materials due to interactions between the radiation and electron cloud of the material (see Figure 3.16.). The resolution of nanostructures depends on the magnitude of the interacting wavelength, which is of the order of 8000 eV for X-rays. In this sense, the theoretical limit of resolution using X-ray is given by the Bragg´s law equation, which relates the angle at which a beam of X-rays of a particular wavelength diffracts and inter-plane distance.

$$\lambda = 2d\sin\theta \tag{3. 4}$$

Where λ is the wavelength of the radiation, θ is the scattering angle and d is the inter-plane distance of atoms, ions or molecules. For clays, this separation length generally corresponds to the interplatelet distance, also called as basal spacing (d_{001}).

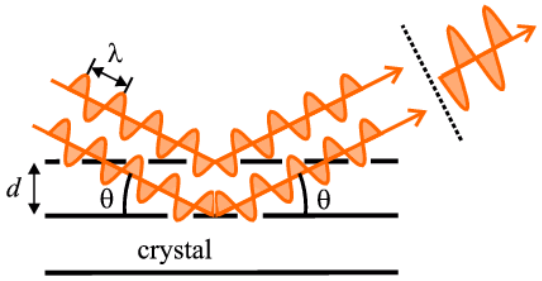

Figure 3. 16. Schematic representation of diffraction phenomena

The diffraction pattern, which results from the constructive interference when X-rays pass through a crystalline material, is recorded by an array detector. The X-ray diffraction results are represented by an X-ray diffractograms which show the intensity of the scattered X-rays as function of *2θ* (two times the angle of incidence/diffraction (Essington, 2004). The peaks in this type of plots corresponds to lattices planes of a crystalline material. Because of unequivocal signal obtained from XRD pattern, the diffractogram is like a footprint of the solid material, and hence XRD is considered as a powerful technique for identifying clay minerals. Moreover, XRD analysis of data can be used to quantitate various crystalline phases in a multicomponent mixture using the basic equation proposed:

$$I = \frac{Kx_i}{u^*} \tag{3. 5}$$

Where I is the intensity of peak, x_i is the mass concentration of the phase i, K is a factor, and u^* is the mass absorption coefficient of the sample.

X-ray diffraction measurements of organoclay and oily suspensions were carried out at room temperature, using a Bruker S8 Advance diffractometer (Germany) (see Figure 3.17.). The equipment has a vertical Brentano Bragg geometry goniometer of two-circles with independent stepper and optical encoders. It also possesses a secondary monochromator, and a copper cathode as X-ray source. The samples were subjected to Cu Kα radiation with a wavelength of 0.15406 nm. This diffractometer can run either in *θ/θ* and *θ/2θ* configuration with a smallest stepsize angle of 0.0001º in the maximum

usable 2θ angular range comprised -110º and 168º. In this study, the 2θ angles were varied from 1.5 to 20º, single scanning step of 0.017º and measurement time of 6s per step. The diffraction data were collected and treated by DIFFRACplus software installed on a computer connected to the diffractometer.

Figure 3. 17. Bruker S8 Advance diffractometer

3.7. References

Private Communication from Anton Paar. , **2007**.

Wagner, W.; Pruss, A. **2002**. The IAPWS Formulation 1995 for the thermodynamic properties of ordinary water substance for general and scientific use. *J. Phys. Chem. Ref. Data*, 31, 387-535.

Lemmon, E.W.; Huber, M.L. **2004**. Thermodynamic properties of n-dodecane. *Energy Fuels*, 18, 960-967.

Sandler, S.R.; Karo, W.; Bonesteel, J.-A.; Pearce, E.M. **1998**. Polymer Synthesis and Characterization. London (UK): Academic Press.

Pearce, E.M.; Wright, C.E.; Bordoloi, B.K. **1982**. Laboratory Experiments in Polymer Synthesis and Characterization. The Pennsylvania State University, University Park, PA.

Scharman, L.L. **2005**. Emulsions, Foams, and Suspensions: Fundamentals and Applications. First Ed. Wiley-VCH Verlag GmbH.

Allegra, G.; Famulari, A.; Meille, S.V. **2006**. Mechanism of smectic arrangement of montmorillonite and bentonite clay platelets incorporated in gels of poly(acrylamide) induced by the interaction with cationic surfactants. *Langmuir* 1, 369-374.

Pavlidou, S.; Papaspyrides, C.D. **2008**. A review on polymer-layered silicate nanocomposites. *Prog. Polym. Sci.* 33, 1119-1198.

Essington, M.E. **2004**. Soil and Water Chemistry: An Integrative Approach. First Ed. CRC Press.

Los artículos publicados en revistas científicas han sido retirados del apartado "Resultats and discussions" de esta tesis debido a las restricciones relativas a los derechos de autor. Dichos artículos han sido sustituidos por las referencias bibliográficas de más abajo, además si la UHU tiene suscripción a la versión electrónica de las revistas se añade un enlace que será de acceso restringido a miembros de la UHU.

Referencias bibliográficas:

- Hermoso Limón, J., Jofere, B.D., Martínez Boza, F.J., Gallegos Montes, C.: **"High Pressure Mixing Rheology of Drilling Fluids".** Ind. *Eng. Chem. Res.*, 2012, 51 (44), pp 14399–14407. DOI: 10.1021/ie301835y

Enlace al texto completo del artículo (solo para miembros de la UHU):

http://pubs.acs.org/doi/abs/10.1021/ie301835y#citing

- Hermoso Limón, J., Martínez Boza, F.J., , Gallegos Montes, C.: **"Influence of viscosity modifier nature and concentration on the viscous flow behaviour of oil-based drilling fluids at high pressure"**. Applied Clay Science. Vol. 87, January 2014, Pages 14–21. DOI: 10.1016/j.clay.2013.10.011

Enlace al texto completo del artículo (solo para miembros de la UHU)

http://www.sciencedirect.com/science/article/pii/S0169131713003414

- Hermoso Limón, J., Martínez Boza, F.J., Gallegos Montes, C.: **"Combined Effect of Pressure and Temperature on the Viscous Behaviour of All-Oil Drilling Fluids"**. Oil and Gas Science and Technology. Rev. IFP Energies nouvelles, 2014. DOI: 10.2516/ogst/2014003

Enlace al texto completo del artículo

http://ogst.ifpenergiesnouvelles.fr/articles/ogst/abs/first/ogst130139/ogst130139.html

- Hermoso Limón, J., Martínez Boza, F.J., Gallegos Montes, C.: **"Influence of aqueous phase volume fraction, organoclay concentration and pressure on invert-emulsion oil muds rheology"**. Journal of Industrial and Engineering Chemistry. 2014. DOI: 10.1016/j.jiec.2014.07.028. Article in press

Enlace al texto completo del artículo (solo para miembros de la UHU).

http://www.sciencedirect.com/science/article/pii/S1226086X14003724#

4. Results and Discussions

4.1. Design and Calibration of non-Conventional Geometries

4.1.1. Abstract

Drilling fluids, used in oil well drilling operations, are suspensions/emulsion of various constituents and solid particles. These fluids usually behave as rheologically complex materials. They show non-Newtonian behavior, such as shear-thinning, yield stress, thixotropy, and strong thermal and pressure dependence. For these reasons, the rheological characterization of this type of fluids using conventional geometries can be a difficult task due to the complex nature and the presence of solids.

Consequently, the overall objective of this first chapter was to design and calibrate special non-conventional geometries, such as helical ribbons and blade turbines, for characterizing the flow behavior of drilling fluids as a function of pressure.

Hence, the idea of applying the basic principles used in the derivation of mixer power curves to estimate the viscosity in the vessel bulk could be valuable methodology for characterizing the rheological behavior of these dispersed systems. In this sense, the well-known Metzner-Otto method, which has been extensively used for the design of mixers at atmospheric pressure, and the Couette analogy method were used to calibrate these special geometries. In order to do this, a commercial Glycerin was used as Newtonian fluid, and power law fluids with different flow indexes, from 0.1 to 0.6, were tested. These fluids are different aqueous solutions of carboxymethyl cellulose (CMC), guar gum and xanthan gum prepared by mechanical agitation, at room temperature, until complete homogenization. In addition, an oil-based drilling fluid for testing was formulated by dispersing 5% w/w organoclay in naphthenic oil.

Mixing rheology measurements were performed in a pressure cell D400/200 (diameter D = 39 mm and height H =140 mm) capable of collecting rheological data up to 400 bar and 200ºC. This cell consists of a non-baffled static vessel with a cylindrical closed head and truncated conical bottom. The cell was completely filled with the fluid to be

tested. Two conventional coaxial cylinder geometries, PZ (d = 38mm) and Z (d = 41mm), were used to validate the flow properties of the fluids used. Besides, two non-conventional geometries, a four flat-blade turbine of 32 mm diameter (FL-4) and 40 mm blade length (L), and a double helical ribbon of 36 mm diameter (DHR-2) and 78 mm impeller length, were supported and centered between two sapphire bearings at the top and bottom of the pressure cell. The pressure cell was pressurized by a hydraulic system, using the fluid to be tested as pressurizing liquid. This pressurization system consisted of a high pressure valve and a hand pump connected by a high pressure line. Samples were carefully introduced from the valve until all the air bubbles inside the vessel were completely expelled.

From the Newtonian data obtained at high pressure, it is apparent that the power consumption only depends on the viscosity-pressure relationship of the fluid. Consequently, this suggests that the efficiency of the two impellers studied is not influenced by viscosity variations due to pressure increase.

The Metzner-Otto constant (K_s) values of blade turbine and helical ribbon shows different pressure and flow index combined dependence. In case of helical ribbon, K_s exponentially increases with the flow index for any pressure evaluated between 1 to 390 bar. Whereas Metzner-Otto constant, K_s, for flat-blade turbine geometry, is affected by the combined influence of both pressure and index flow. According to the Couette analogy treatment, the predicted K_s value is in relative agreement with the experimental K_s values obtained for helical ribbon, although the value for the flat-blade turbine geometry is considerably overestimate compared to the values obtained from Metzner-Otto method. These results seem to indicate that the Couette analogy treatment is principally suitable for geometries with flow patterns similar to those generated by a conventional coaxial cylinder, such as the double helical ribbon.

The application of the flow index-pressure-dependent relationship $K_s\ (n,P)$ of each geometry to the both raw torque and rotational speed data allows an excellent agreement between flow curves from both conventional and mixing geometries, in the pressure ranged scoped. Likewise, both mixing geometries match the pressure

dependence of viscosity, obtained with conventional geometries for the testing drilling fluid, even though the shear-thinning behavior varies over the whole pressure range studied. In addition, it must be emphasized that these mixing geometries extend the experimental range of shear rate down to a much lower shear-rate region, showing that pressure has a little influence at the lowest limit of measurable shear rates. Therefore, these tools extend the experimental shear-rate window covered by the coaxial cylinders conventional geometry allowing the measurement of the measurement of important engineering parameter, such as the apparent yield stress.

4.2. Effect of Organoclay Nature, Concentration and Pressure on Flow Behaviour of All-oil Suspension Drilling Fluids

4.2.1. Abstract

In the first chapter has been demonstrated that drilling fluid are rheologically complex suspensions. Both clays nature and composition are the main key factors that control the development of the specific flow properties of drilling fluids. This rheological behaviour may change when the material is submitted to the extreme pressure and temperature conditions of the wellbore. In case of oil-based drilling fluids, organophilic bentonites have been extensively used due to both good dispersing properties in the oil phase and filtration characteristics. However, little attention has been devoted to the effect that nature and concentration of these viscosity modifiers exert on the rheological properties of oil dispersions submitted to high pressure.

In this chapter, the overall objective was to study the effect that organoclay nature and concentration exert on the viscous flow properties of model all-oil drilling fluid submitted to high pressure. In this sense, a factorial Sisko-Barus model, which takes into account both shear and pressure effects in the same equation, was used to fit the experimental pressure-viscosity data.

The model drilling fluids were formulated with two commercially available organobentonites and mineral based lubricating oil. The samples were prepared by mixing organoclay (at concentration of 1, 3 and 5 % w/w) in the oily base, at room temperature, using a high mixer Ultraturrax for five minutes. Prior high shear processing, the organoclays were wetted with the oil, at room temperature, in a low shear mixer using a conventional four blade impeller.

The high pressure rheological characterization of all-oil drilling fluids was carried out using the set-up configuration described in the experimental section. In this case, a coaxial cylinder geometry (41 mm inner diameter, 1 mm gap, 60 mm length) was used for atmospheric pressure measurements, and a coaxial cylinder-pressure (36 mm inner diameter, 8 mm length) for high pressure measurements. In addition, microstructural

characterization of these oily suspensions was performed using both X-ray diffraction and microscopic techniques.

Atmospheric rheological experiments as well as X-ray diffraction and microscopic techniques suggest that microstructures resulting from interactions among organic ions and solvent should be completely different, yielding significant differences in the bulk viscous flow behaviour, in spite of the fact that both organoclays display many similarities at the nanoscale level. In addition, these interactions, which normally increase with clay concentration, lead to an increase in viscosity.

As expected, viscosity increases with pressure in the whole range of shear rate tested. The viscous flow behaviour of the organoclay suspensions with pressure was modelled satisfactorily using the Barus´ model in combination with Sisko´s model. In this sense, it is interesting to note that the piezoviscous coefficients of the oil-based drilling fluids analysed are quite similar to that of the oil base, being the effect of pressure on particles negligible as compared to the effect on the continuous oil medium.

In addition, oil drilling fluids formulated with B34 organoclay exhibit a remarkable pressure dependence of the flow index for B34-based fluids, suggesting that a higher number of interparticle contacts could be induced by pressure packing. On the other hand, the flow indexes of B128-based drilling fluids dramatically depend on organoclay concentration, whilst it is almost independent of pressure probably due to the microstructure developed would be more robust against pressure changes.

The experimental data confirms that helical ribbon geometry is an appropriate tool to cover accurately a wide shear rate range of the oil-based drilling fluids tested. From the experimental results obtained at atmospheric pressure, it can be concluded that the viscous flow behaviour of these drilling fluids is strongly affected by both the organically modified surface-oil pair solvency and oil viscosity, in the temperature range studied.

Moreover, both Bingham's and Herschel-Bulkley's model fitted the complex viscous flow behaviour of these drilling fluids, at different pressures and temperatures, fairly well. Drilling fluids yield stresses increase with pressure, whilst their temperature dependence is related to the type of organoclay used. This behaviour may be explained on the basis of oil compression and thermally-induced changes in the effective organoclay volume fraction. Further, a factorial WLF-Barus model satisfactorily describes the temperature/pressure evolution of the plastic viscosity for both drilling fluids, being the viscosity at high shear rate mainly influenced by the piezo-viscous properties of the continuous phase.

4.4. Effect of Aqueous Phase, Organoclay Concentration and Pressure on Rheological Behaviour of Invert Emulsions

4.4.1. Abstract

The previous chapters have been devoted to the design and rheological characterization of model all oil drilling fluid, fluids formulated as oily suspension or organobentonites. In this chapter oil-based fluids containing up to 40 wt.% of water soluble polar component, which are classified as invert oil muds or suspoemulsions, will be formulated and characterised. These systems are of mayor interest to understand the interaction between the bentonite structure and both the organic and inorganic components. For these systems, the viscous flow properties are affected by, for instance, water/oil ratio, size of water droplets, organoclay concentration and interfacial interactions. Consequently, the main objective of this chapter was to find the influence of aqueous phase volume fraction on high pressure rheology of suspoemulsions at a given temperature.

Two all-oil drilling fluids formulated by mixing the B128 organoclay (1 and 3 wt.%) in the oil base were used as base fluid for the invert-muds preparation. These organoclay suspensions were emulsified with different fractions (5, 15 and 30 wt.%) of a blend of methanol and water (5:95 v/v) using a high mixer for five minutes.

Isothermal viscous characterization was carried out using the same geometries described in Chapter 4.3. Further, in this work, the pressure cell was connected to a hydraulic pressurization system designed in our laboratory. This system is composed of the following parts: a high pressure hand pump, three high pressure valves, and a chamber. Before pressurizing, a vacuum pump, which was connected to a high pressure line through a high pressure valve, was switched on to avoid bubbles in the circuit. Subsequently, the sample was introduced into the high pressure line with a syringe attached to another valve. Between the hand pump and the high pressure circuit, a chamber, consisting of a cylinder fitted to a piston, separated the pressurizing fluid and the sample. This cylinder-piston arrangement provided the requested pressure to the sample, by the displacement of the piston along the cylinder.

In addition, small amplitude oscillatory shear measurements, in the linear viscoelastic region, were performed between 0.02 rad/s and 100 rad/s, using plate-and-plate geometry (60 mm diameter, 1 mm gap). Besides, microstructural characterization of the invert-muds was performed using both particle size distribution analyser and microscope.

The droplet size of these systems seems to increase with the disperse phase volume fraction from micrographs and light-scattering measurements, whereas it is apparent that the mean droplet diameter decreases by increasing the organoclay concentration. All the suspoemulsions studied present a shear-thinning behaviour with a clear tendency to reach a low-shear-rate-limiting shear stress value. The Herschel-Bulkley model fits the experimental results obtained fairly well.

From the experimental results obtained, it can be concluded that the viscous and viscoelastic behaviour of suspoemulsions, used as invert-muds in drilling industry, are strongly affected by both the organoclay concentration and internal aqueous phase volume fraction. This rheological behaviour has been associated with repulsive forces derived from the surrounding organic ions layer, which provides a steric barrier against droplet flocculation.

At high pressures, the yield stress depends on internal disperse phase volume fraction and organoclay concentration. Its increase has been related to both oil phase compression and water-oil interfacial interactions characteristics. Barus' model fits the pressure dependence of suspoemulsion viscosity, for different disperse phase volume fractions and organoclay concentration, fairly well. In case of 1% w/w organoclay suspoemulsions show similar piezoviscous coefficients no matter internal disperse phase volume fraction. On the contrary, 3% w/w organoclay suspoemulsions piezoviscous coefficients are lower than the one of the corresponding suspension, fact that may be related to the elasticity of the interfacial layer surrounding the emulsified droplets.

4.5. Pressure-Density-Temperature Behaviour of All-oil Suspension Drilling Fluids as a function of Organoclay Concentration

4.5.1. Abstract

From a technological point of view, the knowledge of the effect of high pressure and high temperature on the volumetric properties of drilling fluids is a critical issue worth to be studied, since the successful of the completion operation in the oil well and its cost depend, on a considerable extent, on the evolution of the volumetric properties with these variables. However, the influence of both clay nature and concentration on the volumetric properties of oily suspension for designing drilling fluid is not well understood yet. In this sense, this chapter focuses on the study of the influence that both organoclay nature and concentration exert on the density of the organoclay suspensions as function of both pressure and temperature.

With this aim, two vibrating tube densimeters were used to measure the densities, ρ, of the organoclay suspension formulated in Chapter 4.2. An Anton Paar DMA 5000 densimeter (Austria) was employed to measure the density of SR-10 oil and organoclay suspensions between 40 and 100ºC, at atmospheric pressure. An Anton Paar DMA HPM high-pressure vibrating tube (Austria) was used to measure the densities of the samples studied in a temperature range comprised between 40 and 140ºC, and pressures up to 1200 bar. The temperature of the high-pressure vibrating tube was controlled by an external circulating bath containing silicone. The temperature was maintained constant within ±0.01ºC. A manual piston intensifier (HiP, USA) was used to control the pressure of the system. The pressure applied was measured by a pressure transducer model HP-2-S (Wika, Germany), with an uncertainty of less than 0.5% between 0 and 1600 bar. Among the different ways to transform the vibrating periods into densities, the calibration of the high-pressure vibrating cell in the entire range of pressure and temperature analysed was performed by using a polynomial equation, function of temperature, pressure and oscillation period. For calibration purposes, calibration fluids have been selected on the following basis: the oil and organoclay

suspensions densities are inside the density range defined by these calibration fluids, and there are also some correlations available in the literature.

A modified Tait's equation has been used to fit the experimental density values over the whole temperature (*t*) and pressure (*p*) range studied. The Tait equation describes the pressure-temperature-density behaviour of the organoclay suspensions studied fairly well, with a maximum relative error lower than 0.21%. As expected, organoclay suspension density decreases as temperature increases, and increases with pressure.

From our results, density shows a linear dependency on organoclay concentration, no matter temperature and pressure (40 to 120ºC and 1 to 1200 bar) are. Likewise, the influence of pressure, and also temperature, on density for each organoclay suspension is different. The physical origin of the different PVT behaviour could be related to the non-ideal volumetric behaviour with a positive deviation, which is dampened by increasing pressure. This expansive volumetric behaviour might be attributed to the swelling capacity of organoclays in non-aqueous solvents, associated with interactions between the clay surface and the oil medium.

Similarly, the influence of pressure and temperature on isothermal compressibility and isobaric expansivity of the suspensions is a function of organoclay nature and concentration.

PVT Behavior of Organoclay Suspensions

Hermoso, J.; Martínez-Boza, F.J.; Gallegos, C.

Departamento de Ingeniería Química, Centro de Investigación de Tecnología de Productos y Procesos Químicos (Pro^{2}TecS). Universidad de Huelva. Facultad de Ciencias Experimentales. Campus del Carmen. 21071 Huelva (Spain)

Phone: +34 959219993; Fax: 34 959219983; e-mail: martinez@uhu.es

Keywords: density, temperature, pressure, organoclay.

* Author to whom correspondence should be addressed

Abstract

Two organoclays, commonly used in the formulation of drilling fluids, were dispersed in a mineral oil. Organoclay mass fraction ranged from 0.01 to 0.05. PVT data for the mineral oil and all the suspensions studied were obtained by using a high pressure vibrating tube densimeter, in a temperature range comprised between 40 and 140 ºC and pressures up to 1200 bar. The main objective of this work was to study the influence of organoclay nature and concentration on the density of organoclay suspensions in a wide range of pressure and temperature. A Tait-like equation fitted the volumetric behavior of these suspensions fairly well. Organoclay addition to the liquid matrix yielded a significant increase in density values in the whole range of temperature and pressure tested. These suspensions showed non-ideal volumetric behavior, which was significantly influenced by organoclay nature and concentration.

1. Introduction

Suspensions are of major interest concerning a wide range of industrial applications[1-4]. In particular, the use of organoclay particles, which result from the reaction of smectite clay and amine cation groups[5], has received a growing attention in recent years, due to their remarkable physicochemical properties [6-9].

The addition of organophilic clays to a matrix, such as polymers, notably improves their barrier properties, and thermo-mechanical resistance[10,11,12]. Furthermore, organoclays are widely used for improving the rheological properties of different products[13,14], such as cosmetics, pharmaceuticals, drilling fluids[15,16], paints or lubricating greases[17]. In general, the organoclay needs to be dispersed into hydrocarbon media, in order to achieve the desired properties. The properties of the organoclay suspensions depend on the following determining factors: interactions between the organophilic ions and the solvent, type of the exchanged ion, and chemical characteristics of the solvent[9,17].

Organoclay suspensions are commonly used as drilling fluids, due to their capacity to form gels and their suitable viscous properties. These fluids are submitted to high pressure and temperature in the well during drilling operations[18,19,20]. The successful completion of an oil well and its cost depend, on a considerable extent, on the properties of these fluids. Hence, one of the crucial aspects of organoclay suspensions in the drilling industry is related to the characterization of their thermo-physical properties. Both, viscosity and density have been the two most extensively studied properties of organoclay dispersions concerning this application[21,22,23]. When drilling fluids are pumped down, they experience compression and expansion effects, related to the changes in temperature and pressure conditions along the wellbore. Density variations might be significant and their control is a challenging goal to minimize associated risks,

and improve security and efficiency, particularly for non-aqueous systems[24,25]. Hence, the knowledge of the effect of high pressure and high temperature on the volumetric properties of drilling fluids is a critical issue worth to be studied. Several authors have investigated the combined influence of pressure and temperature on the density of drilling fluids[26, 27, 28]. However, the influence of both clay nature and concentration is not well understood yet.

Consequently, the overall objective of this work was to study the influence of organoclay nature and concentration on the density of organoclay suspensions in a wide range of pressure and temperature. With this aim, the pressure-temperature dependence of the volumetric properties was modelled by using the Tait equation.

Experimental

1.1. Materials

N-dodecane ($C_{12}H_{26}$, molar mass 170.34 g·mol^{-1}, CAS 112-40-3, GC purity higher than 90%) was supplied by Sigma-Aldrich (Germany). This chemical was not submitted to further purification. It was directly injected into both the glass vibrating tube and high pressure cell immediately after the bottle was open.

Two commercially available organoclays, denoted as B34 and B128, provided by Elementis (Belgium), were used in the present study. The density values for B34 and B128 were given by the manufacturer (1.7 g·cm^{-3} and 1.6 g·cm^{-3}, respectively).

A mineral-based lubricating oil, SR-10 (0.114 Pa·s at 40ºC) supplied by Verkol (Spain), was used as base oil for the formulation of organoclay suspensions.

1.2. Preparation of organoclay suspensions

Organoclay suspensions were prepared by mixing, at room temperature, the organoclay in SR-10 base oil (1, 3 and 5% wt. organoclay concentration), using an Ultraturrax high-

shear mixer (Ika, Germany) at 9000 rpm for five minutes. Prior to their high shear processing, the organoclays were wetted with the oil for 1 hour, at room temperature.

1.3. Density measurements

Two vibrating tube densimeters were used to measure the densities, ρ, of the samples studied. An Anton Paar DMA 5000 densimeter (Austria) was employed to measure the density of SR-10 oil and organoclay suspensions between 40 and 100ºC, at atmospheric pressure. Prior to performing these measurements, the densimeter was calibrated, as a function of temperature, using both dry air and degasified bi-distilled water, as recommended by the manufacturer. The results obtained were compared with the values reported in Anton Paar's manual for air and water in the temperature range tested. For this device, the manufacturer reported uncertainties for temperature of ±0.01ºC, and density of $\pm 5 \cdot 10^{-6}$ g·cm^{-3}, between 0 and 100 ºC.

An Anton Paar DMA HPM high-pressure vibrating tube (Austria) was used to measure the densities of the samples studied in a temperature range comprised between 40 and 140ºC, and pressures up to 1200 bar. The temperature of the high-pressure vibrating tube was controlled by an external circulating bath containing silicone. The temperature was maintained constant within ±0.01ºC. A manual piston intensifier (HiP, USA) was used to control the pressure of the system. The pressure applied was measured by a pressure transducer model HP-2-S (Wika, Germany), with an uncertainty of less than 0.5% between 0 and 1600 bar.

Among the different ways to transform the vibrating periods into densities[29,30], the calibration of the high-pressure vibrating cell in the entire range of pressure and temperature analyzed was performed by using a polynomial equation, function of temperature, pressure and oscillation period[31]:

$$\rho = A_1 + A_2 t + A_3 t^2 + A_4 p + A_5 p^2 + A_6 t \cdot p + (A_7 + A_8 t + A_9 t^2 + A_{10} p + A_{11} p^2 + A_{12} t \cdot p) \cdot \tau^2 \qquad (1)$$

where, ρ is the density of the fluid in g·cm^{-3}, t is the temperature in ºC, p is the pressure applied in bar, τ is the oscillation period in ms, and A_i the coefficients of the high-pressure densimeter. These coefficients were evaluated using a non-linear regression from the high pressure/high temperature density data of both n-dodecane and water. The values of the A_i coefficients are shown in Table 1. These calibration fluids have been selected on the following basis: the oil and organoclay suspensions densities are inside the density range defined by these calibration fluids, and there are also some correlations available in the literature. Thus, in the case of water, the experimental data obtained in this work were compared to those obtained from Wagner and Pruss' equation of state[32]. On the other hand, the equation of state proposed by Lemmon and Huber[33] was used for this comparison in the case of n-dodecane. Taking into account the uncertainties in temperature, pressure, period of oscillation, water and n-dodecane densities, and equation (1) fitting for the reference fluids (0.07% for water and 0.1% for n-dodecane), the overall experimental uncertainty in oil and organoclay suspensions densities was estimated to be $\pm 1 \cdot 10^{-3}$ g·cm^3. This uncertainty is similar to that previously reported when using an Anton Paar densimeter[34, 35].

It should be taken into account that the systematic errors in the densities measured with a vibrating tube depend, among others, on sample viscosity[36,37] and U-tube design[38]. The viscosity correction curve for the Anton Paar densimeter model DMA HPM used in this study was provided by the manufacturer[39]. However, the largest corrections concerning the viscosity influence on the measurements of the density, in the whole range of temperature and pressure tested, were lower than the estimated uncertainty.

2. Results and Discussion

2.1. Base oil and suspensions densities

Experimental densities of SR-10 base oil and organoclay suspensions, at three different mass fractions (x_i = 0.01, 0.03 and 0.05), were measured in a temperature range from 40 to 140ºC, and pressures up to 1200 bar. These density values are gathered in Table 2.

A modified Tait's equation[40] has been used to fit the experimental density values over the whole temperature (t) and pressure (p) range studied:

$$\rho(t,P) = \frac{\rho_0(t)}{\left[1 - C\cdot\ln\left(\frac{B(t)+p}{B(t)+p_0}\right)\right]} \tag{2}$$

being p_0 (1 bar) the reference pressure.

The term $\rho_0(t)$ is the dependence of density with temperature at pressure p_0, given by a second-order polynomial equation:

$$\rho_0(t) = a_0 + a_1 t + a_2 t^2 \tag{3}$$

The fitting parameter C is considered independent of temperature; whilst the parameter $B(t)$ is given by a second-order polynomial equation:

$$B(t) = b_0 + b_1 t + b_2 t^2 \tag{4}$$

All these parameters for the base oil and each organoclay suspension result from equation (1) fitting, over the whole range of temperatures and pressure tested, using the least square method. It is important to mention that the values of a_i, b_i and C were obtained by correlating simultaneously the experimental densities as a function of both pressure and temperature. In addition, aiming to check the accuracy of the modified Tait equation employed in this work, the absolute average deviation (AAD) and the standard deviation, σ, have been calculated:

$$AAD = \frac{100}{N}\sum_{i=1}^{N}\left|\frac{\rho_i^{\exp} - \rho_i^{calc}}{\rho_i^{\exp}}\right| \tag{5}$$

$$\sigma = \sqrt{\frac{\sum_{i=1}^{N}(\rho_i^{\exp} - \rho_i^{calc})^2}{N-m}} \quad (6)$$

where N is the number of experimental data and m the number of correlation parameters.

Figure 1 shows the evolution of the experimental density with pressure, at three different temperatures, and the modified Tait equation fitting, for the organoclay suspensions studied. As expected, organoclay suspension density decreases as temperature increases, and increases with pressure. It can be also noticed that the modified Tait equation fits the evolution of the isothermal density fairly well. Tait-like equations have been extensively used by others authors to model volumetric changes of oils as function of pressure and temperature[41,42]. Nevertheless, its application to drilling and completion fluids is very scarce[43]. In Table 3, the fitting parameters values, along with the corresponding AADs and standard deviations, σ, are reported. As can be observed, both the standard deviation and AAD for B34-based fluids are higher than for B128-based ones. The maximum standard deviation and AAD values ($8.24 \cdot 10^{-4}$ g·cm^{-3} and 0.060%, respectively) correspond to the most concentrated B34-based suspension.

The relative deviations of the experimental and calculated densities, $100(\rho_{exp}-\rho_{calc})/\rho_{exp}$, for the SR-10 base oil and suspensions containing 0.03 mass fraction organoclay, in the range of temperature and pressure tested, are shown in Figure 2. As can be noticed, the relative deviations for all these samples are lower than ±0.10%, except for the B34 suspension at 1 bar. Besides, the maximum deviation found in all the organoclay suspensions studied is 0.208% for x_{B34} = 0.01 at 1 bar and 40ºC (see Table 2). Similar deviations have been previously reported when using a Tait-like equation to calculate the densities of liquids systems[44,45,46]. Furthermore, it is worth mentioning that both type of organoclay suspensions show similar density-temperature dependence to that of

synthetic oil-based drilling fluids, as has been reported elsewhere[47]. In addition, it is important to remark that these fluids, at high pressure, are more susceptible to changes in temperature[48].

These results seem to confirm that the proposed modified Tait equation is appropriate to estimate densities under downhole conditions with enough accuracy, from an engineering point of view, to predict possible influx from formations.

In Figure 3, the dependence of the density with the organoclay (B34 left; B128 right) mass fraction in the suspension, at atmospheric pressure and three selected temperatures, is displayed. As expected, the density increases with organoclay concentration, as previously reported by Kole[49] for copper particles in gear oil.

Density shows a linear dependency on organoclay concentration, no matter temperature and pressure (40 to 120ºC and 1 to 1200 bar) are. Table 4 gathers the values of the slope (*r* parameter) of the above-mentioned linear dependence, for the organoclay suspensions studied, at different temperatures and pressures. As can be observed, *r* shows an overall tendency to decrease, at atmospheric pressure, as temperature increases. On the other hand, the values of the slope are higher for B34 than for B128 organoclay suspensions. In addition, the influence of temperature (above 60°C) on the slope for B128 organoclay suspension is much lower than for B34 organoclay suspensions. This fact seems to indicate that the addition of B128 organoclay leads to suspensions with lower susceptibility to temperature, at atmospheric pressure.

Likewise, the influence of pressure on density for each organoclay suspension is also different. For B34 organoclay suspensions at 1200 bar, the slope increases with temperature, showing, in general, lower values than at atmospheric pressure, although the differences decrease as temperature increases. Conversely, higher temperatures yield

a slight reduction in the slope, at 1200 bar, for B128 organoclay suspensions, being its values larger than at atmospheric pressure.

The physical origin of the effect of organoclay concentration on changes in suspension density is not clear. A possible explanation for the different volumetric behavior of the oily fluids studied may be related to the *excess specific volume*. This excess property can be calculated, on mass basis, according to:

$$V^E = \frac{1}{\rho_{susp}} - \sum_{i=1}^{n} \frac{x_i}{\rho_i} \quad (7)$$

where x_i and ρ_i are the mass fraction and density of each component and ρ_{susp} is the suspension density.

In Table 5, the excess volume values for both types of organoclay suspensions, in the range of pressure and temperature studied, are shown. Despite not being strictly an excess property from the thermodynamic point of view, its calculation has been previously carried out aiming to take into account the non-additivity of volume in dispersions[50]. The excess volume values are generally positive for both organoclay suspensions, in the temperature range of 40 to 140º C, at atmospheric and high pressure, except for the least concentrated B128 organoclay suspension. As shown in Table 5, the relationship between excess specific volume and B34 organoclay suspension concentration does not show a clear tendency, at constant temperature and pressure. Otherwise, the B128 suspensions shift, in general, from contractive volumetric behavior to expansive with increasing organoclay concentration. In the case of the lowest concentrated B128 suspension, the negative V^E values might be due to the accommodation of small molecules in the voids provided by the organoclay interlayers, as has been suggested elsewhere[51]. In addition, the non-ideal and predominant expansive volumetric behavior observed for both suspensions might be attributed to the swelling capacity of organoclays in non-aqueous solvents. The macroscopic swelling of

these particles is associated with interactions between the clay surface and the oil medium, as has been previously reported[7,52].Hence, the particular volumetric behavior of each organoclay suspensions could result from the different organic ions/base oil interactions.

Finally, at high pressure, the V^E values for both organoclay suspensions are generally lower, whereas temperature has not a clear effect on this property, as shown in Table 5.

2.2. Derived thermodynamic properties

From the Tait equation proposed to fit the PVT data, the isothermal compressibility, κ_T, has been obtained from an analytical differentiation with respect to pressure, as follows[53]:

$$\kappa_T = \left(\frac{1}{\rho}\right)\left(\frac{\partial \rho}{\partial p}\right)_t = \frac{C}{(B(t)+p)\left[1 - C\ln\left(\frac{(B(t)+p)}{(B(t)+1)}\right)\right]} \tag{8}$$

Similarly, the isobaric thermal expansivity, α_p, can be analytically obtained by differentiating equation (2) with respect to temperature. It is important to mention that the calculated isobaric expansivity depends on the type of $B(t)$ and $\rho_0(t)$ functions used. According to its definition, and the temperature dependence of both $B(t)$ and $\rho_0(t)$, the thermal expansivity can be expressed by the following equation:

$$\alpha_p = \left(-\frac{1}{\rho}\right)\left(\frac{\partial \rho}{\partial t}\right)_p = -\frac{a_1 + 2a_2 t}{\rho_0(t)} - \frac{C(1-p)}{(B(t)+p)(B(t)+1)} \cdot \frac{b_1 + 2b_2 t}{\left[1 - C\ln\left(\frac{(B(t)+p)}{(B(t)+1)}\right)\right]} \tag{9}$$

where the values of C, a_i and b_i parameters are shown in Table 3.

Figure 4 shows the pressure dependence of the isothermal compressibility, calculated from equation (8), for suspensions with different organoclay concentrations, at three selected temperatures; and Table 6 gathers the values of the isothermal compressibility of all the samples studied in the whole temperature and pressure ranges tested. It is

apparent that the isothermal compressibility for the organoclay suspensions decreases as pressure increases, and increase with temperature, as expected. For B34 suspensions, the isothermal compressibility decreases as organoclay concentration increases, although a tendency to reach quite similar values is apparent as pressure increases. However, in the case of B128 suspensions, the influence of organoclay concentration on κ_T is much less significant.

Figure 5 shows the evolution of the isobaric thermal expansivity with pressure for the organoclay suspensions studied, at 100ºC. In addition, Table 7 gathers the values of α_p for the base oil and organoclay suspensions, in the whole range of temperature and pressure tested. As expected, the isobaric thermal expansivity decreases as pressure increases. The thermal expansivity for the B34 suspension with the highest organoclay concentration exhibits a larger pressure susceptibility. On the contrary, the thermal expansivity for B128 organoclay suspensions does not seem to depend on organoclay concentration. Besides, the expansivity-pressure relationship for this type of suspension is very similar to that of the base oil, showing a little decrease in the α_p values of the base oil. These results clearly indicate that the differences found in the derived volumetric properties of these organoclay suspensions are related to suspended particle interactions.

3. Conclusions

The Tait equation describes the pressure-temperature-density behavior of the organoclay suspensions studied fairly well, with a maximum relative error lower than 0.21%. Organoclay addition to the liquid matrix causes a significant increase in density in the whole range of temperature and pressure tested. The organoclay suspensions show a non-ideal volumetric behavior with a positive deviation, which is dampened by increasing pressure. This expansive volumetric behavior is essentially influenced by

organoclay nature and concentration. Similarly, the influence of pressure and temperature on isothermal compressibility and isobaric expansivity of the suspensions is a function of organoclay nature and concentration.

4. References

(1) Liang, Y.; Hilal, N.; Langston, P.; Starov, V. Interactions forces between colloidal particles in liquid: Theory and experiment. *Adv. Colloid Interface Sci.* **2007**, *134 –135*, 151–166.

(2) Stenicka, M.; Pavlínek, V.; Sáha, P.; Blinova, N.V.; Stejskal, J.; Quadrat, O. The electrorheological efficiency of polyaniline particles with various conductivities suspended in silicone oil. *Colloid Polym. Sci.* **2009**, *287*, 403 – 412.

(3) Sinha, R.S. A new possibility for microstructural investigation of clay-based polymer nanocomposites. *Polymer* **2010**, *51*, 3966 – 3970.

(4) Park, B.J.; Fang, F.F.; Choi, H.J. Magnetorheology: Materials and application. *Soft Matter* **2010**, *6*, 5246 – 5253.

(5) Jordan, J.W. Organophilic bentonites. I. Swelling in organic liquids. *J. Phys. Colloid Chem.* **1949**, *53*, 294 – 306.

(6) Hato, M.J.; Zhang, K.; Ray, S.S.; Choi, H.J. Rheology of organoclay suspension. *Colloid Polym. Sci.* **2011**, *289*, 1119 – 1125.

(7) Burgentzle, D.; Duchet, J.; Gérard, J.F.; Jupin, A.; Fillon, B. Solvent-based nanocomposite coatings I. Dispesions of oganophilic montmorillonita in organic solvents. *J. Colloid Interf. Sci.* **2004**, *278*, 26 – 39.

(8) Le Pluart, L.; Duchet, J.; Sautereau, H.; Halley, P.; Gerard, J.F. Rheological properties of organoclay suspensions in epoxy network precursors. *Appl. Clay Sci.* **2004**, *25*, 207 – 219.

(9) Moraru, V.N. Structure formation of alkylammonium montmorillonites in organic media. *Appl. Clay Sci.* **2001**, *19*, 11 – 26.

(10) Paul, D.R.; Robenson, LM. Polymer nanotechnology: Nanocomposites. *Polymer* **2008**, *49*, 3187 – 3204.

(11) Zanetti, M.; Costa, L. Preparation and combustion behavior of polymer/layered silicate nanocomposites based upon PE and EVA. *Polymer* **2004**, *45*, 4367 – 4373.

(12) Kokabi, M.; Sirousazar, M.; Hassan, Z.M. PVA-clay nanocomposite hydrogels for wound dressing. *Eur. Polym. J.* **2007**, *43*, 779 – 781.

(13) Stefanescu, E.A. Recent Industrial Developments in the Fields of Clay-Based Nanocomposites. *Recent Pat. Mater. Sci.* **2010**, *3*, 1 – 12.

(14) Patel, H.A.; Somani, R.S.; Bajaj, H.C.; Jasra, R.V. Nanoclays for polymer nanocomposites, paints, inks, greases, and cosmetics formulations, drug delivery vehicule and waste water treatment. *Bull. Mater. Sci.* **2006**, 29, 133 – 145.

(15) Hermoso, J.; Martínez-Boza, F.; Gallegos, C. Influence of viscosity modifier nature and concentration on the viscous flow behavior of oil-based drilling fluids at high pressure. *Appl. Clay Sci.* **2014**, *87*, 14-21.

(16) Hermoso, J.; Martínez-Boza, F.; Gallegos, C. Combined effect of pressure and temperature on the viscous behaviour of all-oil drilling fluids. *Oil Gas Sci. Technol.* **2014**, *In press* DOI: 10.2516/ogst/2014003.

(17) King, Jr., H.E.; Milner, S.T.; Lin, M.Y.; Singh, J.P.; Mason T.G. Structure and rheology of organoclay suspensions. *Phys. Rev. E.* **2007**, *75*, 021403-1 – 021403- 20.

(18) Williams, H.; Khatri, D.; Vaughan, M.; Landry, G.; Janner, L.; Mutize, B.; Herrera, M. Particle Size Distribution-Engineered Cementing Approach Reduces Need for Polymeric Extenders in Haynesville Shale Horizontal Reach Wells. *SPE Annual Technical and Exhibition Conference*, **2011**, *5*, 4141 – 4161.

(19) Yue, Q.-S.; Yang, Q.Z.; Liu, S.-J.; He, B.-S.; Hu, Y.-L. Rheological properties of water based drilling fluid in deep water drilling conditions. *Appl. Mech. Mater.* **2013**, *318*, 507 – 512.

(20) Luckham, P.F.; Rossi, S. The colloidal and rheological properties of bentonite suspensions. *Adv. Colloid Interface Sci.* **1999**, *82*, 43 – 92.

(21) Demirdal, B.; Cunha, J.C. Importance of drilling fluids´rheological and volumetric characteristization to plan and optimize managed pressure drilling operations. *J. Can. Pet. Technol.,* **2009**, 48, 8 – 14.

(22) Xu, L.; Zhao, L.; Xu, M.B.; Xu, J.; Wang, X. Lab investigations into high temperature high pressure rheology of water-based drilling fluid. *Appl. Mech. Mater.* **2013**, 418, 191 – 195.

(23) Zamora, M.; Roy, S.; Slater, K.; Troncoso, J. Study on the volumetric behavior of base oils, brines, and drilling fluids under extreme temperaturas and pressures. *SPE Drill. Completion.* **2013**, 28, 278 – 288.

(24) Hussein, A.M.O.; Amin, R.A.M. Density measurement of vegetable and mineral based oil used in drilling fluids. *SPE Nigeria Annual International Conference and Exhibition,* **2010**, *1*, 237 – 242.

(25) Demirdal, B.; Miska, S.; Takach, N.; Cunha, J.C. Drilling fluids rheological and volumetric characterization under downhole conditions. *Proceedings of the SPE Latin America and Caribbean Petroleum Engineering Conference*, **2007**, *3*, 1616 – 1623.

(26) Peters, E.J.; Chenevert, M.E.; Zhang, C. Model for predicting the density of oil-based muds at high pressures and temperatures. *SPE Drill. Completion,* **1990**, *5*, 141 – 148.

(27) Demirdal, B.; Cunha, J.C. Olefin-based synthetic-drilling fluids volumetric behavior under downhole conditions. *SPE Drill. Completion,* **2009**, *24*, 239 – 248.

(28) Babu, D.R. Effect of P-ρ-T behavior of water muds on static pressures during deep well drilling. *J. Pet. Sci. Eng.* **1993**, *9*, 341 – 349.

(29) Bouchot, C.; Richon, D. An enhanced method to calibrate vibrating tube densimeters. *Fluid Phase Equilib.* **2001**, *191*, 189 – 208.

(30) Lagourette, B.; Boned, C.; Saint-Guirons, H.; Xans, P.; Zhou, H. Densimeter calibration method versus temperature and pressure. *Meas. Sci. Technol.* **1992**, *3*, 699 – 703.

(31) Niesen, V.G. (Vapor + liquid) equilibria and coexisting densities of (carbon dioxide + n-butane) at 311 to 395 K. *J. Chem. Thermodyn.* **1989**, 21, 915 – 923.

(32) Wagner, W.; Pruss, A. The IAPWS Formulation 1995 for the Thermodynamic Properties of Ordinary Water Substance for General and Scientific Use. *J. Phys. Chem. Ref. Data* **2002**, *31*, 387 – 535.

(33) Lemmon, E.W.; Huber, M.L. Thermodynamic Properties of *n*-Dodecane. *Energy Fuels* **2004**, *18*, 960 – 967.

(34) Davila, M.J.; Alcalde, R.; Aparicio, S. Compressed liquid density measurements for {methylbenzoate + (cyclohexane or 1-hexanol)} binary systems. *J. Chem. Thermodyn.* **2011**, *43*, 1017 – 1022.

(35) Davila, M.J.; Alcalde, R.; Atilhan, M.; Aparicio, S. PρT measurements and derived properties of liquid 1-alkanols. *J. Chem. Thermodyn.* **2012**, *47*, 241 – 259.

(36) Ashcroft, S.J.; Booker, D.R.; Turner, J.C.R. Density measurement by oscillating tube. Effects of viscosity, temperature, calibration and signal processing. *J. Chem. Soc., Faraday Trans.* **1990**, *86*, 145 – 149.

(37) Fandiño, O.; Comuñas, M.J.P.; Lugo, L.; López, E.R.; Fernández, J. Density Measurements under Pressure for Mixtures of Pentaerythritol Ester Lubricants. Analysis of a Density-Viscosity Relationship. *J. Chem. Eng. Data* **2007**, *52*, 1429 – 1436.

(38) Comuñas, M.J.P.; Bazile, J-P.; Baylaucq, A.; Boned, C. Density of Diethyl Adipate using a New Vibrating Tube Densimeter from (293.15 to 403.15 K) and up to 140 MPa. Calibration and Measurements. *J. Chem. Eng. Data* **2008**, *53*, 986 – 994.

(39) Private Communication from Anton Paar. , **2007**.

(40) Taguchi, R.; Machida, H.; Sato, Y.; Smith Jr., R.L. High-pressure densities of 1-alkyl-3-methylimidazolium hexafluorophosphates and 1-alkyl-3-methylimidazolium tetrafluoroborates at temperatures from (313 to 473) K and at pressures up to 200 MPa. *J. Chem. Eng. Data* **2009**, 54, 22 – 27.

(41) Thern, A.; Lüdemann, H.-D. p, T dependence of the self diffusion coefficients and densities in liquid silicone oils. *Z Naturforsch A* **1996**, *51*, 192 – 196.

(42) Regueira, T.; Lugo, L.; Fandiño, O.; López, E.R.; Fernández, J. Compressibilities and viscosities of reference and vegetables oils for their use as hydraulic fluids and lubricants. *Green Chem.* **2011**, *13*, 1293 – 1302.

(43) Khalil, M.; Jan, B.M.; Raman, A.A.A. A tait-like equation for estimating the density of nontraditional super lightweight completion fluid at high pressure and temperature. *Pet. Sci. Technol.***2013**, 31, 44 – 50.

(44) Caudwell, D.R.; Trusler, J.P.M.; Vesovic, V.; Wakeham, W.A. The Viscosity and Density of n-Octadecane at Pressure up to 200 MPa and Temperatures up to 473K. *Int. J. Thermophys.* **2004**, *25*, 1339 – 1352.

(45) Alaoui, F.; Montero, E.; Bazile, J.P.; Comuñas, M.J.P.; Galliero, G.; Boned, C. Liquid density of 1-butanol at pressures up to 140 MPa and from 293.15 K to 403.15 K. *Fluid Phase Equilib.* **2011**, *301*, 131 – 136.

(46) Sagdeev, D.I.; Fomina, M.G.; Mukhamedzyanov, G.Kh.; Abdulagatov, I.M. Experimental study of the density and viscosity of polyethylene glycols and their

mixtures at temperatures from 293 to 465 and at high pressures up to 245 MPa. *Fluid Phase Equilib.* **2012**, *315*, 64 – 76.

(47) Demirdal, B.; Miska, S.; Takach, N.; Cunha, J.C. Drilling fluids rheological and volumetric characterization under downhole conditions. *Proceedings of the SPE Latin America and Caribbean Petroleum Engineering Conference* **2007,** 3, 1616 – 1623.

(48) Demirdal, B.; Cunha, J.C. Olefin-based synthetic-drilling-fluids volumetric behaviour under downhole conditions. *SPE Drilling & Completion* **2009**, 24, 239 – 248.

(49) Kole, M.; Dey, T.K. Enhanced thermophysical properties of copper nanoparticles dispersed in gear oil. *Appl. Therm. Eng.* **2013**, *56*, 45 – 53.

(50) Pastoriza-Gallego, M.J.; Lugo, L.; Legido, J.L.; Piñeiro, M.M. Enhancement of thermal conductivity and volumetric behavior of Fe_xO_y nanofluids., *J. Appl. Phys.* **2011**, *110*, 014309.

(51) Zafarani-Moattar, M. T.; Magdan-Cegincara, R. Effect of temperature on volumetric and transport properties of nanofluids containing ZnO nanoparticles poly(ethylene glycol) and water. *J. Chem. Thermodyn.* **2012**, *54*, 55 – 67.

(52) Minase, M.; Kondo, M.; Onikata, M.; Kawamura, K. The viscosity of organic liquid suspensions of trimethyldococylammonium-montmorillonite complexes. *Clays Clay Miner*. **2008**, *56*, 49 – 65.

(53) Fandiño, O.; Pensado, A.S.; Lugo, L.; Comuñas, M.J.P.; Fernández, J. Compressed liquid densities of squalene and pentaerythritol tetra(2-ethylhexanoate). *J. Chem. Eng. Data*. **2005**, 50, 939 – 946.

Tables

Table 1. Values of A_i coefficients in equation 1.

Coefficients	
A_1 (g·cm^{-3})	-16.13663
A_2 (g·cm^{-3}·ºC^{-1})	-0.00118
$10^6 \cdot A_3$ (g·cm^{-3}· ºC^{-2})	6.71
$10^5 \cdot A_4$ (g·cm^{-3}·bar^{-1})	-5.12
$10^8 \cdot A_5$ (g·cm^{-3}· bar^{-2})	3.83
$10^7 \cdot A_6$ (g·cm^{-3}· ºC^{-1}· bar^{-1})	4.34
$10^6 \cdot A_7$ (g·cm^{-3}·ms^{-2})	2.41
$10^{10} \cdot A_8$ (g·cm^{-3}·ºC^{-1}·ms^{-2})	-4.65
$10^{13} \cdot A_9$ (g·cm^{-3}·ºC^{-2}·ms^{-2})	-9.81
$10^{12} \cdot A_{10}$ (g·cm^{-3}·bar^{-1}·ms^{-2})	6.08
$10^{15} \cdot A_{11}$ (g·cm^{-3}·bar^{-2}·ms^{-2})	-5.31
$10^{14} \cdot A_{12}$ (g·cm^{-3}·ºC^{-1}· bar-1·ms^{-2})	-5.96

Table 2. Experimental density values[a] (ρ_{exp}), and calculated from a modified Tait equation (ρ_{calc}), of the SR-10 oil and the organoclay suspensions, for different mass fractions (x_i), temperatures (t[b]) and pressures (p[c]).

t /ºC	p (bar)	ρ (g·cm^{-3})	$100\cdot(\rho_{exp} - \rho_{calc})/\rho_{exp}$	t /ºC	p (bar)	ρ (g·cm^{-3})	$100\cdot(\rho_{exp} - \rho_{calc})/\rho_{exp}$
SR-10 Base oil						**x_{B34} = 0.01**	
40	1	0.90122	0.047	60	200	0.90043	-0.083
40	200	0.91087	-0.030	60	400	0.91125	-0.061
40	400	0.92068	0.008	60	600	0.92092	-0.030
40	600	0.92948	0.020	60	800	0.92920	-0.049
40	800	0.93714	-0.021	60	1000	0.93720	-0.015
40	1000	0.94494	0.012	60	1200	0.94430	-0.011
40	1200	0.95198	0.012	80	1	0.87600	0.027
60	1	0.88758	-0.001	80	200	0.88948	0.032
60	200	0.89826	-0.060	80	400	0.90116	0.050
60	400	0.90883	-0.014	80	600	0.91117	0.042
60	600	0.91812	-0.011	80	800	0.92015	0.040
60	800	0.92690	0.017	80	1000	0.92809	0.019
60	1000	0.93478	0.013	80	1200	0.93562	0.029
60	1200	0.94227	0.022	100	1	0.86272	-0.018
80	1	0.87474	0.003	100	200	0.87805	0.056
80	200	0.88630	-0.065	100	400	0.89031	0.039
80	400	0.89785	0.010	100	600	0.90090	0.020
80	600	0.90787	0.027	100	800	0.91031	0.009
80	800	0.91672	0.008	100	1000	0.91892	0.015
80	1000	0.92466	-0.036	100	1200	0.92684	0.032
80	1200	0.93232	-0.046	120	1	0.85105	0.088
100	1	0.86301	0.088	120	200	0.86619	-0.004
100	200	0.87488	-0.054	120	400	0.87914	-0.038
100	400	0.88664	-0.041	120	600	0.89052	-0.034
100	600	0.89773	0.029	120	800	0.90008	-0.080
100	800	0.90727	0.030	120	1000	0.90908	-0.070
100	1000	0.91563	-0.015	120	1200	0.91751	-0.031
100	1200	0.92393	0.006	140	1	0.83724	-0.098
120	1	0.85045	0.039	140	200	0.85544	0.042
120	200	0.86379	-0.051	140	400	0.86954	0.057
120	400	0.87737	0.083	140	600	0.88081	-0.011
120	600	0.88787	0.018	140	800	0.89138	0.014
120	800	0.89781	0.010	140	1000	0.90074	0.031
120	1000	0.90706	0.019	140	1200	0.90876	-0.002
120	1200	0.91536	0.001			**x_{B34} = 0.03**	
140	1	0.83823	-0.014	40	1	0.91103	-0.152
140	200	0.85280	-0.077	40	200	0.92346	0.040
140	400	0.86690	0.034	40	400	0.93300	0.023
140	600	0.87830	0.006	40	600	0.94178	0.013
140	800	0.88900	0.030	40	800	0.94968	-0.017
140	1000	0.89836	0.010	40	1000	0.95715	-0.031
140	1200	0.90651	-0.061	40	1200	0.96410	-0.049
		x_{B34} = 0.01		60	1	0.89963	0.072
40	1	0.90442	0.208	60	200	0.91126	0.075
40	200	0.91317	-0.044	60	400	0.92167	0.070
40	400	0.92298	-0.038	60	600	0.93099	0.052
40	600	0.93178	-0.030	60	800	0.93952	0.034
40	800	0.93995	-0.001	60	1000	0.94733	0.010
40	1000	0.94737	0.018	60	1200	0.95461	-0.014
40	1200	0.95441	0.055	80	1	0.88625	0.015
60	1	0.88745	-0.174	80	200	0.89905	0.044

Table 2. Continued

t /ºC	p (bar)	ρ (g·cm^{-3})	$100\cdot(\rho_{exp} - \rho_{calc})/\rho_{exp}$	t /ºC	p (bar)	ρ (g·cm^{-3})	$100\cdot(\rho_{exp} - \rho_{calc})/\rho_{exp}$
		x_{B34} = 0.03				**x_{B34} = 0.05**	
80	400	0.91022	0.042	100	800	0.92349	-0.069
80	600	0.92012	0.023	100	1000	0.93222	-0.059
80	800	0.92903	-0.007	100	1200	0.94134	0.049
80	1000	0.93733	-0.023	120	1	0.86874	0.036
80	1200	0.94499	-0.043	120	200	0.88187	0.024
100	1	0.87400	0.020	120	400	0.89326	-0.041
100	200	0.88795	0.077	120	600	0.90600	0.161
100	400	0.89984	0.079	120	800	0.91409	-0.055
100	600	0.91032	0.062	120	1000	0.92384	-0.008
100	800	0.91977	0.042	120	1200	0.93326	0.068
100	1000	0.92848	0.028	140	1	0.85392	-0.003
100	1200	0.93637	-0.001	140	200	0.86875	-0.031
120	1	0.86206	-0.002	140	400	0.88202	-0.050
120	200	0.87630	-0.004	140	600	0.89617	0.180
120	400	0.88809	-0.081	140	800	0.90458	-0.114
120	600	0.90040	0.056	140	1000	0.91508	-0.077
120	800	0.91019	0.030	140	1200	0.92556	0.035
120	1000	0.91912	0.008			**x_{B128} = 0.01**	
120	1200	0.92730	-0.018	40	1	0.90402	-0.098
140	1	0.85173	0.096	40	200	0.89254	0.065
140	200	0.86567	-0.015	40	400	0.87918	0.030
140	400	0.87805	-0.079	40	600	0.86753	-0.002
140	600	0.89047	0.033	40	800	0.85408	0.026
140	800	0.90068	0.024	40	1000	0.84365	-0.009
140	1000	0.90997	0.015	40	1200	0.91675	0.028
140	1200	0.91839	-0.005	60	1	0.90387	0.071
		x_{B34} = 0.05		60	200	0.90387	-0.015
40	1	0.91774	-0.187	60	400	0.88147	-0.008
40	200	0.92924	0.064	60	600	0.86997	-0.029
40	400	0.93732	0.008	60	800	0.85984	-0.020
40	600	0.94599	0.072	60	1000	0.92642	-0.028
40	800	0.95250	-0.042	60	1200	0.91456	-0.014
40	1000	0.95966	-0.044	80	1	0.90357	-0.008
40	1200	0.96706	0.017	80	200	0.89310	-0.016
60	1	0.90942	0.186	80	400	0.88317	-0.005
60	200	0.91817	0.058	80	600	0.87369	-0.047
60	400	0.92710	0.027	80	800	0.93510	-0.035
60	600	0.93649	0.113	80	1000	0.92386	-0.007
60	800	0.94309	-0.043	80	1200	0.91321	0.007
60	1000	0.95084	-0.025	100	1	0.90381	0.067
60	1200	0.95851	0.025	100	200	0.89431	0.052
80	1	0.89478	-0.061	100	400	0.88496	0.001
80	200	0.90573	-0.039	100	600	0.94353	0.015
80	400	0.91573	-0.033	100	800	0.93251	0.025
80	600	0.92459	-0.071	100	1000	0.92231	0.031
80	800	0.93310	-0.080	100	1200	0.91335	0.001
80	1000	0.94155	-0.039	120	1	0.90424	-0.107
80	1200	0.94995	0.045	120	200	0.89553	-0.023
100	1	0.88199	-0.026	120	400	0.95069	0.014
100	200	0.89379	-0.031	120	600	0.94026	0.008
100	400	0.90469	-0.024	120	800	0.93076	0.011
100	600	0.91568	0.087	120	1000	0.92195	0.005

Table 2. Continued

t /ºC	p (bar)	ρ (g·cm^{-3})	$100\cdot(\rho_{exp} - \rho_{calc})/\rho_{exp}$	t /ºC	p (bar)	ρ (g·cm^{-3})	$100\cdot(\rho_{exp} - \rho_{calc})/\rho_{exp}$
		x_{B128} = 0.01				x_{B128} = 0.03	
120	1200	0.92128	0.010	140	800	0.89892	0.005
140	1	0.84365	0.032	140	1000	0.90802	-0.031
140	200	0.85984	0.005	140	1200	0.91666	-0.024
140	400	0.87369	0.021			**x_{B128} = 0.05**	
140	600	0.88496	-0.039	40	1	0.91965	0.195
140	800	0.89553	-0.018	40	200	0.92709	-0.121
140	1000	0.90501	0.003	40	400	0.93716	-0.046
140	1200	0.91340	-0.002	40	600	0.94584	-0.031
		x_{B128} = 0.03		40	800	0.95376	-0.024
40	1	0.91118	0.076	40	1000	0.96143	0.017
40	200	0.92083	-0.032	40	1200	0.96858	0.054
40	400	0.93051	-0.200	60	1	0.90235	-0.085
40	600	0.93932	-0.006	60	200	0.91444	-0.029
40	800	0.94749	0.019	60	400	0.92501	-0.006
40	1000	0.95491	0.027	60	600	0.93444	0.003
40	1200	0.96181	0.035	60	800	0.94309	0.017
60	1	0.89649	-0.021	60	1000	0.95096	0.020
60	200	0.90782	-0.059	60	1200	0.95844	0.040
60	400	0.91851	-0.024	80	1	0.88895	-0.029
60	600	0.92793	-0.013	80	200	0.90218	0.008
60	800	0.93633	-0.021	80	400	0.91336	-0.012
60	1000	0.94421	-0.012	80	600	0.9235	-0.011
60	1200	0.95156	0.003	80	800	0.93273	-0.005
80	1	0.88324	-0.016	80	1000	0.94104	-0.013
80	200	0.89595	-0.024	80	1200	0.94869	-0.024
80	400	0.90751	0.012	100	1	0.87652	0.041
80	600	0.91740	0.001	100	200	0.89071	0.044
80	800	0.92638	-0.004	100	400	0.90285	0.025
80	1000	0.93457	-0.009	100	600	0.91319	-0.034
80	1200	0.94209	-0.017	100	800	0.92335	0.010
100	1	0.87107	0.052	100	1000	0.93195	-0.021
100	200	0.88476	0.022	100	1200	0.94025	-0.006
100	400	0.89677	0.013	120	1	0.86404	0.012
100	600	0.90698	-0.036	120	200	0.87919	-0.002
100	800	0.91689	0.004	120	400	0.89264	0.037
100	1000	0.92562	0.009	120	600	0.90390	0.012
100	1200	0.93367	0.018	120	800	0.91421	0.019
120	1	0.85862	0.029	120	1000	0.92345	0.015
120	200	0.87363	0.017	120	1200	0.93161	-0.019
120	400	0.88671	0.034	140	1	0.85220	-0.044
120	600	0.89771	0.002	140	200	0.86851	-0.012
120	800	0.90765	-0.010	140	400	0.88249	0.026
120	1000	0.91689	0.008	140	600	0.89414	0.001
120	1200	0.92531	0.021	140	800	0.90470	0.002
140	1	0.84604	-0.073	140	1000	0.91418	-0.003
140	200	0.86298	0.014	140	1200	0.92268	-0.022
140	400	0.87671	0.019				
140	600	0.88848	0.011				

[a]Density uncertainty $u(\rho) = 1\cdot10^{-3}$ g·cm^{-3}
[b] Temperature uncertainty $u(t) = 0.01$ ºC
[c] Pressure uncertainty $u(p) = 8$ bar

Table 3. Modified Tait's equation parameters, and deviations, for SR-10 oil and different organoclay suspensions, in the whole range of pressure and temperature tested

Sample	SR-10	B34			B128		
x_i		0.01	0.03	0.05	0.01	0.03	0.03
a_0 (g·cm^{-3})	0.92829	0.93062	0.94096	0.94085	0.93196	0.93970	0.94988
$10^4 \cdot a_1$ (g·cm^{-3}·ºC^{-1})	-7.05	-7.18	-7.42	-5.00	-6.94	-7.57	-8.43
$10^7 \cdot a_2$ (g·cm^{-3}·ºC^{-2})	4.49	4.09	7.05	-8.60	4.36	6.56	1.06
b_0 (bar)	1841.10	1437.69	1780.57	2357.80	1400.55	1637.74	1835.38
b_1 (bar·ºC^{-1})	-8.95	-8.68	-9.66	-8.38	-6.11	-9.24	-12.69
b_2 (bar·ºC^{-2})	0.01776	0.02160	0.02579	-0.00385	0.00890	0.02145	0.03788
C	0.09190	0.07425	0.08909	0.10518	0.07822	0.08131	0.08335
$10^4 \cdot \sigma$ (g·cm^{-3})	3.99	6.53	6.59	8.24	3.87	3.01	4.89
AAD (%)	0.028	0.044	0.043	0.060	0.025	0.021	0.028

Table 4. Influence of organoclay mass fraction on suspension density: values of the slope *r*, estimated from the linear fitting of both variables (see Figure 4)

t (ºC)	*r* (g·cm^{-3})			
	B34		B128	
	p (bar)		*p* (bar)	
	1	1200	1	1200
40	0.331	0.323	0.370	0.309
60	0.469	0.349	0.279	0.304
80	0.421	0.366	0.271	0.304
100	0.412	0.363	0.255	0.307
120	0.395	0.376	0.264	0.304
140	0.370	0.397	0.254	0.295

Table 5. Influence of organoclay concentration on suspension *excess specific volume*, at different temperatures and pressures.

t (ºC)	$10^3 \cdot V^E$ (cm^3·g^{-1})					
	p (bar)					
	1			1200		
	x_{B34} = 0.01	x_{B34} = 0.03	x_{B34} = 0.05	x_{B34} = 0.01	x_{B34} = 0.03	x_{B34} = 0.05
40	1.288	3.693	6.095	1.948	0.661	6.730
60	5.549	1.062	-0.136	2.449	0.472	5.671
80	3.905	1.802	2.144	1.060	0.150	4.312
100	6.095	3.121	3.577	1.543	0.444	4.687
120	5.047	1.792	4.625	2.482	1.060	4.258
140	7.458	-0.766	8.318	2.418	1.177	3.040
	x_{B128} = 0.01	x_{B128} = 0.03	x_{B128} = 0.05	x_{B128} = 0.01	x_{B128} = 0.03	x_{B128} = 0.05
40	0.920	2.409	4.257	-2.325	2.027	3.269
60	-1.244	3.852	6.641	-1.618	2.727	3.909
80	-0.591	4.544	7.636	-2.485	2.304	3.872
100	-0.700	5.290	8.827	-1.913	2.429	4.081
120	0.511	5.337	9.048	-2.345	2.277	4.318
140	-1.984	6.027	8.843	-3.540	2.129	4.574

Table 6. Isothermal compressibility values for SR-10 oil and organoclay suspensions with different disperse phase mass fractions

$10^5 \cdot \kappa_T$ (bar^{-1})	p (bar)						
	1	200	400	600	800	1000	1200
t (°C)	SR-10 (base fluid)						
40	6.08	5.43	4.91	4.49	4.14	3.84	3.58
60	6.71	5.94	5.32	4.83	4.43	4.09	3.80
80	7.42	6.48	5.76	5.19	4.72	4.34	4.02
100	8.17	7.05	6.21	5.55	5.03	4.60	4.24
120	8.98	7.64	6.66	5.92	5.33	4.85	4.45
140	9.81	8.24	7.11	6.27	5.61	5.09	4.66
	x_{B34}= 0.01						
40	6.59	5.67	4.98	4.44	4.02	3.67	3.37
60	7.46	6.30	5.46	4.82	4.33	3.92	3.59
80	8.41	6.97	5.96	5.21	4.64	4.18	3.81
100	9.43	7.66	6.46	5.59	4.94	4.43	4.01
120	10.48	8.33	6.93	5.95	5.22	4.65	4.20
140	11.47	8.95	7.36	6.26	5.46	4.85	4.36
	x_{B34}= 0.03						
40	6.20	5.51	4.96	4.52	4.15	3.84	3.57
60	6.88	6.04	5.39	4.87	4.45	4.09	3.79
80	7.59	6.58	5.82	5.22	4.73	4.34	4.01
100	8.30	7.11	6.22	5.55	5.01	4.57	4.20
120	8.96	7.59	6.59	5.84	5.24	4.77	4.37
140	9.53	7.99	6.90	6.08	5.44	4.93	4.51
	x_{B34}= 0.05						
40	5.21	4.79	4.44	4.13	3.87	3.64	3.44
60	5.71	5.21	4.79	4.44	4.14	3.88	3.65
80	6.32	5.72	5.22	4.80	4.46	4.16	3.90
100	7.10	6.34	5.74	5.24	4.83	4.48	4.18
120	8.11	7.14	6.38	5.78	5.28	4.87	4.52
140	9.48	8.18	7.20	6.45	5.84	5.35	4.94
	x_{B128}= 0.01						
40	6.68	5.78	5.10	4.57	4.14	3.79	3.49
60	7.33	6.26	5.47	4.87	4.38	3.99	3.67
80	8.07	6.79	5.87	5.18	4.64	4.21	3.85
100	8.90	7.37	6.30	5.52	4.91	4.43	4.04
120	9.83	8.00	6.76	5.86	5.19	4.65	4.22
140	10.86	8.68	7.24	6.23	5.47	4.88	4.41
	x_{B128}= 0.03						
40	6.24	5.47	4.88	4.41	4.02	3.70	3.43
60	7.00	6.05	5.34	4.78	4.33	3.96	3.65
80	7.84	6.67	5.82	5.16	4.64	4.23	3.88
100	8.75	7.32	6.30	5.54	4.95	4.48	4.10
120	9.69	7.97	6.78	5.91	5.25	4.72	4.30
140	10.61	8.59	7.23	6.25	5.52	4.94	4.48
	x_{B128}= 0.05						
40	6.00	5.31	4.76	4.32	3.96	3.65	3.40
60	6.88	5.99	5.30	4.76	4.33	3.97	3.67
80	7.84	6.70	5.85	5.21	4.69	4.28	3.93
100	8.81	7.40	6.38	5.62	5.03	4.56	4.17
120	9.70	8.02	6.84	5.98	5.32	4.79	4.37
140	10.39	8.48	7.18	6.24	5.52	4.96	4.51

Table 7. Isobaric expansivity values for SR-10 oil and organoclay suspensions with different disperse phase mass fractions

$10^4 \cdot \alpha_p$ (°C^{-1})				p (bar)			
	1	200	400	600	800	1000	1200
t (°C)				SR-10 (base fluid)			
40	7.43	6.89	6.45	6.09	5.78	5.52	5.29
60	7.34	6.75	6.28	5.90	5.58	5.30	5.07
80	7.24	6.61	6.11	5.71	5.38	5.10	4.87
100	7.14	6.46	5.95	5.54	5.21	4.93	4.70
120	7.03	6.33	5.81	5.41	5.08	4.81	4.58
140	6.91	6.22	5.71	5.32	5.01	4.75	4.54
				x_{B34}= 0.01			
40	7.60	6.90	6.37	5.95	5.62	5.34	5.10
60	7.53	6.76	6.20	5.76	5.42	5.13	4.90
80	7.46	6.64	6.05	5.61	5.27	4.99	4.76
100	7.38	6.53	5.95	5.53	5.19	4.93	4.71
120	7.29	6.48	5.93	5.54	5.24	5.00	4.81
140	7.21	6.48	6.01	5.68	5.44	5.24	5.08
				x_{B34}= 0.03			
40	7.51	6.93	6.47	6.08	5.76	5.49	5.25
60	7.31	6.70	6.22	5.83	5.51	5.24	5.01
80	7.10	6.48	6.01	5.63	5.32	5.06	4.84
100	6.88	6.28	5.84	5.49	5.20	4.97	4.77
120	6.64	6.12	5.73	5.42	5.18	4.98	4.82
140	6.40	5.99	5.68	5.45	5.27	5.12	4.99
				x_{B34}= 0.05			
40	6.19	5.78	5.43	5.12	4.86	4.62	4.41
60	6.65	6.15	5.73	5.37	5.06	4.79	4.55
80	7.13	6.51	6.00	5.57	5.20	4.88	4.60
100	7.62	6.84	6.21	5.68	5.24	4.86	4.52
120	8.14	7.12	6.31	5.66	5.11	4.65	4.25
140	8.68	7.29	6.23	5.39	4.70	4.12	3.63
				x_{B128}= 0.01			
40	7.28	6.75	6.34	6.02	5.76	5.54	5.35
60	7.19	6.60	6.16	5.81	5.53	5.30	5.11
80	7.10	6.44	5.96	5.59	5.30	5.06	4.86
100	7.00	6.27	5.76	5.37	5.06	4.82	4.61
120	6.89	6.09	5.54	5.13	4.82	4.57	4.36
140	6.78	5.91	5.33	4.90	4.58	4.32	4.12
				x_{B128}= 0.03			
40	7.73	7.10	6.61	6.21	5.88	5.60	5.36
60	7.56	6.87	6.34	5.92	5.57	5.29	5.05
80	7.38	6.63	6.08	5.64	5.30	5.01	4.77
100	7.18	6.41	5.84	5.41	5.08	4.80	4.57
120	6.98	6.21	5.66	5.25	4.94	4.68	4.47
140	6.77	6.04	5.55	5.19	4.91	4.68	4.50
				x_{B128}= 0.05			
40	8.26	7.53	6.94	6.46	6.06	5.72	5.43
60	7.93	7.13	6.51	6.01	5.61	5.26	4.97
80	7.58	6.75	6.12	5.64	5.24	4.92	4.64
100	7.21	6.42	5.83	5.39	5.04	4.75	4.51
120	6.82	6.16	5.68	5.32	5.04	4.82	4.63
140	6.42	5.98	5.68	5.45	5.27	5.13	5.02

Figure Captions

Figure 1. Evolution of the experimental density with pressure, at three different temperatures, and modified Tai's equation fitting, for the organoclay suspensions studied.

Figure 2. Relative deviations of experimental and calculated (modified Tait's equation) densities for SR-10 oil and organoclay suspensions (x_i = 0.03).

Figure 3. Influence of organoclay mass fraction on suspension density (temperature: 40, 100 and 140ºC; pressure: 1 bar).

Figure 4. Pressure dependence of the compressibility, as a function of suspension organoclay concentration, at different temperatures.

Figure 5. Pressure dependence of the thermal expansivity, as a function of suspension organoclay concentration, at 100ºC.

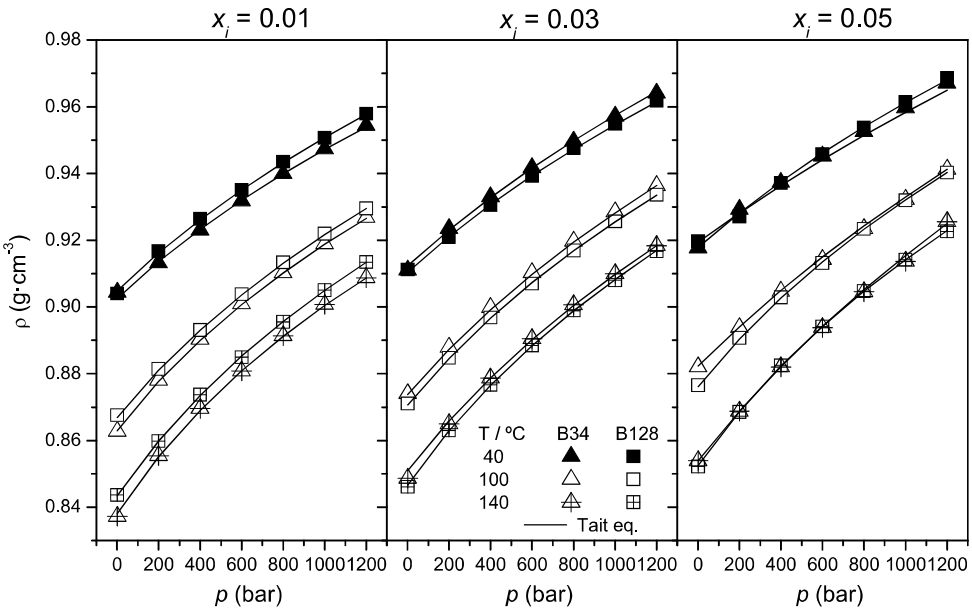
x_i = 0.01
x_i = 0.03
x_i = 0.05
ρ (g·cm^{-3})
0.98
0.96
0.94
0.92
0.90
0.88
0.86
0.84
0 200 400 600 800 1000 1200
p (bar)
T / °C
B34
B128
40
100
140
Tait eq.

Figure 1

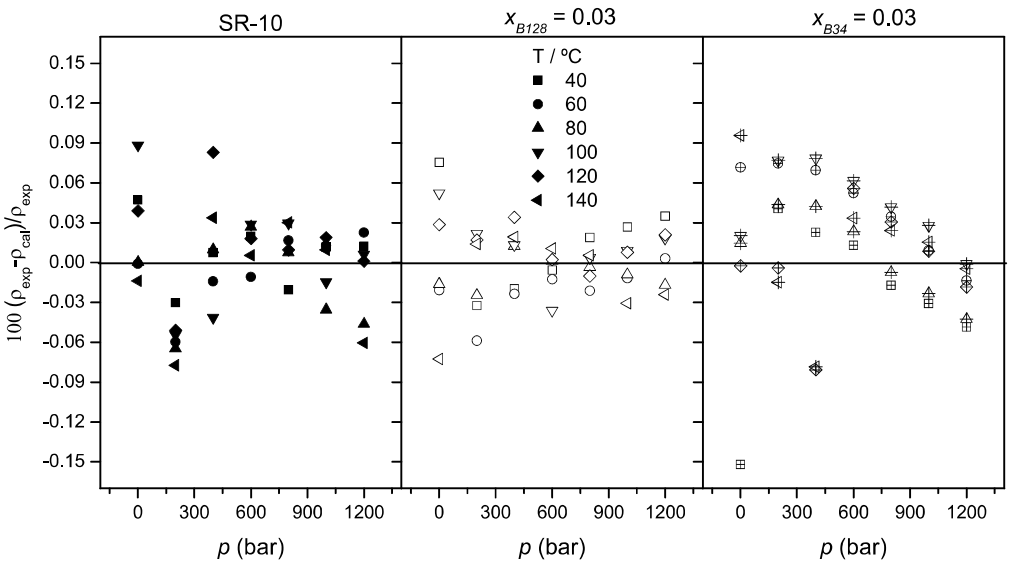
SR-10
x_{B128} = 0.03
x_{B34} = 0.03
T / °C
40
60
80
100
120
140
100 (ρ_{exp} -ρ_{cal})/ρ_{exp}
0.15
0.12
0.09
0.06
0.03
0.00
-0.03
-0.06
-0.09
-0.12
-0.15
0
300
600
900
1200
p (bar)

Figure 2

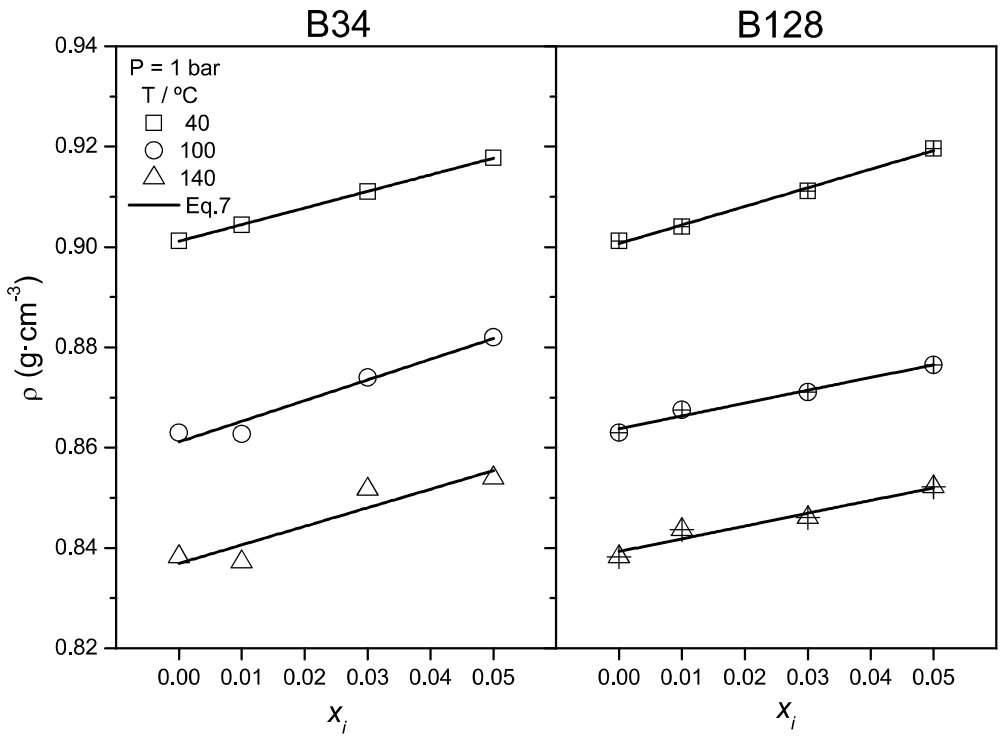
B34
B128
P = 1 bar
T / °C
40
100
140
Eq.7
ρ (g·cm-3)
0.94
0.92
0.90
0.88
0.86
0.84
0.82
0.00
0.01
0.02
0.03
0.04
0.05
xi

Figure 3

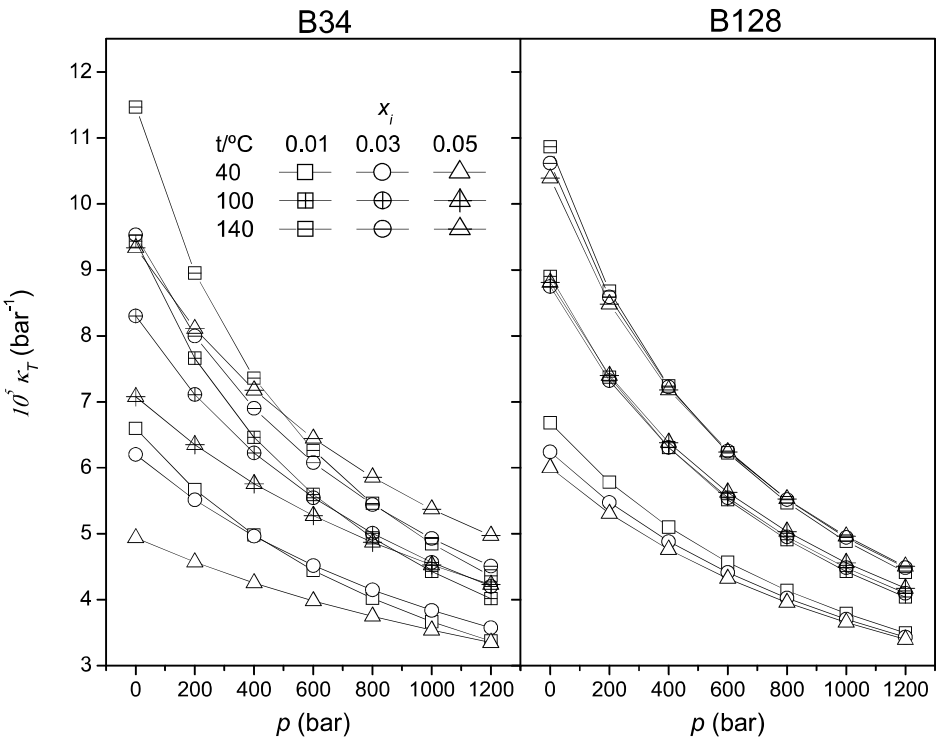

Figure 4

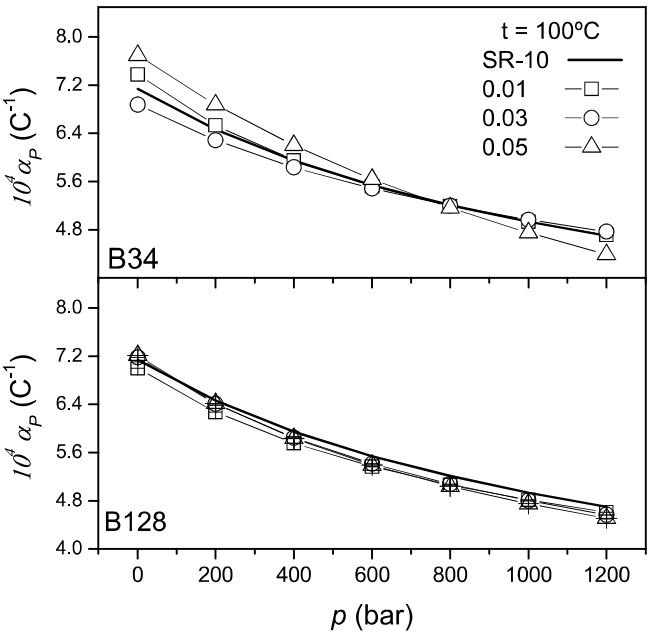
t = 100ºC
SR-10
0.01
0.03
0.05
B34
B128
$10^4 \alpha_P$ (C^{-1})
p (bar)
8.0
7.2
6.4
5.6
4.8
4.0
0
200
400
600
800
1000
1200

Figure 5

4.6. Viscosity-Pressure-Temperature Behaviour of All-oil Suspensions Drilling Fluids

4.6.1. Abstract

Finally, in this chapter the pressure-density-temperature data (PρT), presented in Chapter 4.5., the pressure-viscosity-temperature data (PηT), presented in chapter 4.2 and 4.3, and calorimetric data were used to model the evolution with both pressure and temperature of the viscosity of the drilling fluids, by using the different Equation of State (EoS) and empirical model such as Murnaghan EoS, Fillers-Moonan-Tschoegl's (FMT), Yasutomi's and the WLF-Barus' models.

Differential scanning calorimetry (DSC) tests were carried out with a DSC-Q100 calorimeter to determine the glass transition of the samples. Density and viscosity determination was conducted as has been explained in previous chapters.

As expected, a nearly linear decrease in density with temperature is observed for all samples in the range of temperature studied. Temperature and pressure exert an opposite influence on the volumetric behaviour, being the influence of temperature more relevant as compared to that of pressure. Likewise, bentonite suspensions are slightly more susceptible to temperature than the base oil. In the range of pressure tested, both oil and organoclay suspensions show a qualitatively similar linear increase in the bulk modulus with pressure suggesting that the volumetric behaviour for these suspensions is determined by that of the base oil.

The thermopiezoviscous behaviour of these materials can be modelled using equations developed for thermopiezorheologically simple materials, such as the FMT, the Yasutomi or the empirical WLF-Barus factorial model. In this work, the approach is based on selecting characteristic rheological parameters, such as the Newtonian viscosity, in the case of the base oil, or the plastic viscosity (η_p) of the organoclay suspensions, to eliminate the complex shear-rate dependence of the piezoviscous behaviour, fitting the model equations to these selected shear-rate independent parameters.

At constant temperature, viscosity increases exponentially with pressure in the range of pressure tested, and all the three models tested can predict the evolution of the viscosity of drilling fluids with pressure and temperature. In this sense, free-volume models, based on physical parameters, do fit the viscosity-pressure-temperature data fairly well, showing similar or even lower error than some well-known empirical exponential equations.

Pressure-volume-temperature and pressure-temperature-viscosity behaviours of organobentonite suspensions

J. Hermoso*, F. Martínez-Boza, C. Gallegos

Departamento de Ingeniería Química, Centro de Investigación de Tecnología de Productos y Procesos Químicos (Pro^{2}TecS). Universidad de Huelva. Facultad de Ciencias Experimentales. Campus del Carmen. 21071 Huelva (Spain)

Phone: +34 959219985; juan.hermoso@diq.uhu.es

Keywords: High pressure rheology, viscosity, PVT, suspension

* Author to whom correspondence should be addressed

Abstract

Organoclays suspensions are commonly used as drilling fluids in environments where they are submitted to high pressure and temperature for long periods of time. Consequently, both volumetric and thermorheological properties are among their most important quality parameters concerning this application.

The overall objective of this work was to study the pressure and temperature dependence of both viscosity and density for organoclay suspensions. With this aim, pressure-density-temperature data (PVT) were used to model the evolution with pressure and temperature of the volumetric properties of the drilling fluids, by using the Murnaghan equation. On the other hand, the pressure-temperature-viscosity behaviour was modelled by using different equations, such as Fillers-Moonan-Tschoegl's (FMT), Yasutomi's and WLF-Barus' models. All these models predict the evolution of the viscosity of drilling fluids with pressure and temperature, for engineering purposes, fairly well.

1. Introduction

Organoclay suspensions are commonly used as drilling fluids due to their capacity to form gels and their suitable viscous properties. These fluids are submitted to high pressure and temperature in the well during drilling operations [1, 2]. The successful completion of an oil well and its cost depend, on a considerable extent, on the properties of these fluids. Hence, one of the most interesting points for the drilling industry is the characterization of their thermophysical properties. Both, viscosity and density have been the two most extensively studied properties of organoclay dispersions used as drilling fluids. When drilling fluids are pumped down, they experience compression and expansion effects related to the increase or decrease of temperature and pressure along the wellbore. Density variations might be significant and its control is a challenging goal to minimize associated risks, and improve security and efficiency, particularly for non-aqueous systems [3, 4]. Several authors have investigated the combined influence of pressure and temperature on the density of drilling fluids [5-7]. However, few papers have been focused on the characterisation of the pressure-volume-temperature relationship for this type of dispersions [8].

In addition, the rheological behaviour of organoclay dispersions is a critical issue in the success of drilling operations. Data concerning the influence of high pressure and temperature on the viscous properties of these types of suspensions are relatively scarce [9, 10]. However, knowledge of the flow behaviour of clay-based drilling fluids, as a function of temperature and pressure, is of a paramount importance in order to solve different important issues, such as excessive torque, gelation, hole cleaning, etc [11].

The thermopiezoviscous behaviour of fluids is a relevant issue for engineering applications involving processes at high pressure and temperature. The influence of pressure, temperature and shear rate on the viscosity of fluids has been extensively

analysed [12-18]. In this sense, different equations based on the friction theory [19, 20], the free-volume concept [21-25], and empirical correlations [26-30] have been proposed to model the combined effect of temperature and pressure on the rheological properties of materials.

The overall objective of this work was to study the influence of pressure and temperature on viscosity and density of organoclay suspensions. With this aim, pressure-density-temperature data (PVT) were used to model the evolution with the above-mentioned variables of the volumetric properties of the drilling fluids, by using the Murnaghan equation. Finally, using rheological, PVT, and calorimetric data, the pressure-temperature-viscosity behaviour of these suspensions was modelled using different equations, such as Fillers-Moonan-Tschoegl's (FMT), Yasutomi's and WLF-Barus' models

2. Experimental

2.1. Materials

Two commercially available organoclays, denoted as B34 and B128 and provided by Elementis (Belgium), were used in the present study.

A mineral based lubricating oil, SR10 (0.916 $g \cdot cm^{-3}$ at 40ºC) supplied by Verkol (Spain), was used as base oil for the formulation of organoclay dispersions.

2.2 Preparation of organoclay dispersions

Organoclay dispersions were prepared by mixing the organoclay (5% wt.) in SR10 oil base, using a high mixer Ultraturrax (Ika, Germany), at room temperature, at 9000 rpm for five minutes. Prior to its high shear processing, the organoclay was wetted with the oil for 1 hour at room temperature.

2.3. Density measurements

Two vibrating tube densimeters were used to measure the density, ρ, of the samples studied. At atmospheric pressure, an Anton Paar DMA 5000 (Austria) was employed to measure the density of SR10 oil and organoclay dispersions between 40ºC and 100ºC. Prior to performing density measurements with oil and organoclay dispersions at atmospheric pressure, the DMA 5000 densimeter was calibrated, as function of temperature, using both dry air and degasified bi-distilled water as recommended by the manufacturer. The results obtained were compared with the values reported in Anton Paar's manual for air and water in the temperature range used. For this densimeter, the manufacturer cited an uncertainty for temperature of ±0.01ºC, and density of $\pm 5 \cdot 10^{-6}$ $g \cdot cm^{-3}$, between 0ºC and 100 ºC.

An Anton Paar DMA HPM high-pressure vibrating tube (Austria) was used to measure the density in the temperature range comprised between 40ºC and 140ºC, and pressures up to 1200 bar. The temperature of the high-pressure vibrating tube was controlled by an external circulating bath using silicone. The temperature was maintained constant within ±0.01ºC. A manual piston intensifier (HiP, USA) was used to control the pressure of the system. The pressure applied was measured by a pressure transducer model HP-2-S (Wika, Germany) with an uncertainty of less than 0.5% between 0 and 1600 bar.

The calibration of the HPM vibrating cell, in the entire range of pressure and temperature analysed, was performed by using a polynomial expression as a function of temperature, pressure and oscillation period given by Anton Paar:

$$\rho = A_1 + A_2 T + A_3 T^2 + A_4 P + A_5 P^2 + A_6 T \cdot P + (A_7 + A_8 T + A_9 T^2 + A_{10} P + A_{11} P^2 + A_{12} T \cdot P) \cdot \tau^2 \quad (1)$$

where, ρ is the density of the fluid in $g \cdot cm^{-3}$, T the measured temperature in ºC, P is the pressure applied in bar, τ is the oscillation period in ms, and A_i the coefficients of the

high-pressure densimeter. These coefficients were evaluated by non-linear regression of equation (1) to standard densities for both dodecane [31] and water [32].

Taking into account the accuracies of temperature, pressure, period of oscillation, water and dodecane densities, and equation (1) fitting for the reference fluids (0.07% for water and 0.1% for dodecane), the overall experimental uncertainty in oil and organoclay suspensions densities is estimated to be $\pm 1 \cdot 10^{-3}$ g·cm^{-3}. This uncertainty is similar to that previously reported in the literature [33, 34].

2.4. Rheological measurements

Viscous flow measurements were performed using a controlled stress rheometer, MARS II from Thermo Scientific (Germany). Rheological data were obtained using different geometries: a conventional coaxial cylinder geometry (41 mm inner diameter, 1 mm gap, 60 mm length) and a serrated plate-and-plate geometry (35 mm diameter, 1 mm gap) for rheological tests at atmospheric pressure; a coaxial cylinder geometry (38 mm diameter, 80 mm length) and a double helical ribbon (DHR) geometry (36 mm diameter, 78 mm length), coupled with a pressure cell (D400/200), for measurements at high pressure. DHR is a non-conventional geometry, calibrated with a Newtonian fluid and several shear-thinning fluids, in the pressure range used in the present study [35]. The cell D400/200 is a pressure vessel of 39 mm inner diameter. Inside the cell, the coaxial cylinder and the double helical ribbon geometry were put in contact with a sapphire surface, at the bottom of the vessel, by a steel needle. The inner geometry was equipped, at the top, with a secondary magnetic cylinder (36 mm diameter, 8 mm length), magnetically coupled to a tool outside the cell, which was connected to the motor-transducer of the rheometer. The pressure cell was connected to a hydraulic pressurization system, which consists of two units, a high pressure valve and a hand pump (Enerpac, USA), connected by a high pressure line. The pressure cell was

pressurized using, as pressurizing liquid, the same fluid to be tested. A pressure transducer GMH 3110 (Gresingeg Electronic, Germany), able to measure differential pressures ranging from 0 to 400 bar (0.1 bar resolution), was used.

Steady-state viscosity measurements, at different differential pressures (0, 100, 200, 300 and 390 bar) and temperatures (40, 80, 100, 120 and 140ºC), were performed in a shear rate range dependent on sample viscosity. The temperature in the high pressure cell was regulated with circulating silicone bath (DC30 Thermo Scientific, Germany), with an uncertainty of ±0.1ºC.

2.5 Differential Scanning Calorimetry

Differential scanning calorimetry (DSC) tests were carried out with a DSC-Q100 calorimeter (TA Instruments, USA), using 5-10 mg samples sealed in hermetic aluminium pans. The sample was purged with dry nitrogen at a flow rate of 50 mL/min, to avoid any condensation of moisture. First, the pans where placed onto the cell at room temperature, then were heated at 80ºC, kept at this temperature for 5 minutes to reach the thermodynamic equilibrium, and subsequently, the samples were quenched-cooled to –80ºC, at 10ºC/min, kept for 5 minutes at this temperature to reach the equilibrium, and, finally, heated, at 10ºC/min, up to 180ºC. The glass transition temperature was determined from the inflection point of the step-like decrease in the heat flow.

3. Results and Discussion

3.1. Viscous flow behaviour

Figure 1 shows the steady-state viscous flow curves of the samples studied (SR10 oil, and B34 and B128 suspensions), at 80ºC and pressures of 1 and 390 bar. In the case of the suspensions, the steady-state viscous flow curves were obtained after upward and downward shear stress sweep tests, as has been described by the authors elsewhere [36,

37].

As can be observed in Figure 1, the viscous behaviour of the SR10 oil is Newtonian in the pressure range of 1-390 bar, at 80ºC. This oil also behaves as a Newtonian liquid for the whole range of temperature tested (40-140ºC). In contrast, organoclay suspensions show a shear-thinning behaviour, exhibiting a Bingham-law dependence of viscosity with shear rate in the whole range of pressure and temperature tested (1-390 bar; 40-140ºC), as has been previously reported [36].

The Newtonian viscosity of the SR10 oil sample increases up to 2.13 times from atmospheric pressure to 390 bar, at 80ºC. However, the viscosity-pressure relationship for the organoclay suspensions is more complex, depending on both bentonite nature and shear rate. For example, the plastic viscosity increases ā2.11 times for B34 sample and ā2.22 times for B128 sample, in the above-mentioned range of pressure. Nevertheless, at a shear rate of 1 s^{-1}, the plastic viscosity increases ā2.68 times for B34 sample and ā1.34 times for B128 sample. This complex piezoviscous behaviour has been related to the development of complex molecular structures with different sensitivities to pressure and shear rate [38].

The thermopiezoviscous behaviour of these materials can be modelled using equations developed for thermopiezorheologically simple materials, such as the FMT [39], the Yasutomi [40] or the empirical WLF-Barus factorial model [36]. The approach is based on selecting characteristic rheological parameters, such as the Newtonian viscosity, in the case of the SR10 oil, or the plastic viscosity (η_p) of the organoclay suspensions, to eliminate the complex shear-rate dependence of the piezoviscous behaviour, fitting the model equations to these selected shear-rate independent parameters.

Viscosity-pressure-temperature models can be also classified as either only based on empirical parameters or based on some physical properties. Thus, the FMT model takes

into account the pressure dependence of the bulk modulus and the expansivity. The pressure dependence of these properties can be obtained from the evolution of the density with pressure and temperature using the Murnaghan EoS. The Yasutomi model is described as a function of the glass transition temperature, which can be obtained from DSC measurements. The WLF-Barus model describes the thermopiezoviscous behaviour using empirical parameters for both temperature and pressure. To apply either FMT's or Yasutomi's model based on physical properties, the bulk modulus or the glass transition temperature should be previously determined by additional experiments.

3.2. Density-pressure-temperature behaviour

Figures 2-4 show the values of the density for the different samples studied, as a function of pressure (1-1200 bar) and temperature (40ºC up to 140ºC). As expected, a nearly linear decrease in density with temperature is observed for all samples in the range of temperature studied. Temperature and pressure exert an opposite influence on the volumetric behaviour. The decrease in density when temperature is raised from 40ºC to 140ºC is compensated by an increase in pressure from 1 to ~1056 bar, for the SR 10 oil and even slightly higher for both bentonite suspensions (up to ~1105 and ~1060 for B34 and B128, respectively). Thus, the influence of temperature is more relevant as compared to that of pressure. On the basis of this analysis, both bentonite suspensions, B34 and B128, are slightly more susceptible to temperature than the base oil, showing the B34 suspension the lowest susceptibility to pressure, at 140°C. These drilling fluids show quite similar temperature susceptibility to that of the synthetic oil-based drilling fluids studied by Demirdal et al. [4], at low pressure. On the contrary, these fluids show higher temperature susceptibility than those studied by Demirdal and Cunha [7] at high pressure.

The experimental evolution of the density, ρ, with both temperature and pressure can be

described by the Murnaghan equation [41]:

$$\frac{\rho}{\rho_0(0,T)} = \left(\frac{K_e(T) + k_e P}{K_e(T) + k_e P_{ref}} \right)^{1/k_e} \tag{2}$$

being

$$\rho_0(0,T) = a_0 + a_1(T - T_{ref}) + a_2(T - T_{ref})^2 + a_3(T - T_{ref})^3 \tag{3}$$

$$K_e(T) = K_e^* \exp(-\lambda(T - T_{ref})) \tag{4}$$

The polynomial function, $\rho_0(0,T)$, represents the evolution of the density, at the reference pressure, where T_{ref} is the reference temperature (80ºC) and a_0, a_1, a_2, and a_3 are fitting parameters, whose values, for the samples studied, are presented in Table 1. $K_e(T)$ represents the temperature dependence of the bulk modulus of the entire volume, being K_e^* the bulk modulus at zero pressure and temperature of reference; k_e is an empirical constant, the Bridgman constant, that implies a linear dependence of the bulk modulus with pressure [24]; and λ defines the temperature dependence of the bulk modulus at any given pressure [42] ($\lambda = m \cdot \alpha_e^*$, being m an empirical constant and α_e^* the thermal expansivity of the entire volume at cero pressure and temperature of reference). The values of K_e^*, k_e and λ are also presented in Table 1.

As can be seen in Figures 2-4, the Murnaghan equation describes the density evolution in the range of temperature and pressure studied fairly well. This equation has been extensively used by other authors to fit data of volumetric properties, as a function of temperature and pressure, of rubbery polymers [42] and heavy petroleum fractions [43]. For these samples, the values of the percent average absolute deviation (%AARD), shown in Table 1, are lower than 0.07, indicating that this model is suitable for oil-based drilling fluids.

The evolution of the bulk modulus of the entire volume, K_e, with pressure, at the

reference temperature (80ºC), is shown in Figure 5. The Murnaghan equation predicts a linear increase of the bulk modulus with pressure, as follows:

$$K_e(P) = K_e^* + k_e P \tag{5}$$

In the range of pressure tested, both oil and organoclay suspensions show a qualitatively similar linear increase in the bulk modulus with pressure. This fact suggests that the volume-pressure behaviour for these suspensions is determined by that of the base oil, as has been pointed out by other authors [7]. The values of the bulk modulus, calculated from PVT data, at 1 bar and 80ºC, are similar and slightly higher than those obtained for n-paraffinic based drilling fluids [4] and mineral oil-based mud [5, 6] respectively, being the pressure susceptibility slightly higher for the suspensions studied.

The evolution of the expansivity, $\alpha_e(P)$, at constant temperature (80ºC), for the oil and suspension samples studied is shown in Figure 6. A decrease in the expansivity values with pressure is observed for all the samples. According to the Murnaghan EoS, the isothermal expansivity can be described as follows:

$$\alpha_e(P) = \alpha_e^* \left(1 - \frac{mP}{K_e^* + k_e P} \right) \tag{6}$$

Values for both the expansivity of the entire volume, α_e^*, and the empirical parameter, m, are also presented in Table 1. As can be observed, the organoclay suspensions present expansivity values at cero pressure slightly higher than the SR10 oil, more significantly for B34 suspension, indicating that these suspensions are more compressible than the base oils. This fact suggests an increase in the free volume fraction of the suspension due to interactions between the oil and the organic chains of the organobentonite. Nevertheless, this effect vanishes as pressure increases, being the expansivities of the suspensions similar to that of the base oil at 400 bar, and even lower at higher pressures. These oil-based drilling fluids show lower expansivity values than

those formulated with mineral and vegetal oils, as reported by Hussein et al. [3].

3.3. Temperature-pressure-viscosity relationship

The FMT model has been successfully used for modelling the pressure and temperature dependence of heavy and intermediate fuel and recycled oils viscosities [43, 44, 45]. Models based on molecular theories have the advantage of predicting the evolution of the rheological properties on the basis of the temperature-pressure evolution of some physical properties, such as expansivity and compressibility in the case of the FMT model. This model expresses the viscosity-pressure-temperature relationship as a function of molecular parameters:

$$\ln\left(\frac{\eta}{\eta_{ref}}\right) = -\frac{2.303 \cdot c_1^{00}(T - T_{ref} - \theta(P))}{c_2(P) + (T - T_{ref} - \theta(P))} \tag{7}$$

being

$$\theta(P) = c_3(P)\ln\left(\frac{1 + c_4 P}{1 + c_4 P_{ref}}\right) - c_5(P)\ln\left(\frac{1 + c_6 P}{1 + c_6 P_{ref}}\right) \tag{8}$$

$$c_1^{00} = B / 2.203 f_0 \tag{9}$$

$$c_2(P) = f_0 / \alpha_f(P) \tag{10}$$

$$c_3(P) = 1 / k_e \alpha_f(P) \tag{11}$$

$$c_4 = k_e / K_e^* \tag{12}$$

$$c_5(P) = 1 / k_\phi \alpha_f(P) \tag{13}$$

$$c_6 = k_\phi / K_\phi^* \tag{14}$$

$$\alpha_f(P) = \alpha_e(P) - \alpha_\phi(P) = \alpha_f^*\left(1 - \frac{mP}{K_e^* + k_e P}\right) - m\alpha_\phi^* P\left(\frac{1}{K_e^* + k_e P} - \frac{1}{K_\phi^* + k_\phi P}\right) \tag{15}$$

where, η_{ref} is the viscosity at the reference temperature and pressure; f_0 is the fractional free-volume at the reference temperature; B is a constant; $\alpha_f(P)$ is the expansivity of the

free-volume, considered pressure dependent and temperature independent; α_f^* is the expansivity of the free volume at zero pressure and temperature of reference, $\alpha_{\hat{u}}^*$ is the expansivity of the occupied volume at zero pressure and temperature of reference; K_ϕ^* are the bulk moduli of occupied volume, at zero pressure and temperature of reference; k_ϕ is the Bridgman constant for the occupied volume, the superscript *00* indicates temperature and pressure of reference.

With the coefficients K_e^*, k_e and m determined from density measurements, the experimental viscosities can be used to determine the remaining parameters of the model (η_{ref}, B, f_0, $k_{\hat{u}}$, $K_{\hat{u}}^*$, α_f^*, $\alpha_{\hat{u}}^*$), by fitting the set of equations (7) to (15), where η_{ref} depends on the temperature and pressure of reference, arbitrarily selected, and $\alpha_f^*, \alpha_{\hat{u}}^*$ are constrained by the PVT behaviour since $\alpha_e^* = \alpha_f^* + \alpha_{\hat{u}}^*$. The values obtained for these parameters are shown in Table 2.

Among the models based on the free-volume concept, the Yasutomi model [25] has been extensively applied to model the pressure-temperature-viscosity relationship for polyethylene and different lubricant oils [46]. This model includes material properties at the glassy state:

$$\log\left(\frac{\eta}{\eta_g}\right) = -\frac{c_1(T-T_g)F}{c_2+(T-T_g)F} \tag{16}$$

where η_g is the viscosity at T_g, the glass transition temperature, which is a function of pressure:

$$T_g = T_{go} + A_1 \ln(1 + A_2(P - P_{ref})) \tag{17}$$

and F is the free volume expansivity,

$$F = 1 - B_1 \ln(1 + B_2(P - P_{ref})) \tag{18a}$$

being the expression for an improved definition [40]:

$$F = 1 + B_1 (P - P_{ref})^{B_2} \tag{18b}$$

where T_{go} is the gas transition temperature at reference pressure; and c_1, c_2, A_1, A_2, B_1 and B_2 the parameters to be evaluated.

The range of pressure tested in this research is much narrower than that normally covered for lubricant studies [25]. Consequently, the viscosity-pressure evolution is simpler than that obtained for lubricant oils submitted to higher pressure. In these cases, the Yasutomi equation would be overparameterized, leading to several set of parameters from the regression procedure of the viscosity-pressure data. Consequently, in this fitting process, η_g and B_2 have been arbitrarily set to 10^{12} Pa·s and 1 respectively, using the T_{go} values from DSC measurement as additional fixed parameters. The results obtained for the remaining parameters are shown in Table 3.

Finally, the WLF-Barus model combines two well-known exponential equations, the WLF and a generalized version of the Barus equation, to describe both temperature and pressure effects on the viscosity:

$$\eta = \eta_{ref} \exp\left[\left(-\frac{2.303 \cdot c_1 (T - T_{ref})}{c_2 + (T - T_{ref})}\right)\left((\beta_0 + \beta_1 (T - T_{ref}))(P - P_{ref})\right)\right] \tag{19}$$

where c_1 and c_2 are empirical constants. The piezoviscous coefficient, β_s, has been linearized with temperature in order to generalize the model. The results obtained from the application of the WLF-Barus model to the viscosity data are shown in Table 4.

Figure 7 shows the evolution with pressure of the Newtonian viscosity, for SR10 oil, and the plastic viscosity, for B34 and B128 drilling fluids, at the reference temperature (80ºC). It can be seen that, at constant temperature, viscosity increases exponentially with pressure in the range of pressure tested. In addition, all the three models tested describe the isothermal evolution of viscosity with pressure, for engineering purposes,

fairly well.

In Figure 8, the experimental viscosity data (in the range 1-400 bar and 40-140ºC) of the samples studied and the calculated ones by using different models are compared (Figure 8a: FMT's model; Figure 8b: Yasutomi's model; and Figure 8c: WLF-Barus' model). As can be seen, the largest deviations between experimental and calculated values are observed for B34 and B128 drilling fluids, at 140ºC. These deviations, previously explained by the authors [36], are a consequence of the influence, on the rheological behaviour of these drilling fluids, of the gelation process induced at high temperature. Excluding the results obtained at the above-mentioned temperature (140ºC), the three models fit the experimental results, in the whole range of temperature and pressure tested, fairly well (average error less than 5%). Nevertheless, on the basis of the %AARD and relative deviation, each model behaves differently depending on the sample. Thus, both FMT's and WLF-Barus' models show similar deviations and lower %AARD values for the SR10 oil (~ 2.3%, see Tables 2-4). B34 drilling fluid shows the highest values of %AARD and lowest R^2 correlation coefficient for any model tested, being WLF-Barus' model the best fit for this sample. On the contrary, Yasutomi's model shows the lowest values of the %AARD for the B128 drilling fluid. The use of an empirical exponential function of temperature and pressure to model viscosity data of water-based drilling fluids, oil-based drilling fluids [47] and invert oil mud [48] is very common for engineering purposes, being the average error higher than those found in this research (around 5% [49] or even higher [50]).

4. Conclusions

From the experimental results obtained, it can be concluded that bentonite-in-oil suspension densities are more susceptible to changes in temperature than to pressure. The Murnaghan equation describes the PVT behaviour, in the range of temperature and

pressure studied, fairly well.

Different models can predict the evolution of the viscosity of drilling fluids with pressure and temperature. In this sense, free-volume models, based on physical parameters, do fit the viscosity-pressure-temperature data fairly well, showing similar or even lower error than some well-known empirical exponential equations.

Acknowledgments

This work is part of a research project sponsored by a CICE-FEDER programme (research project TEP-3895). The authors gratefully acknowledge the financial support received.

References

[1] H. Williams, D. Khatri, M. Vaughan, G. Landry, L. Janner, B. Mutize, M. Herrera, Particle size distribution-engineered cementing approach reduces need for polymeric extenders in Haynesville Shale horizontal reach wells. SPE Annual Technical and Exhibition Conference 5 (2011) 4141 – 4161.

[2] Q.-S. Yue, Q.Z. Yang, S.-J. Liu, B.-S. He, Y.-L. Hu, Rheological properties of water based drilling fluid in deep water drilling conditions. Appl. Mech. Mater. 318 (2013) 507 – 512.

[3] A.M.O. Hussein, R.A.M. Amin, Density measurement of vegetable and mineral based oil used in drilling fluids. SPE Nigeria Annual International Conference and Exhibition 1 (2010) 237 – 242.

[4] B. Demirdal, S. Miska, N. Takach, J.C. Cunha, Drilling fluids rheological and volumetric characterization under downhole conditions. Proceedings of the SPE Latin America and Caribbean Petroleum Engineering Conference 3 (2007) 1616 – 1623.

[5] E.J. Peters, M.E. Chenevert, C. Zhang, Model for predicting the density of oil-based muds at high pressures and temperatures. SPE Drilling & Completion 5 (1990) 141 – 148.

[6] T. Hemphill, P. Isambourg, New model predicts oil, synthetic mud densities. Oil Gas J. 103 (2005) 56 – 58.

[7] B. Demirdal, J.C. Cunha, Olefin-based synthetic-drilling-fluids volumetric behaviour under downhole conditions. SPE Drilling & Completion 24 (2009) 239 – 248.

[8] Babu, D.R. Effect of P-ρ-T behaviour of water muds on static pressures during deep well drilling. J. Pet. Sci. Eng. 9 (1993) 341 – 349.

[9] S.-Y. Zhao, J.-N. Yan, Y. Shu, H.-X. Zhang, Rheological properties of oil-based drilling fluids at high temperature and high pressure. J. Cent. South Univ. Technol. 15 (2008) 457 − 461.

[10] R.A. Gandelman, R.A.F. Leal, J.T. Gonyalves, A.F.L. Aragao, R.F. Lomba, Martins, A.L., Study on gelation and freezing phenomena of synthetic drilling fluids in ultradeepwater environments. SPE/IADC Drilling Conference 2 (2007) 1013 – 1020.

[11] K. Shahbazi, S.A. Metha, R.G. Moore, M.G. Ursenbanch, K.C.V. Fraassen, Oxidation as a rheology modifier and a potential cause of explosions in oil and synthetic-based drilling fluids. International Symposium on Oilfield Chemistry, Houston, February 28 – March 2 (2007) 157-165.

[12] J. Hron, J. Málek, K.R. Rajagopal, Simple flows of fluids with pressure-dependent viscosities. Proc. R. Soc. A 457 (2001) 1603 – 1622.

[13] J. Málek, J. Neĉas, K.R. Rajagopal, Global analysis of the flows of fluids with pressure-dependent viscosities. Arch. Ration. Mech. Anal. 165 (2002) 243 – 269.

[14] M. Franta, J. Malek, K.R. Rajagopal, On steady flows of fluids with pressure-and-shear-dependent viscosities. Proc. R. Soc. A 461 (2005) 651 – 670.

[15] J. Málek, K.R. Rajagopal, Incompressible rate type fluids with pressure and shear-rate dependent material moduli. Nonlinear Anal.: Real World Appl. 8 (2007) 156 – 164.

[16] K.R. Rajagopal, G. Saccomandi, The mechanics and mathematics of the effect of pressure on the shear modulus of elastomers. Proc. R. Soc. A 465 (2009) 3859 – 3874.

[17] K.R. Rajagopal, G. Saccomandi, L.Z. Vergori, Stability analysis of the Rayleigh-Benard convection for a fluid with temperature and pressure dependent viscosity. Z. Angew. Math. Phys. 60 (2009) 739 – 755.

[18] M. Bulíček, J. Málek, K.R. Rajagopal, Mathematical analysis of unsteady flows of fluids with pressure, shear-rate, and temperature dependent material moduli that slip at

solid boundaries. SIAM J. Math. Anal. 41 (2009) 665 – 707.

[19] S.E. Quiñones-Cisneros, C.K. Zeberg-Mikkelsen, E.H. Stenby, The friction theory (*f-theory*) for viscosity modeling. Fluid Phase Equilib. 169 (2000) 249 − 276.

[20] S.E. Quiñones-Cisneros, U.K. Deiters, Generalization of the friction theory for viscosity modeling. J. Phys. Chem. B 110 (2006) 12820 − 12834.

[21] A.K. Doolittle, D.B. Doolittle, J. Appl. Phys. 28 (1957) 901− 905.

[22] H. Kashiwagi, T. Makita, Viscosity of twelve hydrocarbon liquids in the temperature range 298-348 K at pressures up to 110 MPa. Int. J. Thermophys. 3 (1982) 289 – 305.

[23] N.W. Tschoegl, W.G. Knauss, I. Emri, The effect of temperature and pressure on the mechanical properties of thermo-and/or piezorheologically simple polymeric materials in thermodynamic equilibrium –a critical review. Mech. Time-Dependent Mat. 6 (2002) 53 – 99.

[24] R.W. Fillers, N.W. Tschoegl, Effect of pressure on the mechanical properties of polymers. Trans. Soc. Rheol. 21 (1977) 51 – 100.

[25] S. Yasutomi, S. Bair, W.O. Winer, An application of a free volume model to lubricant rheology I–Dependence of viscosity on temperature and pressure. J. Tribol. 106 (1984) 291 – 302.

[26] D. Berthe, P. Vergne, High pressure rheology for high pressure lubrication: A review. J. Rheol. 34 (1990) 639-655.

[27] J. Sorab, W. E. Vanarsdale, Correlation for the pressure and temperature dependence of viscosity. Tribol. Trans. 34 (1991) 604 – 610.

[28] S. Bair, J. Jarzynski, W.O. Winer, The temperature, pressure and time dependence of lubricant viscosity. Tribol. Int. 34 (2001) 461 - 468.

[29] K. R. Harris, L. A. Woolf, M. Kanakubo, Temperature and pressure dependence of the viscosity of the ionic liquid 1-butyl-3-methylimidazolium Hexafluorophosphate. J. Chem. Eng. Data 50 (2005) 1777 – 1782.

[30] A. Baylaucq, M.J.P. Comuñas, C. Boned, A. Allal, J. Fernández, High pressure viscosity and density modelling of two polyethers and two dialkyl carbonates. Fluid Phase Equilib. 199 (2002) 249 – 263.

[31] E.W. Lemmon, M. Huber, Thermodynamic properties of n-dodecane. Energy & Fuels 18 (2004) 960 – 967.

[32] W. Wagner, A. Pruss, The IAPWS formulation 1995 for the thermodynamic properties of ordinary water substance for general and scientific use. J. Phys. Chem. Ref. Data 31 (2002) 387 – 535.

[33] M.J. Dávila, R. Alcalde, S. Aparicio, Compressed liquid density measurements for {methylbenzoate + (cyclohexane or 1-hexanol)} binary systems. J. Chem. Thermodyn. 43 (2011) 1017 – 1022.

[34] M.J. Dávila, R. Alcalde, M. Atilhan, S. Aparicio, PρT measurements and derived properties of liquid 1-alkanols. J. Chem. Thermodyn. 47 (2012) 241 – 259.

[35] J. Hermoso, B.D. Jofore, F.J. Martínez-Boza, C. Gallegos, High pressure mixing rheology of drilling fluids. Ind. Eng. Chem. Res. 51 (2012) 14399 – 14407.

[36] J. Hermoso, F.J. Martínez-Boza, C. Gallegos, Combined effect of pressure and temperature on the viscous behaviour of all-oil drilling fluids. Oil & Gas Sci. and Tech. "In press" (2014). DOI: 10.2516/ogst/2014003.

[37] M.J. Martín-Alfonso, F.J. Martínez-Boza, P. Partal, C. Gallegos, Influence of pressure and temperature on the flow behaviour of heavy fuel oils. Rheol. Acta 45 (2006) 357 – 365.

[38] B.E. Poling, J.M. Prausnitz, J.P. O´Connell, The properties of gases and liquids, 5th Ed. McGraw-Hill. New York, 2001.

[39] W.H. Moonan, N.W. Tschoegl, Effect of pressure on the mechanical properties of polymers. 2. Expansivity and compressibility measurements. Macromolecules 16 (1983) 55 – 59.

[40] S. Bair, C. Mary, N. Bouscharain, P. Vergne, An improved Yasutomi correlation for viscosity at high pressure. Proc. Inst. Mech. Eng., Part J. 227 (2013) 1056 – 1060.

[41] F.D. Murnaghan, Finite deformation of an elastic solid. Wiley. New York, 1951.

[42] Y.A.Fakhreddine, P. Zoller, Equation of state of a polydimethylsiloxane fluid. J. App. Polym. Sci. 41 (1990) 1087 – 1093.

[43] M.J. Martín-Alfonso, F.J. Martínez-Boza, F.J. Navarro, M. Fernández, C. Gallegos, Pressure-temperature-viscosity relationship for heavy petroleum fractions. Fuel 86 (2007) 227 – 233.

[44] F. J. Martínez-Boza, M. J. Martín-Alfonso, C. Gallegos, M. Fernández, High-pressure behavior of intermediate fuel oils. Energy & Fuels 25 (2011) 5138– 5144.

[45] F. Martinez-Boza, F. Fernandez-Latorre, and C. Gallegos, High-pressure viscosity of used motor oil/vacuum residue blends. Fuel, 88 (2009) 1595–1601.

[46] S. Bair, High-pressure, high-shear stress rheology of polybutene. J. Non-Newtonian Fluid Mech. 97 (2001) 53 – 65.

[47] O.H. Houwen, T. Geehan, Rheology of oil-base muds. SPE paper 15416. SPE Annual Technical Conference and Exhibition, New Orleans, October 5-8, 1986.

[48] M.D. Politte, Invert oil mud rheology as a function of temperature and pressure. SPE paper 13458. SPE/IADC Drilling Conference, New Orleans, March 6-8, 1985.

[49] B. Demirdal, J.C. Cunha, Importance of drilling fluids´ rheological and volumetric characterization to plan and optimize managed pressure drilling operations. J. Can. Pet. Technol. 48 (2009) 8 – 14.

[50] E. Santoyo, A. Garcia, J.M. Morales, E. Contreras, G. Espinosa-Paredes. Effective thermal conductivity of Mexican geothermal cementing systems in the temperature range from 28 C to 200 C. Appl. Thermal Eng. 21 (2001) 1799–1812.

TABLES

Table 1. Murnaghan's equation fitting parameters of PVT data modelling for the samples studied.

Parameters	**SR10**	**B34**	**B128**
a_0 (g·cm^{-3})	0.8747	0.8946	0.8898
a_1 (g·cm^{-3}ºC^{-1})	-6.24·10^{-4}	-6,6·10^{-4}	-6.46·10^{-4}
a_2 (g·cm^{-3}·ºC^{-2})	4.9·10^{-6}	-5·10^{-7}	7·10^{-7}
a_3 (g·cm^{-3}·ºC^{-3})	-4·10^{-9}	4·10^{-9}	-7·10^{-9}
k_e	9.50	9.51	9.49
K_e* (bar)	1.358·10^{4}	1.49·10^{4}	1.357·10^{4}
λ (ºC^{-1})	4.8·10^{-3}	6.3·10^{-3}	5.3·10^{-3}
m	6.734	8.536	7.290
α_e* (ºC^{-1})	7.14·10^{-4}	7.38·10^{-4}	7.27·10^{-4}
Statistics			
Residual Sum of Squares	4.8·10^{-6}	3.2·10^{-5}	1.4·10^{-5}
R^2	0.999	0.999	0.999
Standard Deviation	3.6·10^{-4}	9.4·10^{-4}	6.3·10^{-4}
% AARD	0.026	0.070	0.041

Table 2. Values of the different FMT model parameters for the samples studied (T_{ref} = 80ºC; P_{ref} = 1 bar).

Parameters	**SR10**	**B34**	**B128**
η_{ref} (Pa·s)	0.016	0.028	0.059
B	0.389	0.419	0.353
f_0	0.091	0.097	0.096
$k_{\hat{u}}$	10.0	8.6	8.4
$K_{\hat{u}}^*$ (bar)	3.1·10^{4}	4.30·10^{4}	4.40·10^{4}
α_f^* (ºC^{-1})	7.10·10^{-4}	7.30·10^{-4}	7.10·10^{-4}
$\alpha_{\hat{u}}^*$ (ºC^{-1})	4·10^{-6}	8·10^{-6}	1.6·10^{-5}
Statistics			
Residual Sum of Squares	0.022	0.103	0.041
R^2	0.998	0.985	0.993
Standard Deviation	0.03	0.08	0.05
% AARD	2.30	5.41	3.93

Table 3. Values of the different parameters of the modified Yasutomi model for the samples studied (T_{ref} = 80ºC; P_{ref} = 1 bar).

Parameters	**SR10**	**B34**	**B128**
η_g (Pa·s)	$1 \cdot 10^{12}$	$1 \cdot 10^{12}$	$1 \cdot 10^{12}$
c_1	16.05	15.81	15.06
c_2 (ºC)	23.71	24.43	20.31
T_{g0} (ºC)	-61.8	-63.5	-63.5
A_1	79689	110.63	197.59
A_2 (bar^{-1})	$5.5 \cdot 10^{-7}$	$4.458 \cdot 10^{-4}$	$2.891 \cdot 10^{-4}$
B_1(bar^{-1})	1	1	1
B_2	$-3.51 \cdot 10^{-3}$	$-1.74 \cdot 10^{-3}$	$-2.73 \cdot 10^{-3}$
Statistics			
Residual Sum of Squares	0.107	0.080	0.026
R^2	0.991	0.988	0.995
Standard Deviation	0.065	0.073	0.041
% AARD	4.84	4.78	2.83

Table 4. Values of the different parameters of the WLF-Barus model for the samples studied (T_{ref} = 80ºC; P_{ref} = 1 bar).

Parameters	**SR10**	**B34**	**B128**
η_{ref} (Pa·s)	0.016	0.029	0.060
c_1	1.69	1.84	1.58
c_2 (ºC)	120.0	137.7	138.7
β_0 (bar^{-1})	$2.00 \cdot 10^{-3}$	$1.94 \cdot 10^{-3}$	$2.04 \cdot 10^{-3}$
β_1 (bar^{-1}·ºC^{-1})	$-1.4 \cdot 10^{-5}$	$-2.2 \cdot 10^{-5}$	$-2.1 \cdot 10^{-5}$
Statistics			
Residual Sum of Squares	0.022	0.073	0.034
R^2	0.998	0.989	0.994
Standard Deviation	0.029	0.070	0.047
% AARD	2.36	3.98	3.43

Figure Captions

Figure 1. Experimental steady-state viscous flow curves, and Bingham's model fitting, for SR-10 oil, B34 and B128-based drilling fluids (T= 80°C; P = 1 and 390 bar).

Figure 2. Experimental density values, and Murnaghan's equation fitting, for SR-10 oil, as a function of pressure and temperature.

Figure 3. Experimental density values, and Murnaghan's equation fitting, for B34-based drilling fluid, as a function of pressure and temperature.

Figure 4. Experimental density values, and Murnaghan's equation fitting, for B128-based drilling fluid, as a function of pressure and temperature.

Figure 5. Evolution of the entire bulk modulus for SR-10 oil, B34 and B128-based drilling fluids, as function of pressure, at 80ºC.

Figure 6. Evolution of the thermal expansivity for SR-10 oil and oil-based drilling fluids, as a function of pressure, at 80ºC.

Figure 7. Experimental and estimated viscosities, using FMT, Yasutomi and WLF-Barus models, for SR-10 oil and drilling fluids, as a function of pressure, at 80ºC.

Figure 8. Comparison of experimental and estimated viscosities by using a) FMT's model; b) Yasutomi's model and c) WLF-Barus' model.

Figure 1
Click here to download high resolution image

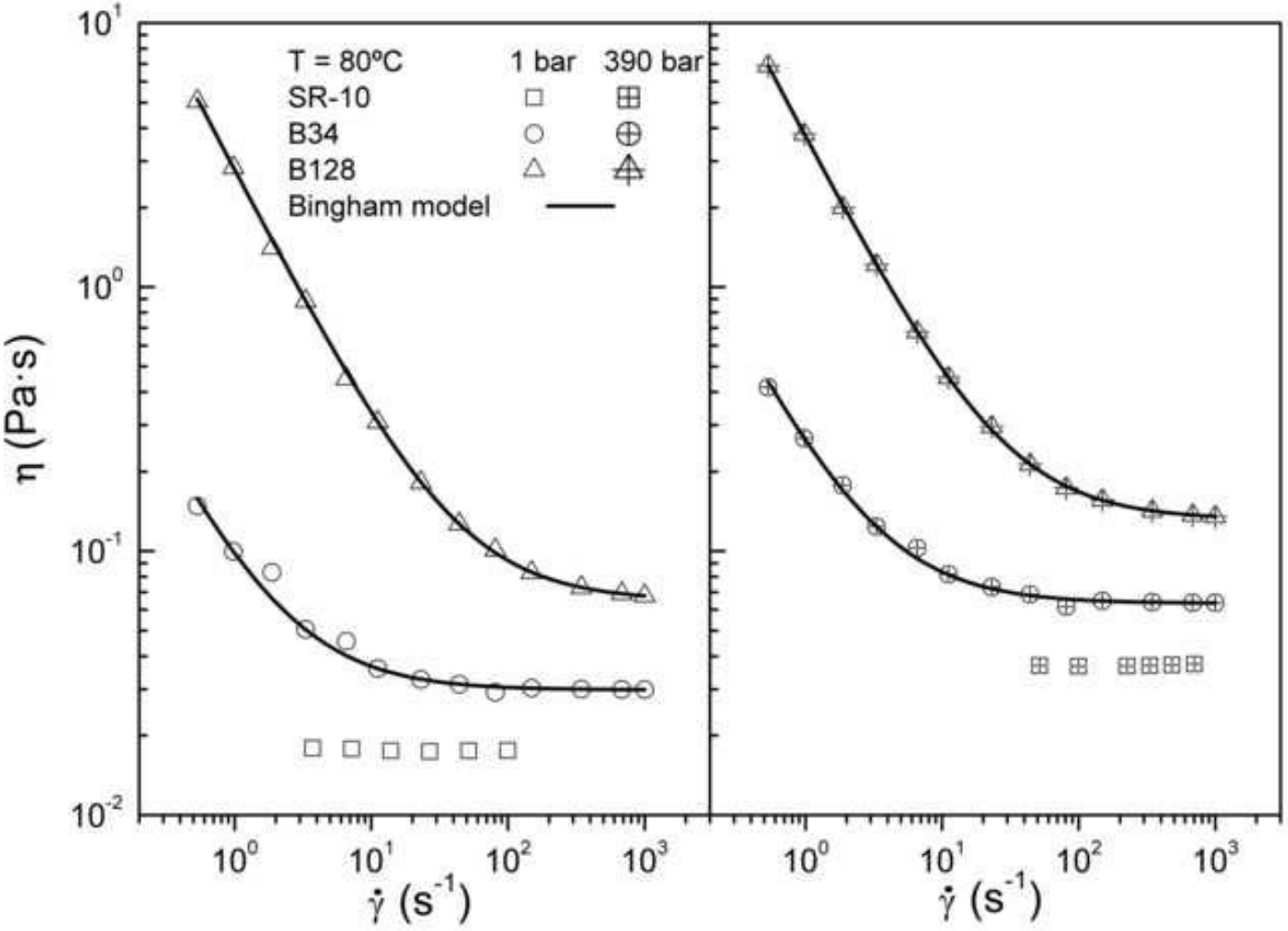

Figure 2

Click here to download high resolution image

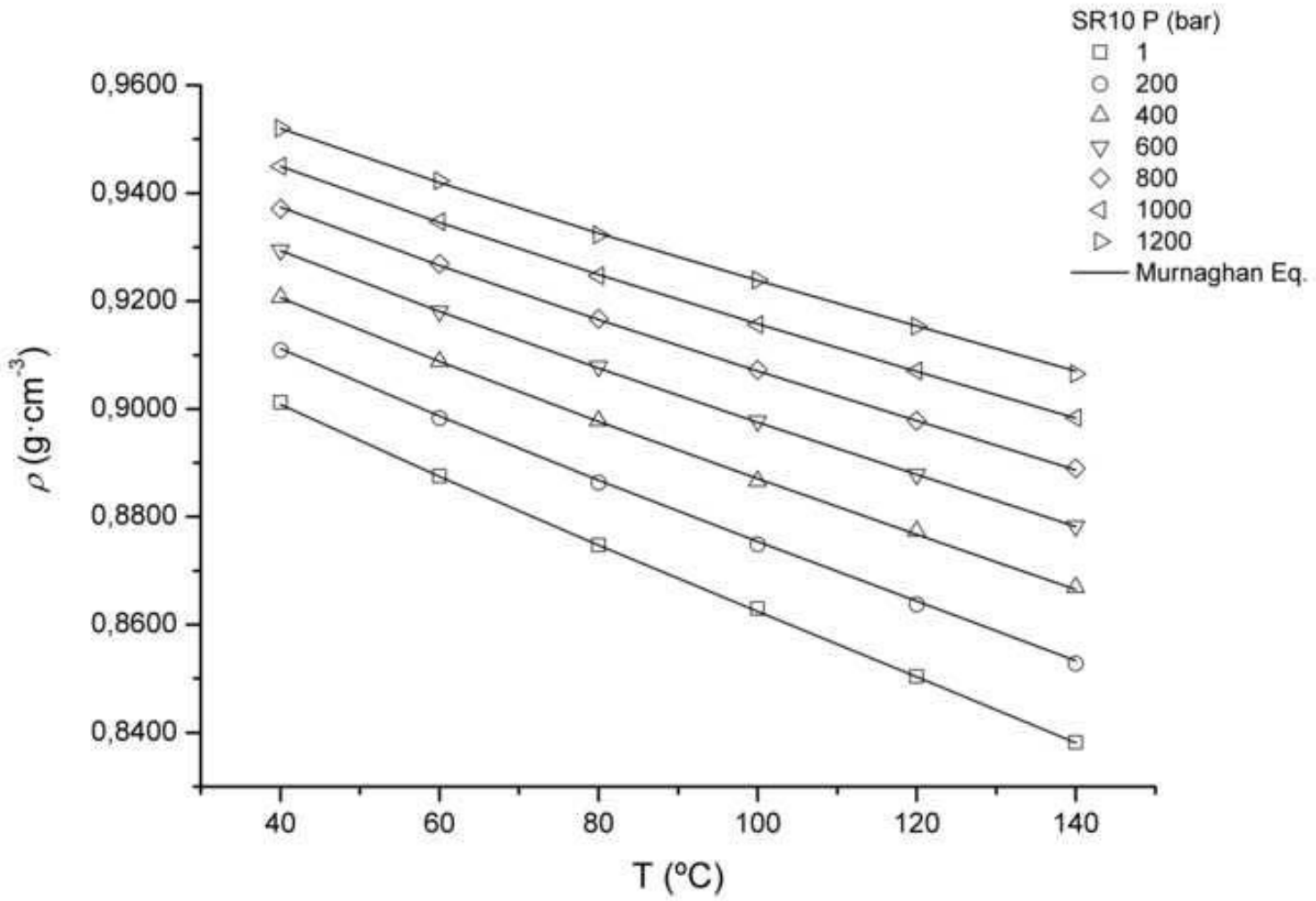

Figure 3
Click here to download high resolution image

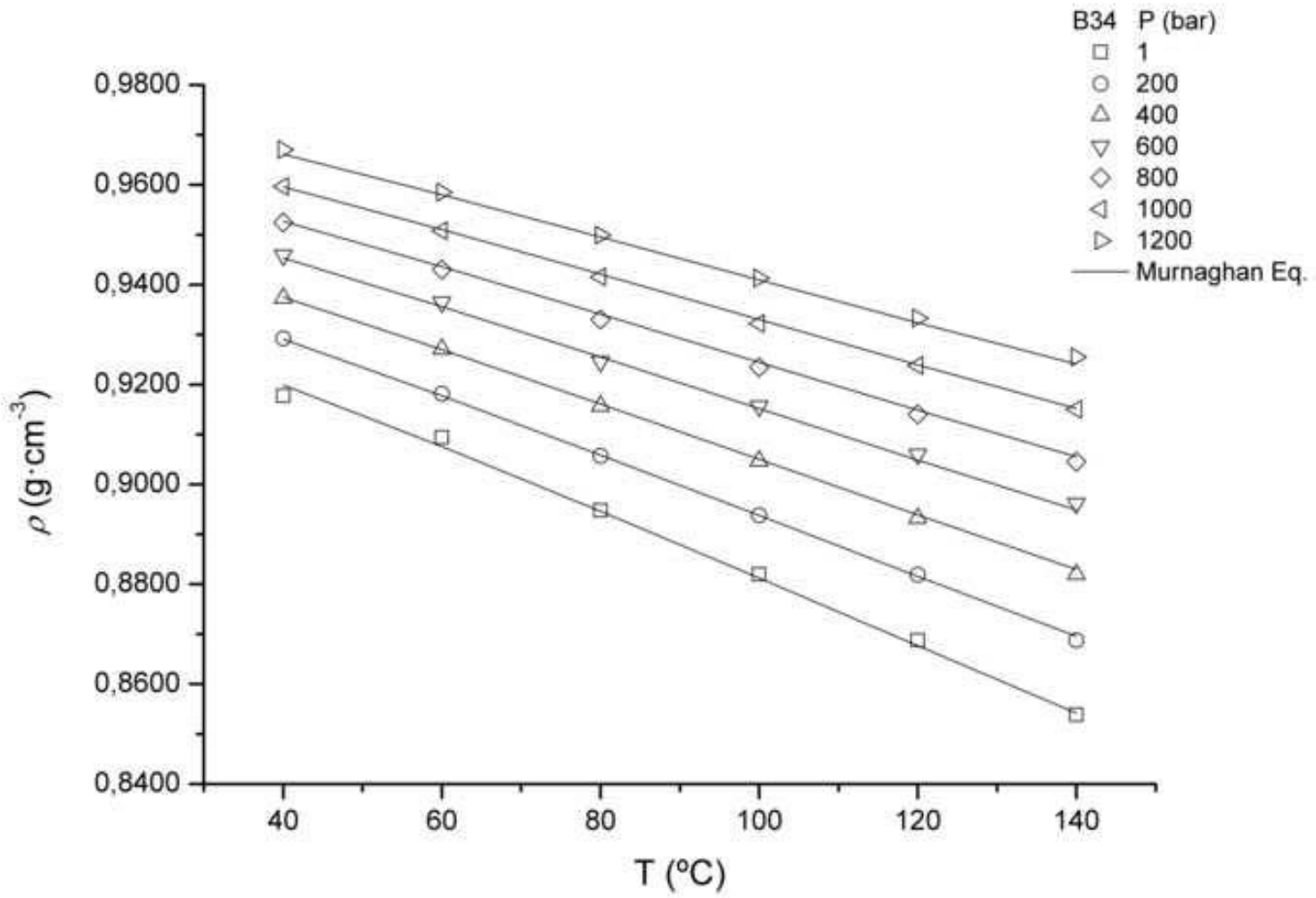

Figure 4
Click here to download high resolution image

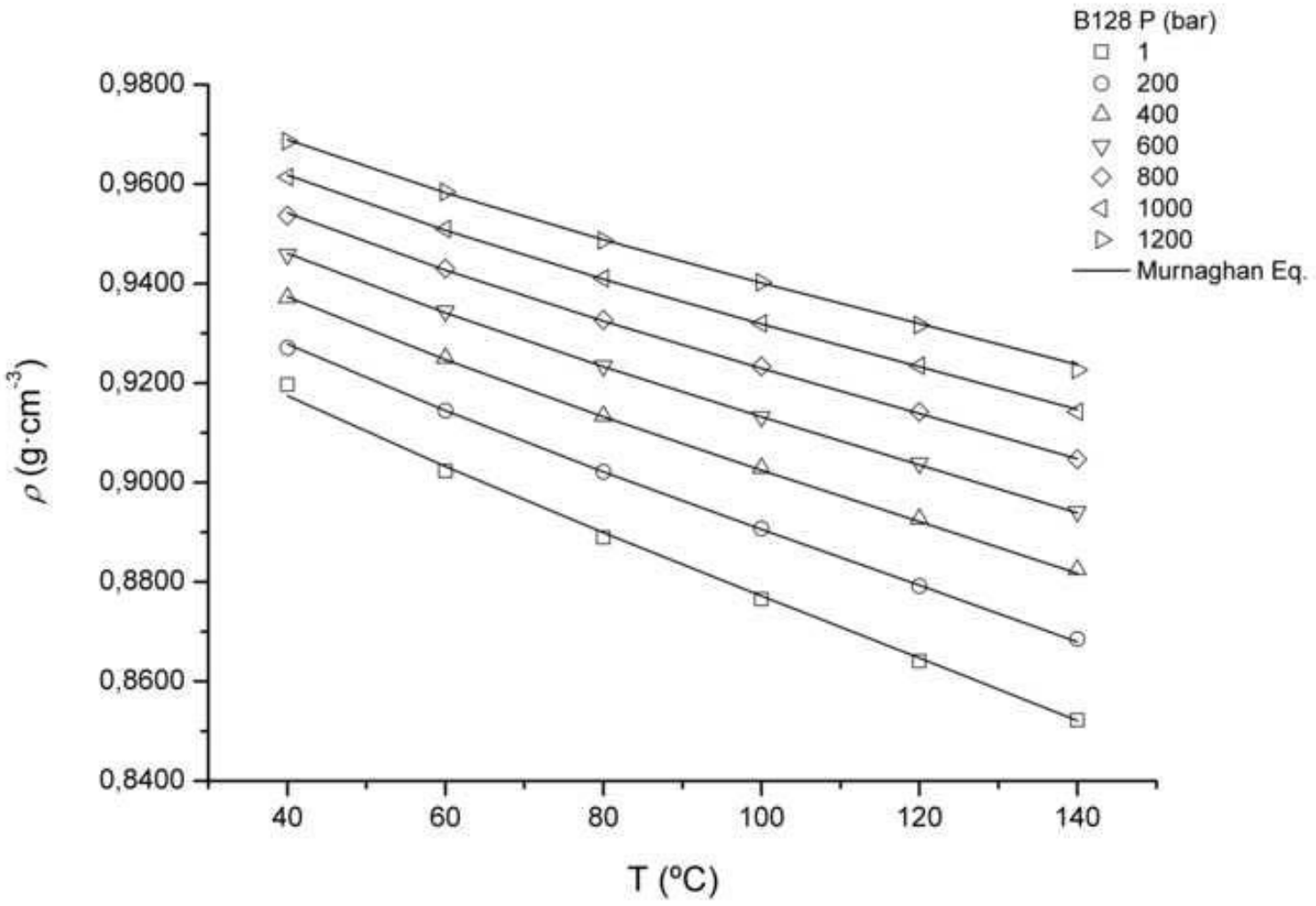

Figure 5
Click here to download high resolution image

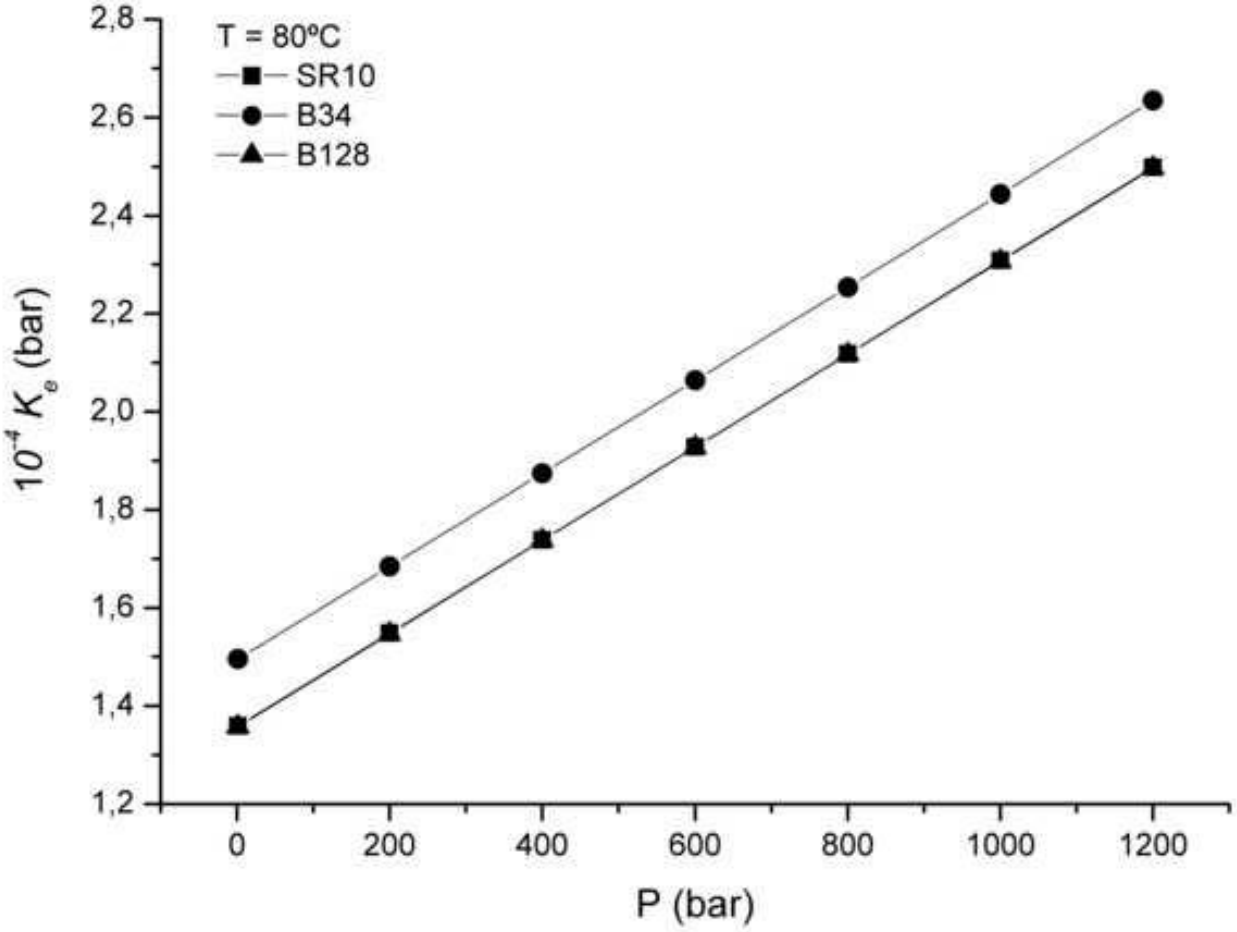

Figure 6
Click here to download high resolution image

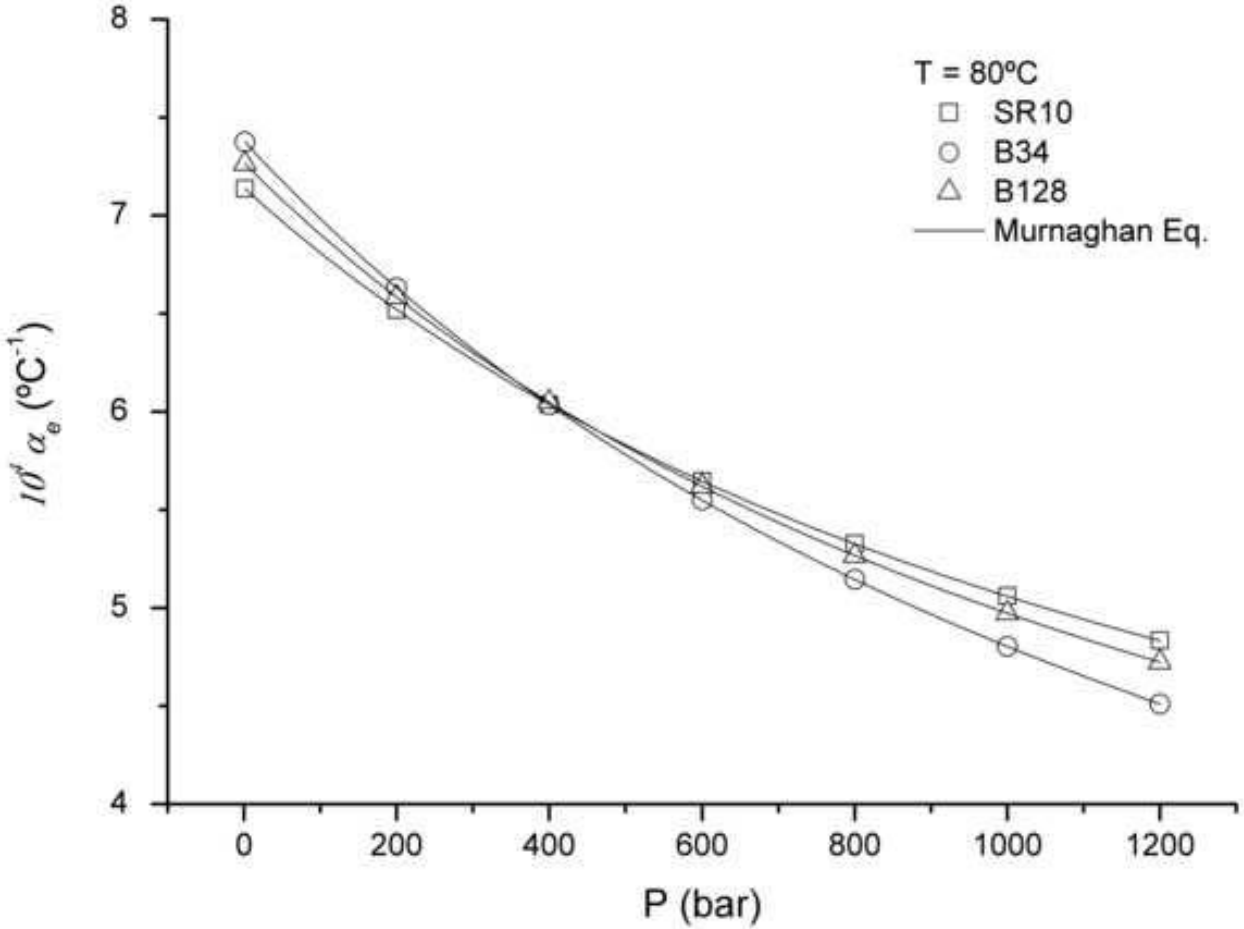

Figure 7

Click here to download high resolution image

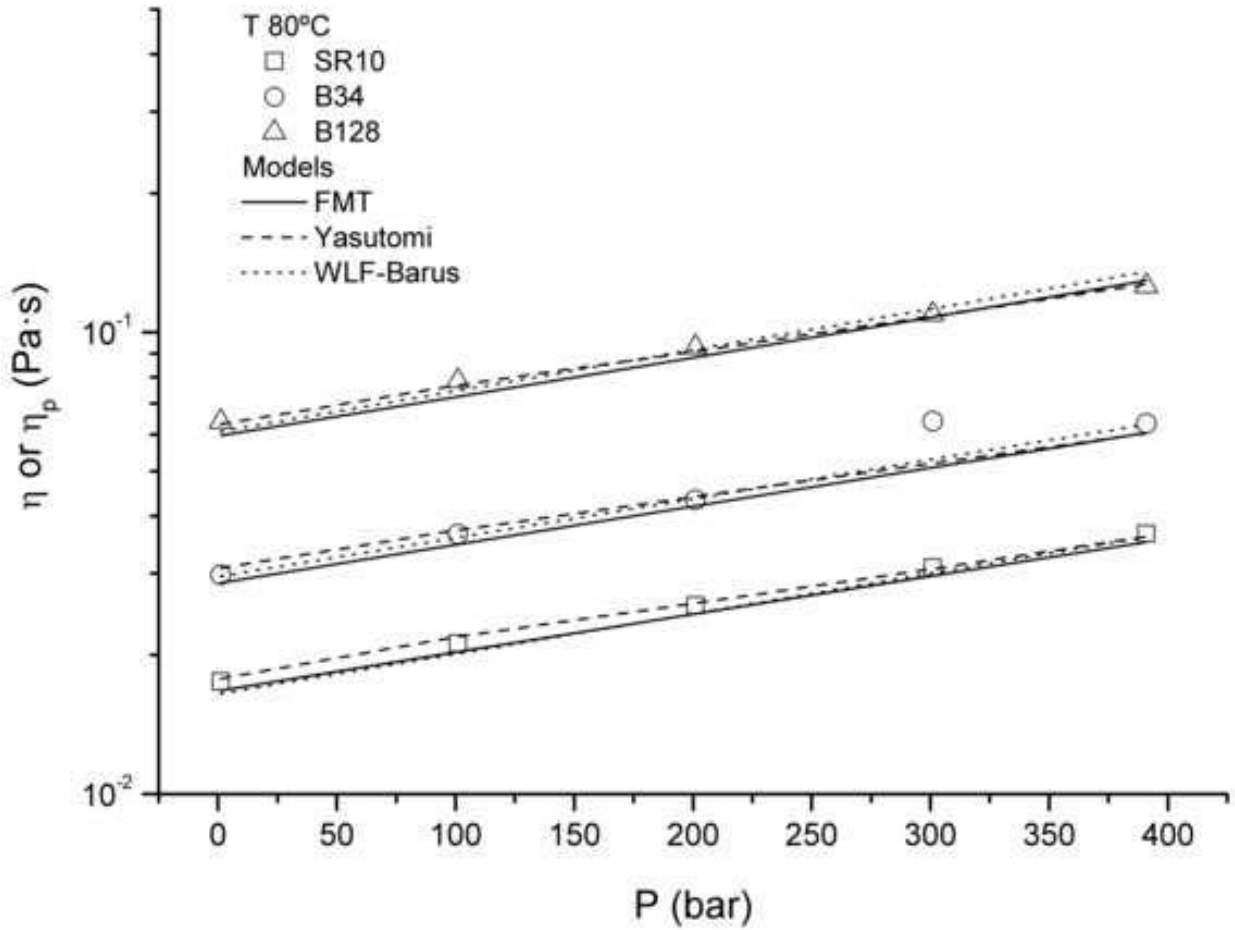

Figure 8

Click here to download high resolution image

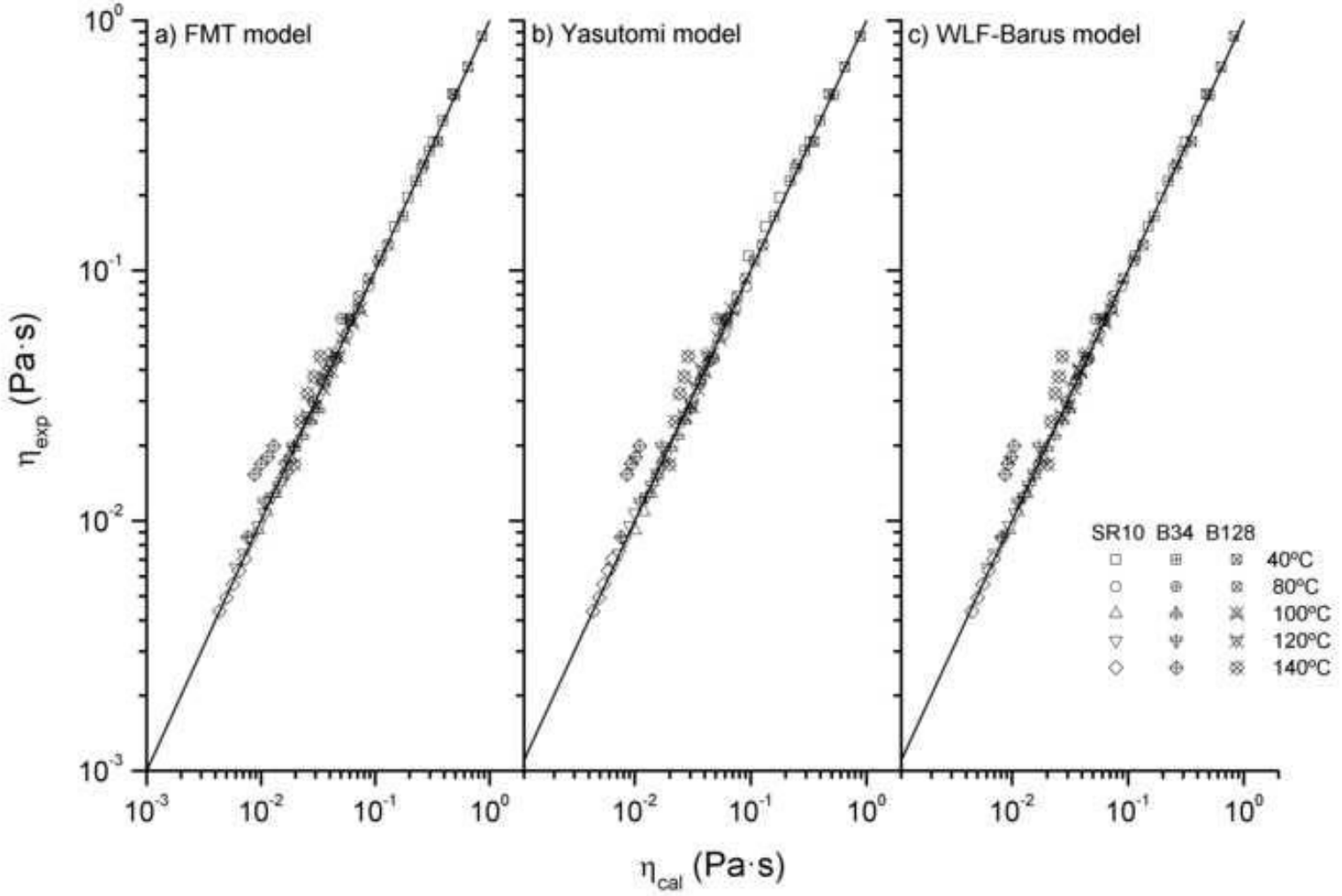

5. Conclusions

Conclusiones

Esta parte de la Tesis Doctoral presenta los resultados más relevantes hallados durante la investigación en el campo de la reologia de alta de fluidos de perforación. Así, a partir del trabajo desarrollado, se enumeran las conclusiones de mayor relevancia:

1. Las geometrías no convencionales, tales como son la cinta helicoidal y la turbina, son dispositivos de medida adecuados para la caracterización de comportamiento de flujo viscoso de los fluidos de perforación en función de la presión cuando se aplica la hipótesis de Metzner-Otto a los datos experimentales. En este sentido, estas geometrías de mezcla extienden el rango experimental de velocidades de cizalla hasta valores muy bajos, permitiendo así la medida de un parámetro ingenieril importante, como es el esfuerzo umbral en función de la presión.
2. Una combinación de los modelos de Sisko y Barus predicen la evolución de la viscosidad no-Newtoniana de los fluidos de perforación “all-oil” con la presión y la velocidad de cizalla bastante bien. El comportamiento viscosidad-presión de los fluidos de perforación tipo “all-oil” está principalmente influido por las propiedades piezoviscosas del aceite y las propiedades de la fase continua. La microestructura resultante también influye en el efecto de la presión sobre la reologia de estos sistemas. De ahí que, las propiedades reológicas de los fluidos de perforación con la organoarcilla B34 dependen de la concentración del organoclay como consecuencia del incremento del incremento en la fracción en volumen efectiva, mientras el comportamiento viscoso de los fluidos de perforación formulados con la organoarcilla B128 es esencialmente independiente de la concentración debido a la alta conectividad de la estructura gel resultante.

3. Los resultados experimentales confirman que la geometría de doble cinta helicoidal es adecuada para caracterizar el comportamiento de flujo viscoso para los fluidos de perforación modelo formulados con 5% en peso de las organoarcillas B34 y B128, bajo condiciones de alta presión y temperatura. Los modelos de Bingham y Herschel-Bulkley describen las propiedades reológicas de los fluidos de perforación modelo en base aceite, a distintas temperaturas y presiones bastante bien. Según estos resultados, el esfuerzo umbral aumenta con la presión, mientras su dependencia con la temperatura, está relacionada con el tipo organobentonita usada. Asimismo, un modelo factorial WLF-Barus describe de forma satisfactoria la variación de la viscosidad plástica con la presión y temperatura de estos fluidos de perforación, estando la viscosidad esencialmente influida por las propiedades piezoviscosas de la fase continua. De todo ello se concluyó que la diferencia en el comportamiento viscoso encontrado para ambos fluidos de perforación están asociadas con la compresión del medio continuo y cambios en la fracción en volumen de la fase dispersa térmicamente inducidos. Este último fenómeno parece estar relacionado con cambios de la solvencia entre el polímero de cubrición de las partículas y el aceite al aumentar la temperatura.
4. El modelo de Herschel-Bulkley ajusta el complejo comportamiento viscoso de las emulsiones inversas formuladas, en un amplio rango de fracciones en volumen de la fase acuosa bastante bien. La dependencia del esfuerzo umbral con la fracción en volumen de la fase acuosas es lineal para las emulsiones formuladas con un 1% en peso de la organoarcilla B128, y sigue una variación potencial cuando la concentración de organoarcilla es del 3% en peso. A altas presiones, el incremento en el esfuerzo umbral con la fracción en volumen y la concentración de organoarcilla ha sido relacionado con la compresión de la fase aceite así como con las interacciones interfaciales agua-aceite. El modelo de Barus ajusta la dependencia de la viscosidad de

las emulsiones inversas con la presión, para distintas fracciones en volumen y concentraciones de organoarcilla, bastante bien. Las emulsiones con un 1% en peso de organoarcilla muestran coeficientes piezoviscosos similares independientemente de la fracción en volumen de fase acuosa. Mientras que por el contrario, las formuladas con un 3% en peso de organoarcilla presentan coeficientes piezoviscosos menores que las de 1%, hecho que podría estar relacionado con la elasticidad de la lámina intefacial que rodea a las gotas emulsionadas.

5. Las densidades de los fluidos de perforación son mas susceptibles a los cambios de temperatura que a los de presión. La densidad muestra un incremento lineal con la concentración de organoarcilla en el rango de temperatura comprendido entre los y los 140ºC, y hasta presiones de 1200 bar. Concretamente, parece que la adición de la organoarcilla B128 da lugar a fluidos con una menor susceptibilidad térmica que en el caso de la organoarcilla B34, tanto a presión atmosférica como a alta presión. Los cambios de densidad de estos fluidos tipo "all-oil" con la presión y la temperatura, los cuales dependen de la naturaleza y la concentración de organoarcilla, han sido atribuidos a comportamiento expansivo no ideal debido a la capacidad de hinchamiento de las organoarcillas en un medio no acuoso.
6. Tanto la ecuación de tipo Tait como la de Murnaghan describen el comportamiento PρT de los fluidos de perforación tipo "all-oil" en el rango de presión y temperatura estudiado bastante bien. Los modelos basados en el volumen libre basado y parámetros físicos, tales como el FMT y el de Yasutomi, correlacionan los datos de viscosidad-presión-temperatura bastante bien, mostrando errores relativos iguales o incluso menores a los modelos conocidos de tipo exponencial, como el WLF-Barus.
7. La determinación y ajuste de los parámetros reológicos de los fluidos de perforación modelo en base aceite, tales como, por ejemplo, el esfuerzo umbral aparente usando sensores de mezclado, en función de

la composición, la presión y la temperatura es esencial para evitar y resolver problemas habituales del pozo, como son la limpieza del pozo, el atasco de la tubería o la sobrepresiones. Asimismo, una predicción fiable de las viscosidades de los fluidos de perforación con la presión y la temperatura, usando modelos de ajuste apropiados, permite un cálculo más aproximado de las pérdidas de presión en distintas secciones del pozo. Por último, una predicción precisa de las propiedades volumétricas de los fluidos de perforación cuando son sometidos a condiciones extremas de presión y temperatura es vital para mantener la estabilidad del pozo.

Conclusions

This part of the Thesis describes the results found during the research on high pressure drilling fluids rheology. From this work, the following conclusions have been highlighted:

1. Non-conventional geometries, such as helical ribbon and blade turbine, are suitable tools for characterizing the flow behaviour of drilling fluids as a function of pressure by applying the Metzner-Otto approach to experimental data. In this sense, these geometries extend the experimental range of shear rate down to a much lower shear-rate, allowing the measurement of important engineering parameter, such as for instance, yield stress as a function of pressure.
2. A combination of both Sisko and Barus models predicts the evolution of the non-Newtonian viscosity of all-oil drilling fluids with pressure and shear rate fairly well. The pressure-viscosity behaviour of all-oil drilling fluids is mainly influenced by the piezoviscous properties of the oil and the properties of the continuous phase. Besides, the resulting microstructure influences the suspension rheology as a

function of pressure. Thus, B34-based drilling fluids rheological properties depend on organoclay concentration as a result of the increase in the effective disperse phase volume fraction, whereas the viscous behaviour of B128-based drilling fluids is essentially independent of concentration due to the significant gel connectivity.

3. Experimental results confirm that double helical ribbon geometry is a very useful tool to characterise the complex viscous flow behaviour of model oil-based drilling fluids formulated with 5% wt. of organobentonite under high pressure high temperature conditions. Both Bingham´s and Herschel-Bulkley´s models describe the rheological properties of model oil-based drilling fluids, at different pressures and temperatures, fairly well. According to these results, drilling fluids yield stresses increase with pressure, whilst their temperature dependence is related to the type of organoclay used. In addition, a factorial WLF-Barus model satisfactorily describes the temperature/pressure evolution of the plastic viscosity for drilling fluids, being the viscosity at high shear rate mainly influenced by the piezo-viscous properties of the continuous phase. Thus, the different viscous flow behaviour encountered for both oil-based drilling fluids as function of pressure and temperature is related to compression of the continuous media and thermally-induced changes in effective disperse volume fraction. This latter phenomenon seems to be attributed to changes in solvency between the polymer-covered particles and the oil media with temperature.
4. The Herschel-Bulkley model fits the complex viscous flow behaviour of invert-muds formulated, in a wide range of internal aqueous phase volume fractions, fairly well. The dependence of the yield stress with internal aqueous phase volume fraction is linear for 1% w/w and power-law for 3% organoclay-based invert muds, respectively. Under pressure, the increase in yield stress with internal disperse phase volume fraction and organoclay concentration has been related to both

oil phase compression and water-oil interfacial interactions characteristics. Furthermore, Barus' model fits the pressure dependence of invert mud viscosity, for different disperse phase volume fractions and organoclay concentration, fairly well. 1% w/w organoclay-based invert muds show similar piezoviscous coefficients no matter internal disperse phase volume fraction. On the contrary, 3% w/w organoclay invert mud piezoviscous coefficients are lower than 1% w/w organoclay-based invert mud, fact that may be related to the elasticity of the interfacial layer surrounding the emulsified droplets.

5. Drilling fluid densities are more susceptible to changes in temperature than to pressure. Density shows a linear dependency with organoclay concentration in the temperature range comprised between 40 and 140ºC and pressures up to 1200 bar. In particular, it seems that the addition of B128 organoclay leads to fluids with lower susceptibility to temperature than B34 organoclay, at atmospheric pressure and high pressure. The density changes of these all-oil drilling fluids with pressure and temperature, which depend on both organoclay nature and concentration, may be attributed to the expansive non-ideal volumetric behaviour originated by the swelling capacity of organoclays in non-aqueous media.
6. Both Tait-like and Murnaghan equation describe the PρT behaviour of all-oil drilling fluids in the range of temperature and pressure studied, fairly well. Models based on the free-volume concept and physical parameters, such as FMT and Yasutomi´s models do fit the viscosity-pressure-temperature behaviour data fairly well, showing similar or even lower error than some well-known empirical exponential equations, such as WLF-Barus model.
7. The determination and modelling of rheological parameters of model oil-based drilling fluids, such as, for instance, the apparent yield stress by using mixing devices, as function of composition, pressure and

temperature is essential for preventing and managing hole challenges to be faced routinely, such as hole cleaning, stuck pipe or surge pressures. Further, a reliable prediction of viscosities of drilling fluids with pressure and temperature, using proper models, allows to calculate more accurate pressure losses in the different sections of the bore. In addition, the accurate modelling of volumetric behaviour of these fluids submitted to extreme conditions is vital to maintain the hole stability.